

Supported lipid bilayer interactions with nanoparticles, peptides and polymers

A Dissertation

Submitted to the Faculty of

Worcester Polytechnic Institute

In Partial Fulfilment of the Requirements for the

Degree of

DOCTOR OF PHILOSOPHY in

Chemical Engineering

December 2017

by

Elaheh Kamaloo

Terri A Camesano, Ph.D.
Professor, Research Advisor
Department of Chemical Engineering
Worcester Polytechnic Institute

Ramanathan Nagarajan, Ph.D.
Research Chemical Engineer
Natick Soldier Research, Development &
Engineering Center (NSRDEC)

Amy M. Peterson, Ph.D.
Assistant Professor of Chemical Engineering
Worcester Polytechnic Institute

Jianyu Liang, Ph.D.
Associate Professor of Mechanical Engineering
Worcester Polytechnic Institute

Dedication

This dissertation is dedicated to Charles C. Morse for his compassion and the endless support during my graduate study at WPI.

*If you could get rid
Of yourself just once,
The secret of secrets
Would open to you.
The face of the unknown,
Hidden beyond the universe
Would appear on the
Mirror of your perception*

~Rumi

Table of Contents

Abstract	7
Authorship.....	11
Acknowledgements.....	12
Glossary of Abbreviations	15
Chapter 1: Introduction	17
1.1 Introduction to supported lipid bilayer (SLB).....	18
1.2 Experimental technique: quartz crystal microbalance with dissipation (QCM-D).....	19
1.3 Research summary	22
1.4 References:	26
Chapter 2: Size Dependence of Gold Nanoparticle Interactions with a Supported Lipid Bilayer:	
A QCM-D study.....	29
2.1 Abstract	30
2.2 Introduction.....	31
2.3 Experimental and Theoretical Methods	34
2.3.1 Gold nanoparticles	34
2.3.2 Vesicle preparation.....	35
2.3.3 QCM-D of formation of supported lipid bilayers.....	36
2.3.4 QCM-D measurements of SLB interactions with gold NPs in water.....	37
2.3.5 QCM-D measurements of SLB interactions with gold NPs in the presence of PMAA38	

2.3.6 Analysis of QCM-D data.....	39
2.4. Results	41
2.4.1 Interactions of gold NPs in water with the supported lipid bilayer	41
2.4.2 Interaction of gold NPs in PMAA solution with the supported lipid bilayer	47
2.4.3 Interaction of PMAA with the lipid bilayer before and after NP exposure.....	48
2.5. Discussion	51
2.5.1 Measured Δf and ΔD represent NP-bilayer interactions and not solvent effects	51
2.5.2 Estimating citric acid-stabilized gold NPs adsorption on bilayer.....	52
2.5.3 Citric acid stabilized gold NP adsorption on bilayer causes some lipid removal.....	53
2.5.4 PMAA coated NPs adsorb more strongly to the bilayer	54
2.5.5 Size-dependent NP engulfment by bilayer causes lipid removal	57
2.6. Conclusions	62
2.7. Acknowledgments	63
2.8. References	63
Chapter 3: Nanoparticle Interactions with Model Membranes Modulated by	
Humic Substances	68
3.1 Abstract	69
3.2 Introduction	70
3.3 Materials and methods	73
3.3.1 Gold nanoparticles	73

3.3.2 Vesicle preparation	73
3.3.3 Humic substances	74
3.3.4 Quartz crystal microbalance with dissipation (QCM-D) monitoring for bilayer formation and NPs interaction.....	75
3.3.5 Relating changes in frequency to mass changes using Sauerbrey relation.....	77
3.4 Results	77
3.4.1 Effect of humic substance on zeta potential of NPs	77
3.4.2 Formation of SLB monitored by QCM-D	79
3.4.3 Monitoring the interactions of NPs with SLBs in the presence of humic substances ..	80
3.4.3 Mass change of bilayer as the result of interactions with different functionalized gold NPs in water and HA	84
3.5 Discussion	87
3.5.1 Humic acids coated the nanoparticles, masking surface charges	87
3.5.2 Interactions between humic substances and a bilayer are affected by the molecular size and structure of the humic substances	88
3.5.3 Mechanism of interactions between NPs and a bilayer are affected by the properties of the humic substances that are present in the media	91
3.6 Summary and conclusions.....	93
3.7 Acknowledgments.....	95
3.8 References	95

Chapter 4: Formation of raft-containing supported lipid bilayers:

A qualitative study by quartz crystal microbalance	103
4.1 Abstract	104
4.2 Introduction	105
4.3 Methods and materials	108
4.3.1 Vesicle preparation	108
4.3.2 Quartz crystal microbalance with dissipation monitoring (QCM-D)	109
4.3.3 Statistical analysis and mathematical modeling	110
4.4 Results and discussion	110
4.4.1 Vesicle containing cholesterol, sphingomyelin, and ganglioside remained unruptured on the surface	110
4.4.2 Effect of experimental parameters on vesicle fusion	114
4.4.3 Effect of vesicle size	115
4.4.4 Effect of Temperature Change	119
4.4.5 Effect of buffer composition and osmotic pressure	122
4.5 Summary	128
4.6 Acknowledgement	128
4.7 References	129
Chapter 5: A QCM-D based mechanistic study of Alzheimer's disease	135
5.1 Abstract	136
5.2 Introduction	137

5.3 Methods and materials	140
5.3.1 Small unilamellar vesicles (SUVs).....	140
5.3.2 Quartz crystal microbalance with dissipation.....	142
5.3.3 A β	142
5.3.4 Thioflavin T (Th-T) assay	143
5.4 Results and discussion.....	143
5.4.1 Kinetics of peptide aggregation characterized by ThT assay	145
5.4.2 Peptide–membrane interactions characterized by QCM-D	146
5.4.3 Peptide–membrane interaction kinetics characterized by QCM-D fingerprint	152
5.5 Conclusions.....	155
5.6 Acknowledgements	156
5.7 References	156
Chapter 6: Conclusions and Future Directions	163

Abstract

Supported lipid bilayers (SLBs) are one of the most common model membranes used in the field of cell membrane biology because they provide a well-defined model membrane platform for determination of molecular-level interactions between different biomolecules (e.g., proteins, peptides) and lipid membranes. Compared to model organisms, the use of SLB is preferable because it mimics cell plasma membrane in a very simple and well-controlled way. Therefore, the molecular structure of the membrane and the experimental conditions (e.g., solution chemistry, temperature, and pH) can be easily adjusted to the required conditions of any systematic research. In addition, SLBs are typically easy to form, cheap, and very reproducible; and they are compatible with different surface characterization techniques such as quartz crystal microbalance with dissipation (QCM-D), ellipsometry, and atomic force microscopy (AFM). This study demonstrates that QCM-D analysis of SLBs serves as powerful tool to investigate and characterize the mechanisms of interactions between lipid membranes and gold nanoparticles (NPs), environmentally relevant polymers, and disease-inducing peptides.

Given the many critical applications of gold NPs in drug delivery and diagnostics, understanding membrane–NP interactions is crucial, especially for determination of NPs cytotoxicity. In this study, we focus on membrane disruption as one of the different mechanisms by which metal NPs induce cytotoxicity. The use of a SLB is beneficial for this goal as it elucidates the unique mechanism of membrane disruption without the interference of other mechanisms taking place simultaneously in biological cells.

For NP–membrane interaction studies, a SLB composed of L- α -phosphatidylcholine (egg PC) was formed on a SiO₂-coated crystal, and QCM-D analysis was performed to obtain information about mass and viscoelastic changes of the SLB resulting from interactions with

gold NPs. In order to better understand the mechanisms of NP–membrane interactions, we systematically changed the NP’s properties and the experimental conditions. In order to understand the effect of NP size, gold NPs with diameters of 2, 5, 10, and 40 nm were tested and compared to each other. NPs were tested in their citric acid–stabilized state as well as in the presence of poly (methacrylic acid) (PMAA), which represents an organic coating that could become associated with NPs in the environment. The results indicated that when dissolved in water, gold NPs with diameters of 2, 5, 10, and 40 nm did not perturb the membrane, but in the presence of environmentally relevant polymers, the larger nanoparticles were found to disrupt the membrane.

In order to elucidate the effect of surface chemistry, 10-nm gold NPs with various functionalizations (i.e., anionic, cationic, and nonionic ligands) were tested. Control experiments were designed to test the effect of NPs in the absence of humic substances, which means the NPs were dissolved in water. In these cases, regardless of the type of NP functionalization, no substantial bilayer mass changes were observed. This suggests that the charge and chemistry of the ligands had a minor effect on NP–membrane interactions. Furthermore, in both the control and humic acid experiments, there were small dissipation changes (less than 1 unit) indicating that the overall membrane structure was not perturbed.

In order to mimic environmentally relevant conditions, the mass and viscoelasticity of the SLB was characterized in the presence of four different natural polymers, also known as natural organic materials (NOMs): fulvic and humic acids extracted from Suwannee River (SRFA and SRHA), which had relatively lower molecular weights; a commercial humic acid (HA); and humic acid extracted from Elliott soil (ESHA), which had a higher molecular weight. The results showed that NOMs with lower molecular weights adsorbed to the bilayer, while higher

molecular weight components did not induce any changes to the bilayers. In addition, the NPs in SRFA and SRHA increased the mass of the bilayer by 20 to 30 ng, while the NPs in HA and ESHA changed the mass of the bilayer by <10 ng. It was concluded that the presence of humic substances, as well as their physical and chemical properties, exerts a direct impact on the interactions between cell membranes and NPs.

In addition to the field of NP toxicity, SLBs play a pivotal role in the field of neurodegenerative diseases, such as Alzheimer's disease (AD), in which the pathological cascade of events starts from interactions of a misfolded peptide with a cell membrane. In this thesis, we confirm the validity of QCM-D analysis of SLB as an important platform for the investigation of amyloid β (the peptide associated with AD) interactions with lipid membranes. Adsorption of A β peptide to cell membrane is known to take place on the so-called "lipid rafts", which are membrane microdomains enriched with cholesterol, sphingomyelin, and ganglioside. The formation of SLBs containing lipid rafts is not only important for the field of AD research, but also it is important for other in vitro studies of cell biology, as the lipid rafts are responsible for a variety of biological functions such as association of some membrane proteins and cellular signaling. However, the presence of lipid raft components such as sphingomyelin and cholesterol makes the formation of the bilayer more challenging because it can lead to adsorption of intact vesicles on the substrate without formation of the bilayer.

In this study, the formation of lipid bilayer composed of 1,2-dioleoyl-sn-glycero-3-phosphocholine (DOPC), 1,2-dioleoyl-sn-glycero-3-phospho-L-serine (DOPS), cholesterol (Chol), sphingomyelin (SM), and ganglioside (GM) was investigated using QCM-D. A challenge was that the raft-containing vesicles remained intact on the SiO₂ crystal. Therefore, different experimental conditions were tested to induce vesicle fusion, such as pH, temperature, osmotic

pressure, and vesicle size. A key parameter in forming the bilayer was found to be applying osmotic pressure to the vesicles by having the vesicles' exterior concentration of NaCl higher than the interior concentration. When this concentration gradient was applied to the vesicles before flowing them on the substrate, vesicle rupture was favored and formation of a complete bilayer could occur. Here, we report the effects of each tested variable on the adsorption and fusion of the raft-containing vesicles, and the results are discussed based on the mechanisms of vesicle-vesicle and vesicle-substrate interactions. After developing a robust method for the formation of SLB with lipid rafts, we used that as a template to characterize the mechanism of interactions between A β peptide and cell membrane which lead to onset of AD.

The mechanism of A β toxicity leading to AD has not been fully discovered yet due to the complexity of the process, which includes several steps: A β peptide adsorption on the membrane, the conformational change from disordered in solution to a membrane-bound α -helix structure, and then formation of β -sheet aggregates that serve as fibrillation seeds. In this study, we showed that the QCM-D technique is a promising tool to conduct systematic studies on the mechanism of interactions between A β peptide and lipid membranes. To our knowledge, this was the first time QCM-D was utilized for characterization of A β fibrillation from monomer states through the formation of mature fibrils. The data indicated that peptide-membrane interactions follow a two-step kinetic pathway starting with the adsorption of small (low-n) oligomers until they cover all the adsorption sites on the surface. In the second step, the membrane structure is destabilized as a result of interaction with oligomers, which leads to lipid loss from the surface. Consistency of the results with data obtained via other techniques substantiates QCM-D technique as a robust approach to answer the remaining unanswered questions in the field of Alzheimer's disease.

Authorship

I hereby declare that the contents of this thesis are a representation of the work done by the main author except for chapter 2, for which contributions were made by Christina M. Bailey, Kellie L. Waterman, Kathleen F. Wang, and Dr. Ramanathan Nagarajan and Dr. Terri Camesano.

Christina M. Baily contributed to performing part of the experiments, the data analysis and preparing the method section, presented in Chapter 3.

Acknowledgements

I want to acknowledge all of the support I received during my journey toward my doctoral degree. A few years ago, when I left my home country to start my graduate study, all I had was a great passion for science. Today I feel blessed, not only for having been able to accomplish my dream, but also for the privilege of knowing the great many people whose support and encouragement has been my motivation for growth.

First, I would like to express my deepest gratitude to my adviser, Dr. Terri A. Camesano, who has supported me intellectually and financially throughout my doctoral program. She was truly patient in mentoring me and very generous in sending me to many conferences to present our scientific work. I am thankful for having the opportunity to work under her supervision to develop the skills to be a scientist. Starting research in her lab was a great turning point in my professional life for which I am grateful beyond words.

I would also like to express my appreciation for all of the support I got from Dr. Ramanathan. He spent countless hours meeting with me and answering my questions. I appreciate his willingness to lend his valuable time and expertise to this project. His passion for genuine research was a great gift.

Besides my advisers, I would like to thank my other committee members, Prof. Peterson and Prof. Liang, for their insightful comments and encouragement and for their hard questions that led me to pursue my project with a more critical and enriched perspective.

My sincere thanks also go to Prof. Gericke, Prof. Peterson, Prof. Zhou, Prof. Roberts, Prof. Duffy, and Prof. Dempsey, who gave me access to their laboratory equipment.

I am very grateful for the funding that I received to conduct this research from the WPI Chemical Engineering Department; the National Science Foundation (CBET 0966496); the Natick Soldier Research, Development & Engineering Center (NSRDEC); the Carl and Inez Weidenmiller Fellowship; the National Science Foundation (EAPSI, 1414982); the Kern Entrepreneurship Education Network Grant; and the Axel F. Backlin Tuition Scholarship.

I am also grateful to my graduate fellows at WPI for their help in the lab and also friendship: Sarah, Kathleen, Prachi, Diego, Lida, Azadeh, Todd, and rest of Prof. Camesano's lab. I want to thank my undergraduate research assistants who helped me with the experiments: Cindy, Ian, and Martin. It was absolutely fun to work with undergraduate assistants and see their excitement for learning about research and working in the lab. I would also like to thank Ellie Lin for all of her great advice on my writing.

My special thanks go to Mohsen, whose love gave me the strength to take the first and most difficult step of my PhD journey: leaving my home country for graduate study. Mohsen was not only my closest friend all these years, he was also a great mentor to me. His persistence in pursuing his professional dreams sets the example of "I will either find a way or I will make one".

I am also grateful for the precious support of my dear friends Yasmin, Leila, Maryam, Leni, Saeedeh, and Parva, who are my soul sisters; and Aida, Pegah, Miad, Nargess, Joe, and Sina. I am blessed to have them all as my friends. I know that without their ongoing support and care, finishing the last chapter of my academic life would not have been possible. I also want to thank Chris for being such a great spiritual support in the last months of my doctoral work. Without her support, I could not have reached the defense milestone.

Finally, I wish to thank my family for supporting me emotionally and spiritually throughout this project, and of course, throughout my life. Thank you, Dad, for teaching me and my sister that there is no limit to the dreams that a woman can pursue in this world. Your love and affection for everyone around you will always warm my heart and motivate me to perform meaningful research that will impact other people's lives. Thank you, Mom, for all the effort you put into my education and for holding education as a core value. The confidence you had in my talents motivated me to set my expectations high and to not give up, even if the road is steep.

Last but not least, I owe a special thank you to my wonderful sister. Atefeh, you have been my buddy through the ups and downs, my role model in professional life, and my best friend forever even if miles away.

Glossary of Abbreviations

$A\beta$	Amyloid beta
$A\beta/GM1$	Peptide to ganglioside ratio
ΔD	Change in energy dissipation
Δf	Change in frequency
Δm	Change in mass
δL	Decay length of the acoustic wave in liquid
ηf	Viscosity of the film
ηL	Viscosity of the liquid
APP	Amyloid precursor protein (APP)
C	Sauerbrey constant
CD	Circular dichroism
D	Dissipation
DOPC	1,2-dioleoyl- <i>sn</i> -glycero-3-phosphocholine
DOPS	1,2-dioleoyl- <i>sn</i> -glycero-3-phospho-L-serine
DLS	Dynamic Light Scattering
ESHA	Elliott soil humic acid
f	Frequency
f_0	Resonant frequency of the quartz crystal (5 MHz)
FTIR	Fourier transform infrared

HA	Commercially available humic acid
NMR	Nuclear magnetic resonance spectroscopy
MUTAB	(11-Mercaptoundecyl)-N,N,N-trimethylammonium bromide
NOM	Natural organic matter
NP	Nanoparticle
PC	L- α -phosphatidylcholine (egg, chicken)
<i>P/L</i>	Peptide-to-lipid ratio
PMAA	Poly(methacrylic acid)
QCM-D	Quartz crystal microbalance with dissipation monitoring
ROS	Reactive oxygen species
SDS	Sodium dodecyl sulfate
SEM	Scanning electron microscopy
SLB	Supported lipid bilayer
SRFA	Suwannee River fulvic acid
SRHA	Suwannee River humic acid
TEM	Transmission electron microscopy
ThT	Thioflavin T
TIRFM	Total internal reflection fluorescence microscopy
Tris	Tris(hydroxymethyl)aminomethane

Chapter 1

Introduction

1.1 Introduction to supported lipid bilayer (SLB)

Supported lipid bilayers (SLBs) are one of the most common model membranes used in the field of cell membrane biology because they provide a well-defined model membrane platform for determination of molecular-level interactions between different biomolecules (e.g., proteins, peptides) and lipid membranes. Compared to model organisms, the use of SLB is preferable because it mimics the cell plasma membrane in a very simple and well-controlled way. Therefore, the molecular structure of the membrane and the experimental conditions (e.g., solution chemistry, temperature, and pH) can be easily adjusted to the required conditions of any systematic research. In addition, SLBs are typically easy to form, cheap, and very reproducible; and they are compatible with different surface characterization techniques such as quartz crystal microbalance with dissipation (QCM-D), ellipsometry, and atomic force microscopy (AFM) [1]. This study demonstrates that QCM-D analysis of SLBs serves as powerful tool to investigate and characterize the mechanisms of interactions between lipid membranes and gold nanoparticles (NPs), environmentally relevant polymers, and disease-inducing peptides.

The most common method for the formation of SLBs is vesicle fusion, which is the spontaneous self-assembly of bilayers from vesicles adsorbed on a surface. Due to its simplicity and reproducibility, the vesicle fusion method is often preferred as it consists of adsorption of vesicles on a surface followed by rupture and fusion of the vesicles to form an extended, uniform bilayer (Fig.1).

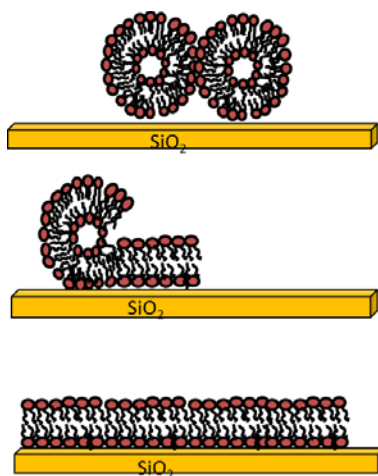


Figure 1. Forming a supported lipid bilayer via vesicle fusion.

1.2 Experimental technique: quartz crystal microbalance with dissipation (QCM-D)

The main experimental technique in this work was quartz crystal microbalance with dissipation (QCM-D), which is a real-time and label-free technique to characterize the mass and viscoelasticity changes of an adsorbed layer on a crystal. Because QCM-D is a sensitive technique (with a mass sensitivity of $\sim 1.8 \text{ ng/cm}^2$ in liquid [2]), it has been used for a wide range of research fields, such as protein-protein interactions, protein-membrane interactions, and membrane-based biosensors [1]. In a QCM-D instrument, a voltage is intermittently applied to a quartz crystal leading to crystal oscillation, and the frequency and dissipation of energy are monitored through each oscillation cycle [3]. An increase in the mass of the film leads to a decrease in the frequency of oscillation (Fig. 2 A), and an increase in the softness of the film leads to an increase in dissipation of energy as shown by dampening of the acoustic waves (Fig. 2 B).

If the film is rigid, the change in mass (Δm) is correlated to a change in frequency (Δf).

This relationship is described by the Sauerbrey equation [4]:

$$\Delta f = \frac{-2f_0^2}{A\sqrt{\rho_q\mu_q}} \Delta m, \quad (1)$$

where f_0 , ρ_q , and μ_q are the resonant frequency of quartz crystal (5 MHz), the density of quartz (2.648 g/cm³), and the shear modulus of the crystal (2.947×10^{11} g/cm·s²), respectively. In the case of less rigid film, the Sauerbrey equation is known to underestimate the mass and needs to be adjusted to the viscoelastic properties of the film and of the bulk solution [5].

Changes in rigidity of the surface lead to changes in the dissipation of energy, which is defined by

$$D = \frac{G''}{2\pi G'} , \quad (2)$$

where G'' and G' are the loss modulus and the storage modulus, respectively [5].

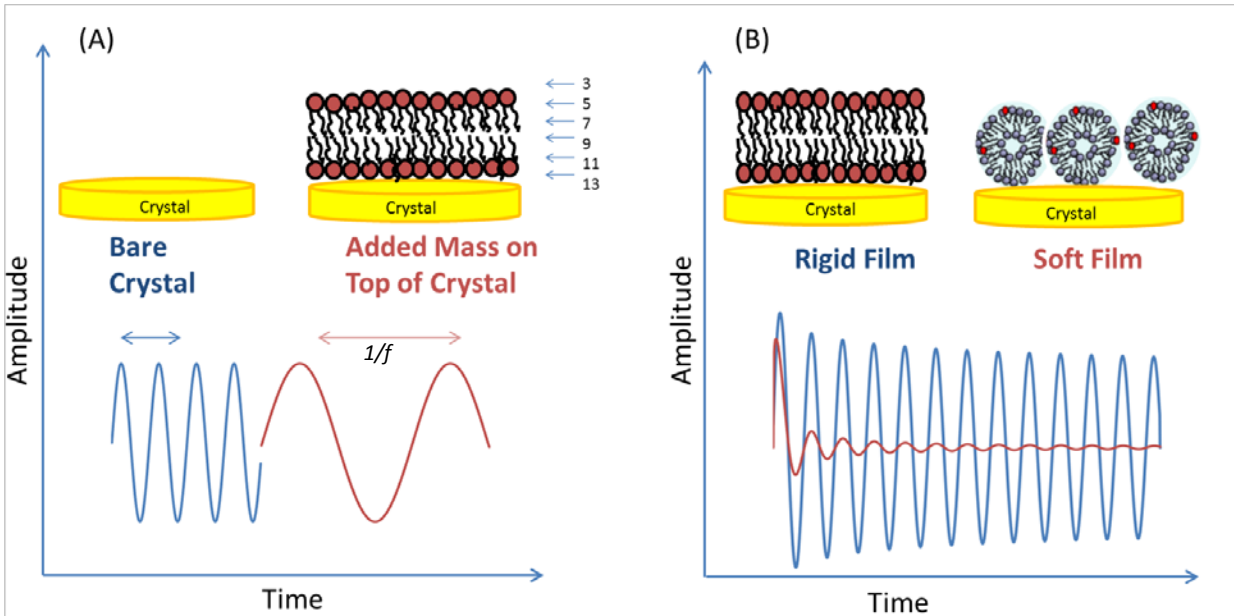


Figure 2. Schematic of QCM-D operation, in which an applied voltage oscillates the crystal and the resonance frequency and dissipation of energy are extracted. (A) The addition of energy causes the crystal to oscillate with at a

lower frequency. The blue and red curves correspond to the oscillation of a bare crystal (less mass) and a crystal carrying a film (increased mass), respectively. (B) Having a softer film on the crystal leads to more dissipation of energy, which is represented by a smaller amplitude. The blue and red decay curves correspond to the oscillation of rigid and soft films, respectively.

QCM-D records the frequency (f) and dissipation of energy (D) at several different harmonics, or overtones. Different overtones are related to the penetration depth (δ) of an acoustic wave throughout the film, defined as

$$\delta = \left(\frac{n_f}{n\pi f_0 \rho_f} \right)^{\frac{1}{2}}, \quad (3)$$

where n_f , n , and ρ_f are the viscosity of the film, the overtone number, and the density of the film, respectively [5]. As described by Eq. 3, the number of the overtone is inversely related to the depth of the film: the 13th overtone describes the closest layer to the crystal surface and 3rd overtone indicates the furthest (Fig. 2 A).

In the present work, we utilized the QCM-D technique to obtain mechanistic knowledge about the interactions of an SLB with three types of species: gold nanoparticles, natural polymers, and amyloid β (A β) peptide. The former two were selected to obtain a more in-depth understanding of NPs' environmental cytotoxicity; it is a high-priority goal of health and safety regulatory agencies and related scientific societies to identify the health, safety, and environmental impacts of engineered nanoparticles [6]. The latter molecule, A β , was chosen because it is known that the interactions between this peptide and brain cell membranes lead to the onset of Alzheimer's disease (AD). The following sections of this document focus on method development, results, and data analysis of SLB interactions with the aforementioned species.

1.3 Research summary

Chapter 2: Interactions of gold nanoparticles with lipid membranes

Nanoparticle (NP)-cell interactions are important to many critical applications such as drug delivery and diagnostics, as well as for determining the safety of NPs to humans and the environment. Gold nanoparticles are especially interesting for toxicity studies due to their wide range of applications in diagnostics and therapeutics. NPs can induce toxicity through different pathways. One of the mechanisms of toxicity for engineered NPs originates from their ability to disrupt the integrity of cell membranes. Studies from mammalian and bacterial cell literature have clearly identified a number of mechanisms by which nanomaterials exhibit toxicity toward biological cells [7], including disruption of cell membrane integrity, cell damage by generation of reactive oxygen species (ROS), damage to DNA, damage to the functionality of cellular proteins/enzymes, triggering of inflammation, oxidative stress, and damage to mitochondrial function. Physicochemical factors, specifically size, surface charge density, and polarity, have been linked to the ability of NPs to interact with cell membranes [8].

In this chapter we focused on the membrane disruption mechanism to answer the following questions: Do interactions between NPs and lipid bilayers lead to membrane disruption? What is the effect of NP size on the interaction of gold NPs with a lipid bilayer? How do environmentally relevant polymers change the interactions of gold NPs with a lipid bilayer? The interactions of 2-, 5-, 10-, and 40-nm-diameter gold NPs with supported lipid bilayers (SLB) of L- α -phosphatidylcholine were investigated via quartz crystal microbalance with dissipation monitoring (QCM-D). NPs were tested in their citric acid-stabilized state as well as in the presence of poly(methacrylic acid) (PMAA), which represents an organic coating that could become associated with NPs in the environment.

Chapter 3: Interactions of natural polymers with lipid membranes

The increasing use of engineered NP leads to the release of such materials into the environment. It is necessary to study the toxicity of NPs in environmentally relevant conditions. Due to the possibility of NPs being released into the natural environment during their life cycle [9], it is necessary to investigate the effects of NPs at the nano–bio interface, where there are other complex chemical species present, such as natural organic material (NOM). NOMs are heterogeneous mixtures of polydispersed materials in soils and natural waters, mainly composed of humic substances (e.g., humic and fulvic acids) and other organic materials such as polysaccharides, proteins, and lipids. Both humic acids (HAs) and fulvic acids (FAs) possess a negative charge due to an abundance of carboxylic and phenolic groups [10], and this can affect the toxicity of NPs as they alter the adsorption, aggregation/stabilization, dissolution, and surface transformation of the nanoparticles.

This chapter provides mechanistic knowledge about SLB–NP interactions to answer the following questions: What is the effect of NP ligands on the interactions of NP with a bilayer? How does natural polymer change the mechanism of NP–bilayer interactions? What is the effect of natural polymer on NPs? What is the effect of natural polymer on bilayers? In order to mimic the natural environment, four humic substances were examined: commercially available humic acid provided by Sigma-Aldrich (HA), humic acid extracted from Elliott soil (ESHA), humic acid extracted from the Suwannee River (SRHA), and fulvic acid extracted from the Suwannee River (SRFA).

Chapter 4: Formation of raft-containing supported lipid bilayers as a template for studying Alzheimer's disease

Alzheimer's disease is related to the presence of amyloid β peptide aggregates on brain cell membranes. The cause of neurotoxicity of A β is not fully understood. Simple SLBs with one or two lipid components are not applicable in Alzheimer's research because the amyloidogenic processing machinery is located in lipid rafts that are rich in cholesterol, sphingomyelin, and gangliosides. The commonly used QCM-D protocol for the formation of simple SLBs does not lead to the formation of bilayer containing lipid rafts. SLBs are important platforms to study the biophysical properties of lipid membranes and protein–lipid interactions. Cellular lipid membranes are lateral heterogeneous structures including highly liquid-ordered domains enriched with cholesterol and sphingomyelin referred as “lipid rafts”. Since these membrane microdomains are responsible for a variety of biological functions, such as association of some membrane proteins and cellular signaling, formation of lipid bilayers containing lipid rafts is important for in vitro studies of cell biology. However, the presence of lipid raft components such as sphingomyelin and cholesterol makes the formation of the bilayer more challenging because it can lead to adsorption of intact vesicles on the substrate without formation of the bilayer. QCM-D provides real-time data on the formation of SLBs. In this study, the formation of lipid bilayer composed of 1,2-dioleoyl-sn-glycero-3-phosphocholine (DOPC), 1,2-dioleoyl-sn-glycero-3-phospho-L-serine (DOPS), cholesterol (Chol), sphingomyelin (SM), and ganglioside (GM) was investigated using QCM-D. A challenge was that the raft-containing vesicles remained intact on the SiO₂ crystal.

In this chapter we systematically studied the effect of different experimental conditions, such as pH, temperature, osmotic pressure, and vesicle size, to induce vesicle rupture and form a

complete bilayer. Here, we report the effects of each tested variable on the adsorption and fusion of the raft-containing vesicles, and the results are discussed based on the mechanisms of vesicle–vesicle and vesicle–substrate interactions.

Chapter 5: Amyloid β aggregation on supported lipid bilayer: QCM-D study of Alzheimer's disease

The mechanism of A β toxicity leading to the onset of Alzheimer's disease has not been fully discovered yet, due to the complex, time-dependent nature of the peptide aggregation and dependence of the aggregation process on the initial state of the peptide, and also the lack of a reproducible technique as a platform for systematic studies. Suggested mechanisms of membrane disruption include three main categories: pore formation, peptide behaving as a detergent, and formation of peptide-rich microdomains inside the bilayer [11,12]. Small oligomers containing 4 to 6 monomers have shown the ability to form pores through membranes and a consequent calcium ion imbalance across the membrane which causes cell apoptosis [13]. Previous study on the interactions of antimicrobial peptides with egg PC supported lipid bilayer (SLB) characterized four different states of peptide–membrane interactions including insertion of a single peptide or peptide clusters, formation of pores, and adsorption of peptides on the surface [14].

In this chapter, we use QCM-D to answer the following questions: How does A β peptide interact with cell membranes? What is the effect of peptide aggregation on the membrane? What is the effect of membrane on aggregation?

Chapter 6: Conclusions and future work

We finish the thesis by summarizing the overall conclusions confirming that supported lipid bilayers provide a powerful model membrane platform allowing for extraction of molecular-scale information in the field of NP cytotoxicity and AD research. Recommendations are made for future directions of AD research using the method developed and discussed in this thesis.

1.4 References:

- [1] N. J. Cho, C.W. Frank, B. Kasemo, F. Höök, Quartz crystal microbalance with dissipation monitoring of supported lipid bilayers on various substrates., *Nat. Protoc.* 5 (2010) 1096–106. doi:10.1038/nprot.2010.65.
- [2] A. Mechler, S. Praporski, K. Atmuri, M. Boland, F. Separovic, L.L. Martin, Specific and selective peptide-membrane interactions revealed using quartz crystal microbalance., *Biophys. J.* 93 (2007) 3907–16. doi:10.1529/biophysj.107.116525.
- [3] I. Reviakine, D. Johannsmann, R.P. Richter, Hearing what you cannot see and visualizing what you hear: Interpreting quartz crystal microbalance data from solvated interfaces, *Anal. Chem.* 83 (2011) 8838–8848. doi:10.1021/ac201778h.
- [4] G. Sauerbrey, Verwendung von Schwingquarzen zur Wagungdiinner Schichten und zur Mikrowagung, *Zeitschrift Fur Phys.* 155 (1959) 206–222. doi:10.1007/BF01337937.
- [5] M. V Voinova, M. Jonson, B. Kasemo, “ Missing mass ” effect in biosensor ’ s QCM applications, *Biosens. Bioelectron.* 17 (2002) 835–841.

- [6] A. Dowling, R. Clift, N. Grobert, D. Hutton, R. Oliver, O. O’neill, J. Pethica, N. Pidgeon, J. Porritt, J. Ryan, Et Al., Nanoscience and nanotechnologies : opportunities and uncertainties, London R. Soc. R. Acad. Eng. Rep. 46 (2004) 618–618. doi:10.1007/s00234-004-1255-6.
- [7] A. Nel, Toxic Potential of Materials at the Nanolevel, Science. 311 (2006) 622–627. doi:10.1126/science.1114397.
- [8] V. V Ginzburg, S. Balijepalli, Modeling the thermodynamics of the interaction of nanoparticles with cell membranes., Nano Lett. 7 (2007) 3716–22. doi:10.1021/nl072053l.
- [9] A.E. Nel, L. Mädler, D. Velegol, T. Xia, E.M. V Hoek, P. Somasundaran, F. Klaessig, V. Castranova, M. Thompson, Understanding biophysicochemical interactions at the nano-bio interface., Nat. Mater. 8 (2009) 543–57. doi:10.1038/nmat2442.
- [10] Z. Wang, L. Zhang, J. Zhao, B. Xing, Environmental processes and toxicity of metallic nanoparticles in aquatic systems as affected by natural organic matter, Environ. Sci. Nano. 3 (2016) 240–255. doi:10.1039/C5EN00230C.
- [11] P. Walsh, G. Vanderlee, J. Yau, J. Campeau, V.L. Sim, C.M. Yip, S. Sharpe, The mechanism of membrane disruption by cytotoxic amyloid oligomers formed by prion protein(106-126) is dependent on bilayer composition., J. Biol. Chem. 289 (2014) 10419–30. doi:10.1074/jbc.M113.515866.
- [12] K. Sasahara, K. Morigaki, K. Shinya, Effects of membrane interaction and aggregation of amyloid β -peptide on lipid mobility and membrane domain structure., Phys. Chem. Chem. Phys. 15 (2013) 8929–39. doi:10.1039/c3cp44517h.

- [13] H. Ding, J. a Schauerte, D.G. Steel, A. Gafni, β -Amyloid (1-40) peptide interactions with supported phospholipid membranes: a single-molecule study., *Biophys. J.* 103 (2012) 1500–9. doi:10.1016/j.bpj.2012.08.051.
- [14] K.F. Wang, R. Nagarajan, T. A. Camesano, Differentiating antimicrobial peptides interacting with lipid bilayer: Molecular signatures derived from quartz crystal microbalance with dissipation monitoring., *Biophys. Chem.* 196 (2015) 53–67. doi:10.1016/j.bpc.2014.09.003.

Chapter 2

Size Dependence of Gold Nanoparticle Interactions with a Supported Lipid Bilayer:

A QCM-D study

Biophysical Chemistry 203–204 (2015) 51–61

2.1 Abstract

Knowledge of nanoparticle (NP) - membrane interactions is important to advances in nanomedicine as well as for determining the safety of NPs to humans and the ecosystem. This study focuses on a unique mechanism of cytotoxicity, cell membrane destabilization, which is principally dependent on the nanoparticle nature of the material rather than on its molecular properties. We investigated the interactions of 2, 5, 10, and 40 nm gold NPs with supported lipid bilayer (SLB) of L- α -phosphatidylcholine using quartz crystal microbalance with dissipation monitoring (QCM-D). Gold NPs were tested both in the absence of and in the presence of polymethacrylic acid (PMAA), used to simulate the natural organic matter (NOM) in the environment. In the absence of PMAA, for all NP sizes, we observed only small mass losses (1 to 6 ng) from the membrane. This small lipid removal may be a free energy lowering mechanism to relieve stresses induced by the adsorption of NPs, with the changes too small to affect the membrane integrity. In the presence of PMAA, we observed a net mass increase in the case of smaller NPs. We suggest that the increased adhesion between the NP and the bilayer, promoted by PMAA, causes sufficient NP adsorption on the bilayer to overcompensate for any loss of lipid. The most remarkable observation is the significant mass loss (60 ng) for the case of 40 nm NPs. We attribute this to the lipid bilayer engulfing the NP and leaving the crystal surface. We propose a simple phenomenological model to show that the competition between the particle-bilayer adhesion energy, the bilayer bending energy, and the interfacial energy at bilayer defect edges allows the larger NPs which become more adhesive because of the polymer adsorption, to be engulfed by the bilayer and leave the crystal surface, causing large mass loss and membrane disruption. The QCM-D measurements thus offer direct evidence that even if NPs are

intrinsically not cytotoxic, they can become cytotoxic in the presence of environmental organic matter which modulates the adhesive interactions between the nanoparticle and the membrane.

2.2 Introduction

Assessing nanomaterial hazards to humans and environmental organisms has proven to be challenging due to the vast diversity in nanomaterial properties (such as molecular composition, aqueous solubility, water-lipid partition coefficient, nanoparticle size, surface area, shape), the wide variations in the biological targets (such as cell lines, biomarkers) and the conditions (such as the dose levels of the nanoparticles, cell contact times) under which the interactions are examined [1]. Many experimental studies of cytotoxicity of engineered nanomaterials have been reported in the literature [2], most using mammalian cells, although there is an increasing body of literature related to bacteria. These studies have helped identify a number of mechanisms by which nanomaterials induce toxicity [3], including: cell damage by generation of reactive oxygen species (ROS), damage to DNA, damage to the functionality of cellular proteins/enzymes, triggering of inflammation, damage to mitochondrial function, and disruption of cell membrane integrity. All of the abovementioned mechanisms of cytotoxicity, with the exception of cell membrane disruption, have been shown possible from the molecular, atomic or ionic species constituting the NP and without requiring the nanoparticle nature of the material. For example, the ROS generation measured with different metal oxide NPs (Fe_2O_3 , Co_3O_4 , Mn_3O_4), and with molecular solutions of the same metal oxides, show that ROS generation occurs readily from molecular solutions [4] and does not require the material to be present in the nanoparticle form. Similar conclusions can be derived from available experimental data for many of the other cytotoxic mechanisms. In contrast, the integrity of the plasma membrane has been studied in the presence of different kinds of NPs such as metallic silver,

semiconductor CdO, and metal oxide MoO₃, and compared against the effects of their corresponding salt solutions: silver carbonate, cadmium chloride, and sodium molybdate [5]. In all cases, the soluble salts did not affect the plasma membrane integrity, while the three NPs reduced the membrane integrity allowing leakage of a cytosolic enzyme to occur. This suggests that the mechanism of cytotoxicity in the form of membrane destabilization requires the nanoparticle nature of the material and is not caused by the molecular scale action of the constituent molecules. It follows that if cell membrane disruption is purely due to physical factors such as the size, surface charge density, and polarity of NPs, then it must be a generic mechanism operative in the case of all nanomaterials. An important complication when studying nanoparticle interactions related to environmental systems arises from the presence of natural organic matter (NOM). Structurally, NOM is extremely complex with a three-dimensional macromolecular architecture and consisting of a diverse group of organic molecules [6]. At present, there is no consensus on the primary binding mechanism responsible for the aggregation of molecules giving rise to NOM. However, the nature of the major functional groups present in NOM has been well characterized, with groups such as carboxyl, hydroxyl, phenolic, alcohol, carbonyl and methoxy, all present. NOM has the ability to modify NP properties by adsorbing to the surface of the particles, which has been found to enhance the stability of aqueous NP dispersions and decrease particle aggregation [7,8]. Typically, NOM is negatively charged, and it impacts the surface properties of NPs by increasing electrostatic repulsion amongst the NPs. Since NOM is ubiquitously found in natural environments, studies of NP activity against environmental organisms should be conducted in the presence of organic species representing NOM.

In this work we focus on how nanoparticle size affects membrane destabilization, in the absence of and in the presence of organic matter simulating NOM. A model membrane system acting as the analog of biological cells is used to obtain systematic information on the nature of NP-membrane interactions. Supported lipid bilayers (SLBs) have become a reliable model system for cell membranes because they exhibit many of the properties of biological membranes, such as lateral fluidity, ability to incorporate proteins, and impermeability to ionic species [9]. The use of supported lipid bilayer, which mimics the basic membrane structure common to all cellular organisms provides a well-defined model membrane platform for studying NP-cell membrane interactions, mitigating data comparison problems arising from the use of different organisms. To simulate the key characteristics of NOM in the environment, we use a polymer, polymethacrylic acid (PMAA) with the carboxyl functional group, which is an important functional unit of NOM. The SLBs are amenable to probing by many advanced surface science techniques. We used quartz crystal microbalance with dissipation monitoring (QCM-D) to study the interaction of gold NPs with a supported lipid bilayer membrane. Gold is generally not believed to be cytotoxic, and is under active investigation for use in gene transfer and drug delivery applications [10][11]. Gold NPs at sizes above 2 nm do not have catalytic activity [12]. Therefore, the predominant mechanism by which gold NPs in the 2 to 100 nm range can cause toxicity is believed to be due only to membrane destabilization. The supported lipid bilayer membrane model is thus ideally suited to explore the mechanistic picture of how gold NPs interact with biological cell membranes, under pristine conditions and simulated environmental conditions.

2.3 Experimental and Theoretical Methods

2.3.1 Gold nanoparticles

Spherical gold NPs were purchased from NANOCS (New York, NY) with diameters of 2, 5, 10, and 40 nm. The manufacturer provided information on the mass concentration of the particles in the aqueous dispersion (all at 0.01 mg/mL) and also the number density of the particles, 1.5×10^{14} , 5×10^{13} , 5.7×10^{12} , and 9×10^{10} particles/mL, corresponding to the 2, 5, 10, and 40 nm particles, respectively. Number densities were chosen as a parameter, since number concentration has been shown to possibly be a more appropriate dosimetric parameter for describing gold NP distribution on SLBs. The manufacturer also reported that the NPs were very narrowly dispersed in size supported by TEM images (data not shown). Zeta potentials were measured in water and PMAA at experimental conditions (pH 7 and a concentration of 7.14×10^{10} particles/mL) using a Malvern Instrument and Zetasizer software. Zeta potentials (Table 1) are essentially the same when NPs are in a water and PMAA environment. The NP solutions were stabilized with small amounts of tri-sodium citrate and tannic acid in de-ionized water at 7°C, in a light impenetrable container. Since these agents are solely used by the manufacturer for decreasing aggregation in solution, we do not study the direct effect of the citric acid on the SLB. The NP solutions (2, 5, 10, and 40 nm) were diluted with ultrapure water (Milli Q) to 7.14×10^{10} particles/mL at a neutral pH of 7 for all QCM-D runs. The corresponding mass concentrations of the NPs in the dispersions are 47.6 ng/mL, 142.8 ng/mL, 1,252.4 ng/mL, and 79,325 ng/mL respectively, for the 2, 5, 10, and 40 nm particles. Zeta potentials were measured using a Nano Series Zetasizer (Malvern, Worcestershire, UK) with folded capillary cells and the NPs of all sizes exhibit negative zeta potential of around -50 mV in ultrapure water.

Size (nm)	Zeta Potential (mV)	Standard Deviation (mV)	Conductivity (mS/cm)
Nanoparticles in Water			
2	-19.9	5.24	0.00205
5	-24.1	6.48	0.0105
10	-23.7	7.31	0.0175
40	-31.2	15.8	0.22
Nanoparticles in PMAA			
2	-29.5	6.6	0.0716
5	-27	6.67	0.0708
10	-29.4	6.32	0.0685
40	-24.6	13.3	0.22

Table 1: Zeta Potentials for 2, 5, 10, and 40 nm Gold NPs in water and PMAA

2.3.2 Vesicle preparation

An egg phosphatidylcholine (PC) vesicle solution was prepared according to published procedures [13]. L- α -phosphatidylcholine (egg, chicken) (PC) with purity > 99% was purchased from Avanti Polar Lipids, Inc. PC powder (1.0 g) was solubilized in 10 mL of ethanol to yield 100 mg/mL, and stored at -20°C. All other chemicals were purchased from Sigma-Aldrich (St. Louis, MO), unless otherwise stated. Briefly, 0.15 mL of 100 mg/mL egg PC solution was dried with nitrogen gas, desiccated for 24 h, and rehydrated with 6 mL of Tris-NaCl buffer, which consisted of 10 mM Tris (hydrozymethyl) aminomethane with \geq 99.9% purity and 100 mM sodium chloride, at pH 7.8. PC vesicles are unilamellar and were measured previously by Wang et al. in Tris NaCl buffer solution to have an average size of 37 nm in diameter. Solutions were

vortexed for 15 s on a mini vortexer (Fisher Scientific Inc., Pittsburgh, PA) and underwent 5 cycles of freeze-thaw-vortex, with the vortex step lasting 15 s each cycle. Small unilamellar lipid vesicles were formed by sonication of the egg PC solution in a glass tube with an ultrasonic dismembrator (Model 150T, Fisher Scientific, Waltham, MA) for 30 min. in pulse mode with a 30% duty cycle (3-second pulse at an amplitude of 60, followed by a 7-second pause) immersed in an ice bath. Probe particles were removed from the solution through centrifugation (Eppendorf Centrifuge 5415 D) at 16000 x g for 10 min. at 23°C. The supernatant was decanted from the pellet and stored under nitrogen gas at 7°C for up to a month. Directly after the lipid was made (day 0) the size was measured by Dynamic Light Scattering using a Malvern Instrument and a diameter Z-average of 124.6 nm was obtained. After 15 days, another size measurement was obtained at a diameter Z-average of 129.7 nm, which demonstrates the size stability of the lipid vesicles. A SLB is able to form with a vesicle solution that has been made a month prior, and is evident through the frequency and dissipation shifts during QCM-D experiments. Before use, lipid vesicle suspensions were diluted to 0.1 mg/mL using Tris-NaCl buffer. All solutions were vortexed for 15 s prior to use. The SLB is kept at a constant temperature of 23°C, which is monitored by the QCM-D, thus a temperature phase transition will not occur in this system. The membrane composition may contain a variety of lipids with different carbon chain lengths and structures

2.3.3 QCM-D of formation of supported lipid bilayers

QCM-D measurements were performed with the Q-sense E4 (Biolin Scientific, Sweden). QCM-D sensor crystals (5 Hz), reactively sputter-coated with silicon dioxide, were purchased from Biolin Scientific (Gothenburg, Sweden). Crystals were re-used up to 10 times. The silica-

coated sensor crystals were placed into the QCM-D flow chambers and cleaned by flowing ethanol, ultrapure water, 2% sodium dodecyl sulfate solution (Sigma, St. Louis, MO), ultrapure water, and then air through the system. The sensors and chambers were dried with nitrogen gas. A Plasma Prep II oxygen plasma cleaner (SPI Supplies, West Chester, PA) was used to etch the sensor surface before each experiment to remove the outer atomic layers of the crystal surface and make it more hydrophilic (two cycles of 45 s each). This latter step facilitated vesicle rupture into a bilayer.

To prepare the supported lipid bilayer [14], Tris-NaCl buffer was flowed over QCM-D sensors at 0.15 mL/min. with a peristaltic pump, for 10 min. for all experiments. The lipid vesicle solution was added for 8 min. to form a stable SLB. The crystals were rinsed with Tris-NaCl buffer for 6 min. to remove any unattached lipids. The frequency change measurements were used to confirm the existence of a stable lipid bilayer for further investigations with NPs.

2.3.4 QCM-D measurements of SLB interactions with gold NPs in water

Measurements of gold NP-SLB interactions were made in ultrapure water. Since the viscosity and density of the solvent contributes to frequency and dissipation changes, the SLB formed using the buffer solution was first rinsed with the flow of ultrapure water for 8 min. All flows through the QCM-D were kept at the rate of 0.15 mL/min. After establishing this baseline in ultrapure water, gold NPs in water (7.14×10^{10} particles/mL) were allowed to flow for 10 min. NP-membrane interactions occur rapidly followed by steady-state frequency and dissipation changes. Thus, a 10 min. time frame was efficient for measuring our observed interactions and allowing enough time to ensure a complete interaction. Previous studies, such as dye-leakage assays, observed several hours to achieve steady state [15]. However, the interactions observed

via QCM-D occurred quickly on the surface of the SLB and did not require this length of measurement. Following the flow of the NP solution in water, the SLB was rinsed in ultrapure water, followed by rinse with Tris-NaCl buffer for 8 min. each. For each NP size (2, 5, 10 and 40 nm), at least 5 replicates were performed.

2.3.5 QCM-D measurements of SLB interactions with gold NPs in the presence of PMAA

To investigate the effect of natural organic matter (NOM) that may be present in the environment on NP-membrane interactions, QCM-D experiments were done with poly(methacrylic acid) (PMAA) chosen as a model organic polymer compound. PMAA is a linear polyelectrolyte with charges from carboxylic groups and displays some features common to NOM. A 0.001 g/mL solution of PMAA (Polymer Source, Inc., Quebec, Canada with average molecular weight of 6800 Da and narrow size distribution) was sonicated for 30 min. in an ultrasonic cleaner (Branson, Danbury, CT) and stored at 7°C. PMAA remained at a constant neutral pH of 7. In the QCM-D experiments, once the stable SLB was formed, the following sequence of flows were allowed to occur: first, the flow of ultrapure water as described above, then the flow of 0.001 g/mL PMAA for 8 min., followed by the flow of gold NP dispersion (7.14×10^{10} NPs/mL in 0.001 g/mL PMAA) for 8 min., then a 0.001 g/mL PMAA rinse at the same flow rate for 8 min., followed by the ultrapure water rinse and finally the buffer rinse. The rinses with ultrapure water before the PMAA flow and after the PMAA flow were done to maintain consistent procedural steps. All four sizes of gold NPs were tested, with at least 5 replicates per NP size.

2.3.6 Analysis of QCM-D data

The QCM-D provides measurements of frequency change and dissipation change. The frequency changes Δf_n measured at various overtones n ($n = 3, 5, 7, 9, 11$) of the natural frequency were normalized by the overtone number ($\Delta f = \Delta f_n / n$). For the analysis, Δf data for the 3rd to 11th overtones were measured and used. Only small changes occur between different overtones, and the 3rd and 11th overtones were chosen to provide a representation of the highest and lowest resonances. The frequency change at the fundamental frequency is not generally analyzed since this is affected by the flow of bulk solution [16]. The QCM-D also measured energy dissipation changes, ΔD , which provided information on the rigidity of the adsorbed film. Typical sensitivities of QCM-D measurements in liquid are ~ 0.1 Hz for frequency (equivalent to an areal mass of ~ 1.7 ng/cm²) and $\sim 0.1 \times 10^{-6}$ for dissipation.

Methods to relate the measured frequency and dissipation changes to changes in mass and in the viscoelastic properties of the membrane on the surface have been described in detail in the literature [17–19] and only a brief summary is provided here. For a rigid film of areal mass m_f (mass per unit area) deposited on the crystal surface and exposed to air, the frequency change Δf which is normalized with respect to the overtone number and the areal mass of the film are related by the Sauerbrey equation, while the dissipation change ΔD is zero.

$$\frac{\Delta f_n}{n} = \Delta f = -\frac{f_n}{n} \frac{m_f}{m_q} = -f_o \frac{m_f}{m_q}, \quad \Delta D = 0 \quad (1)$$

Here, f_n is the natural frequency of the oscillator at the overtone number n , f_o is the fundamental frequency of the oscillator (5 MHz) and m_q is the areal mass of the quartz crystal (0.883 kg/m²). The mass addition due to the film deposited on the crystal surface gives rise to a decrease in the frequency (negative Δf) while net mass loss is indicated by a positive Δf . The

dissipation D is related to the loss modulus G'' and the storage modulus G' in the form $D = G''/(2\pi G')$ and the change in dissipation ΔD can be related to the changes in the rigidity or viscoelasticity of the film attached to the crystal surface. Obviously, for the rigid film, the change in dissipation is zero. The change in mass for a rigid film can be calculated through the Sauerbrey relationship as, $\Delta m = -C \cdot \Delta f$, where Δm is the change in areal mass (mass per crystal area, measured in ng/cm^2) corresponding to the normalized frequency change Δf (in units of Hz) and C the mass sensitivity constant for the sensor crystal ($= 17.7 \text{ ng cm}^{-2} \text{ Hz}^{-1}$ for crystals oscillating at natural frequency of 5 MHz). The areal mass change can be multiplied by the crystal surface area to obtain mass change for the entire crystal.

If the rigid film is immersed in a Newtonian liquid (water or any of the solutions used in our experiments), the frequency and dissipation changes are modified due to the presence of the liquid and are now given by:

$$\Delta f = -\frac{1}{n} \frac{\eta_L}{2\pi\delta_L m_q} - f_o \frac{m_f}{m_q}, \quad \Delta D = \frac{\eta_L}{n\pi f_o \delta_L m_q}, \quad \frac{\eta_L}{\delta_L} = (n\pi f_o \eta_L \rho_L)^{1/2} \quad (2)$$

where η_L is the viscosity of the liquid medium and δ_L is the decay length of the acoustic wave in the liquid medium. The first term in Δf and the term appearing in ΔD represent the contributions coming from the removal of the quartz crystal from air and immersion in a liquid medium and are influenced by the viscosity and density of the solvent. Usually when measurements of any mass changes on the crystal are made using the same liquid, this solvent effect vanishes, since the crystal is in the same liquid both before and after the mass change process. Effectively, the film mass changes are given just by the Sauerbrey term.

If the film is not rigid but viscoelastic, then the frequency and dissipation changes are given by

$$\Delta f = -\frac{1}{n} \frac{\eta_L}{2\pi\delta_L m_q} - f_o \frac{m_f}{m_q} \left[1 - \frac{2}{\rho_f} \left(\frac{\eta_L}{\delta_L} \right)^2 \frac{G''}{G'^2 + G''^2} \right], \quad (3)$$

$$\Delta D = \frac{\eta_L}{n\pi f_o \delta_L m_q} + \frac{m_f}{m_q} \left[\frac{4}{\rho_f} \left(\frac{\eta_L}{\delta_L} \right)^2 \frac{G'}{G'^2 + G''^2} \right]$$

As in Equation (2), the first term in the expressions for Δf and ΔD are due to the solvent effect and they vanish when we consider changes in film properties when the film is immersed in the same liquid both before and after the change. The film mass change is now given by the Sauerbrey term with a correction factor accounting for the viscoelastic properties of the film. Further, there are dissipation changes due to the viscoelastic nature of the film.

2.4. Results

2.4.1 Interactions of gold NPs in water with the supported lipid bilayer

The QCM-D response of frequency and dissipation changes in the experiments involving the citric acid-stabilized gold NPs in water are shown in Fig. 1A for 10 nm NPs and in Fig. 1B for 40 nm NPs. In these figures, the sequence of events ‘a’ through ‘f’ represents the various liquid flow processes over the quartz crystal. In stage (a) a stable lipid bilayer was formed and the bilayer formation was monitored via QCM-D in several steps. As the initial Tris-NaCl buffer on the crystal was replaced by the flow of vesicle solution in the same buffer, the vesicles adsorb on the crystal. This was revealed by the initial large decrease in frequency, or increase in mass, and a sharp increase in dissipation denoting a soft film formation. The vesicles then rupture spontaneously releasing encapsulated aqueous phase and forming the planar supported bilayer. This was indicated by the large increase in frequency, or decrease in mass, associated with the loss of liquid from the vesicle interior and a significant decrease in dissipation denoting that the soft vesicle layer with the liquid encapsulated inside vesicles and trapped between vesicles was being replaced by a more rigid lipid bilayer film. The membrane was then stabilized during

buffer flow in stage (b), which removed any un-ruptured vesicles or not strongly adsorbed lipid fragments. In stage (c) the bilayer was conditioned with the flow of ultrapure water in order to prepare for the nanoparticle contact. The addition of water caused the frequency to increase and dissipation to decrease due to the slightly lower viscosity and density of water that replaced the higher viscosity and density buffer solution. A dispersion of gold NPs in water was then administered to the bilayer and allowed to interact for ten minutes in stage (d). Water was then flowed through the system in stage (e), followed by a final buffer rinse in stage (f). These final rinses allowed for bilayer comparison before and after NP administration.

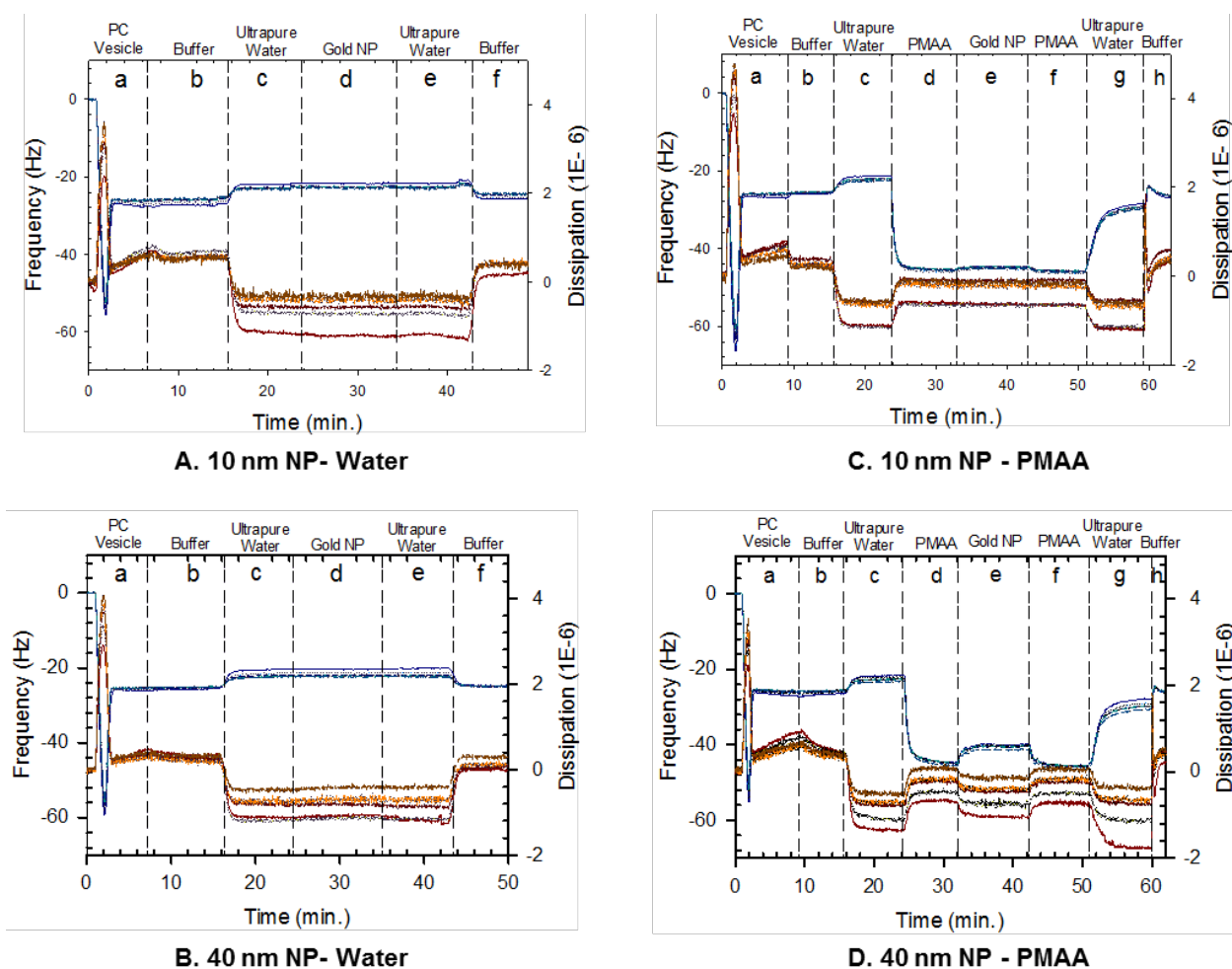


Figure 1. Representative plots showing QCM-D frequency and dissipation changes as a function of time. The blue lines represent frequency and the red lines represent dissipation. Overtones 3, 5, 7, 9, and 11 are shown. Common to

all plots is the formation of the PC bilayer on the SiO₂ crystal, depicted by the large frequency decrease as vesicles adsorbed, followed by a rapid frequency increase as the vesicles ruptured. Buffer was then flowed through the system to stabilize the bilayer by removing un-ruptured or excess vesicles. (A) 10 nm gold NPs in water. (B) 40 nm gold NPs in water. For A and B, following the bilayer formation, the time (in minutes) for each step was: buffer rinse 7:20; water rinse 15:45; gold NPs 24:17; water rinse 34:37; buffer rinse 42:53. (C) 10 nm gold NPs in PMAA solution. (D) 40 nm gold NPs in PMAA solution. For C and D, the time for each step was: buffer rinse 9:25; water rinse 15:52; PMAA solution 23:35; gold NPs in PMAA 32:02; PMAA solution 42:27; water rinse 50:50; buffer rinse 59:04.

The changes in Δf and ΔD observed from the end of stage (c) to the end of stage (d) represent the consequences of NP interactions with the lipid bilayer. Equation (2) demonstrates how the density and viscosity of the solvent affected the frequency and dissipation changes. If the density and viscosity values of the solvent in stage (c) are different from those of the solvent in stage (d), the observed Δf and ΔD values will have contributions arising from the change in the bulk properties of the solvent. We can evaluate whether this is the case in order to decide whether any solvent corrections are needed.

The number of NPs added was consistent for all four NP sizes. The largest volume or mass fraction of NPs added corresponds to the 40 nm NP and therefore it is expected that the density and viscosity changes will be the largest for this system. We estimated the mass concentration of the 40 nm NP in the solvent to be 79,325 ng/mL. Taking the density of water to be 1 g/mL, the density of NP-containing solvent (i.e., water +NPs) was approximately 1.0000793 g/mL, which was not significantly different from that of the NP-free solvent (water). For the three smaller sized NPs, the density of the NP-containing solvent will be even smaller and virtually the same as the density of NP-free solvent (water). Noting that the density of gold is 19.3 g/mL, the volume fraction of the NPs in the solvent, ϕ_{NP} , was $\sim 0.0000793/19.3 \sim 4 \times 10^{-6}$

⁶. The ratio between the viscosity of the NP-containing solvent (η_{w+NP}) and the NP-free solvent (η_w) as a function of the volume fraction ϕ_{NP} of spherical NPs was calculated from the Einstein equation [20]:

$$\frac{\eta_{w+NP}}{\eta_w} = 1 + 2.5 \phi_{NP} \quad (4)$$

Since the particle volume fraction ϕ_{NP} is small, $\sim 4 \times 10^{-6}$, the viscosity of the NP containing solvent will be practically identical to the viscosity of the NP-free solvent. This conclusion is also valid for the other three smaller sized NPs examined in this work, since their volume fractions will be even smaller than that for the 40 nm NP. Since both the density and the viscosity of NP-containing solvent and NP-free solvent are practically the same, the measured Δf and ΔD values will have no contributions from the solvent bulk properties when we replace the solvent in stage (c) by the solvent in stage (d). Therefore, all observed changes in Δf and ΔD can be confidently assigned solely to the interactions of the NPs with the bilayer.

The observed dissipation changes for all four sizes of NPs at various overtone numbers are negligible (Fig. 2). This implies that the lipid bilayer on the quartz surface can be treated as a rigid film and the frequency changes observed can be directly connected to mass changes through the Sauerbrey relationship Equation (2). From the frequency change measured as the difference in frequency at the end of stage (c) and stage (d), areal mass changes were determined for each NP size and at each overtone. Using this areal mass change and taking the crystal active area to be 1 cm^2 , the total mass changes on the crystal at various overtones were calculated (Fig. 3). The calculated mass change values at all overtone numbers were small but negative, indicating that a small mass was lost from the system for all sizes of the NPs, implying the removal of some lipid molecules (Fig. 3). The mass loss is in the 1 to 6 ng range indicating that

at best 1 or 2% of the lipids in the bilayer would have to be removed to explain the observed QCM-D response.

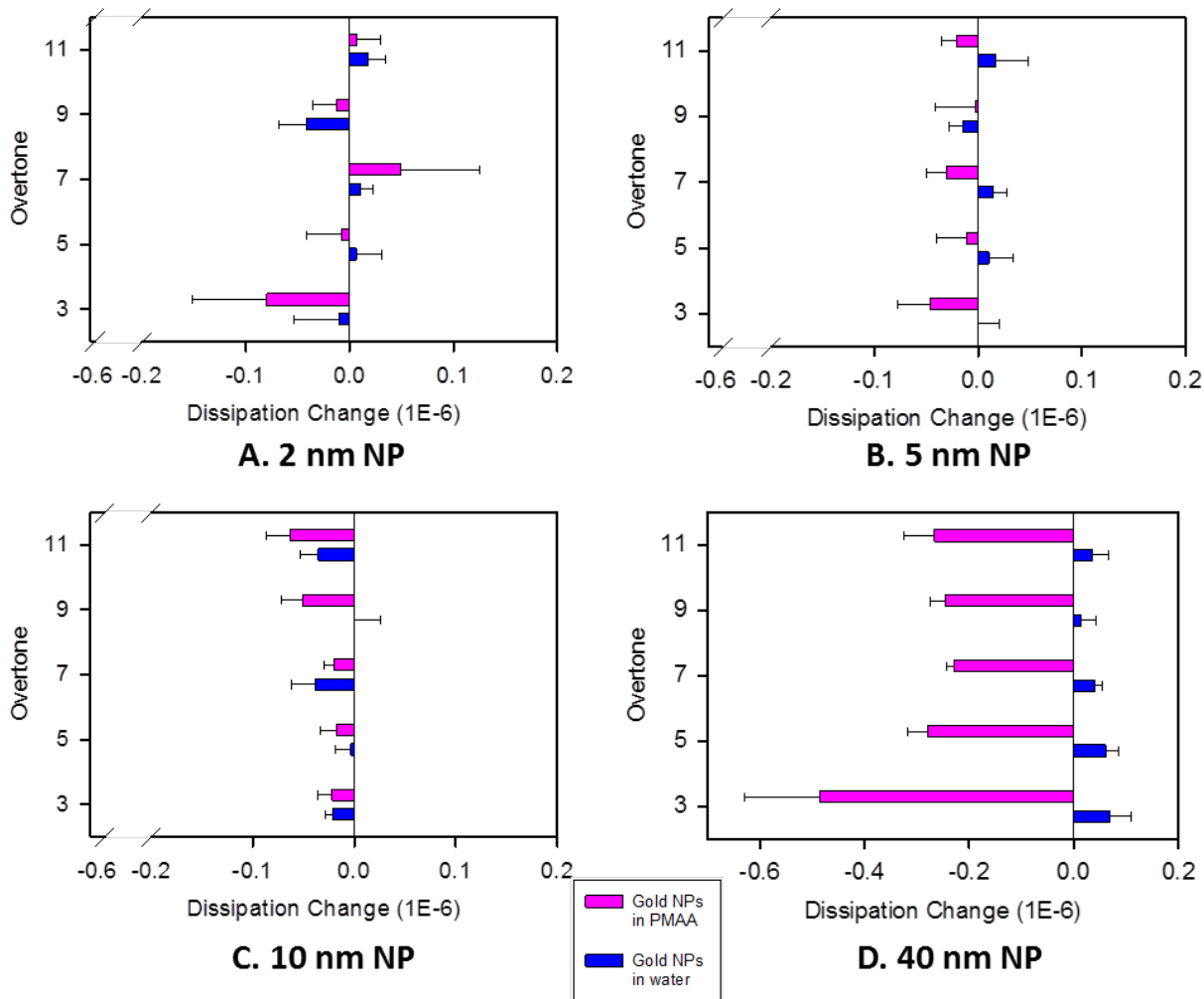


Figure 2. Dissipation changes associated with the nanoparticle-bilayer interactions for gold NPs of size (A) 2 nm; (B) 5 nm; (C) 10 nm; and (D) 40 nm. Blue bars are for NPs in water, and pink are for NPs in PMAA solution. Error bars show the standard error values. Each data point is based on at least 5 experimental samples at a constant concentration of 7.14×10^{10} particles/mL. Statistical analysis was performed with SigmaPlot 12.5 software at a 95% confidence interval ($\alpha=0.05$). The results of one-way analysis of variance (ANOVA) test showed that the results of different sizes have statistically significant difference ($P = <0.001$).

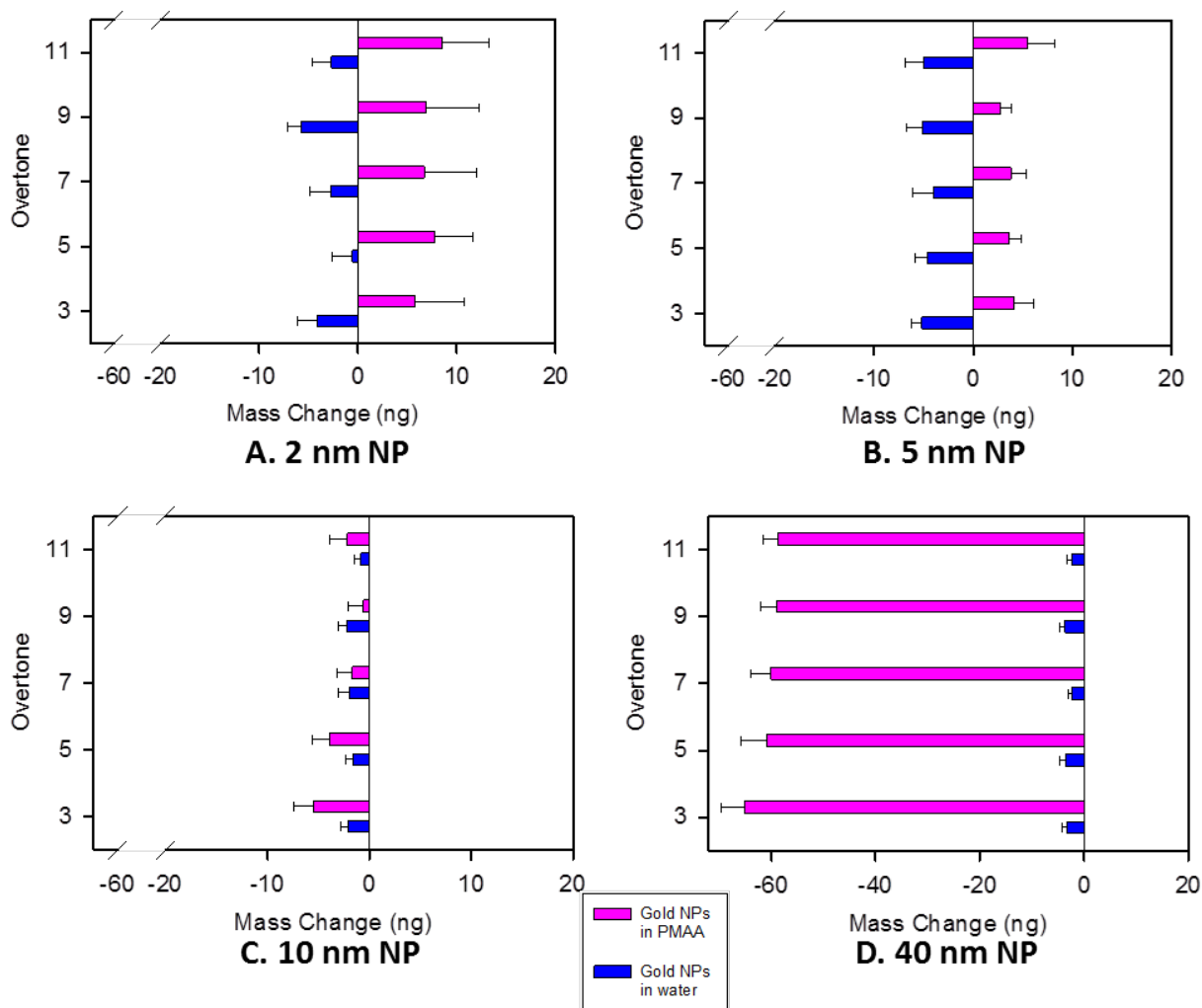


Figure 3. Mass changes estimated from Sauerbrey relationship for interactions of gold NPs with PC bilayer, for NPs of size (A) 2 nm; (B) 5 nm; (C) 10 nm; and (D) 40 nm. Blue bars are for NPs in water, and pink are for NPs in PMAA solution. Error bars show the standard error values. Each data point reported is based on at least 5 experimental samples at a constant concentration of 7.14×10^{10} particles/mL. Statistical analysis was performed with SigmaPlot 12.5 software at a 95% confidence interval ($\alpha=0.05$). The results of one-way analysis of variance (ANOVA) test showed that the results of different sizes have statistically significant difference ($P < 0.001$). The mass calculated is per 1 cm^2 of crystal area.

2.4.2 Interaction of gold NPs in PMAA solution with the supported lipid bilayer

We investigated the influence of large organic molecules present in water on the NP-lipid bilayer interactions by selecting a linear ionizable polymer, poly(methacrylic acid) (PMAA) as an illustrative organic matter. The QCM-D response of frequency and dissipation changes in the experiments involving the NPs in PMAA+water are shown in Fig. 1C and Fig. 1D for the 10 nm and 40 nm NPs, respectively. As in the case of citric acid-stabilized gold NPs in water, the sequence of events 'a' through 'h' in Fig. 1C and Fig.1D represent the various liquid flow processes over the quartz crystal, with the first three stages (a, b, and c) being identical to those discussed. In stage (d) a solution of 0.001 wt% PMAA in water was allowed to flow over the bilayer. Gold NPs equilibrated in the PMAA solution (0.001 wt% PMAA in water) were then allowed to interact with the SLB in stage (e). A rinse in the PMAA solution followed in stage (f), followed by a water rinse in stage (g), and a final buffer rinse in stage (h). The water rinses in stages (c) and (g) were performed to maintain the same sequence of steps as for the experiment with NPs in water.

The mass concentration of PMAA used in the experiments was 10^{-5} g/mL and the mass concentration of the 40 nm NP in the solvent was 79,325 ng/mL. As the molecular weight of PMAA is 6.8 kDa, we do not expect to see a large effect on solution properties from the presence of the polymer. Given these values, using the same quantitative arguments discussed in section 3.1, we can conclude that the viscosities of PMAA + water + NPs and PMAA + water were practically identical to the viscosity of water; and the densities of PMAA + water + NPs and PMAA + water were practically identical to the density of water. Therefore, all frequency and

dissipation changes monitored were free of any contributions due to solvent bulk property changes.

The changes in Δf and ΔD observed from the end of stage (d) to the end of stage (e) represent solely the consequences of NP interactions with the lipid bilayer in the presence of PMAA. The addition of PMAA to the system caused a size-dependent mechanism for the NP-bilayer interaction (Fig. 3). The 2 nm and 5 nm gold NPs contributed to a small mass increase on the bilayer surface, indicating NP adsorption on the bilayer while the 10 nm NPs exhibited a small mass decrease on the surface, which indicated some lipid removal. All of these changes were relatively quite small. The most prominent change was seen with the 40 nm gold NPs, which caused a large mass decrease on the surface, causing approximately 22% of the bilayer to be removed. The frequency changes for each overtone were fairly similar, indicating that the lipid loss was a homogenous process along the depth of the bilayer. The dissipation change for the 40 nm NP was still quite small and negative, implying that the rigidity of the bilayer was maintained even if there was a significant lipid loss from the bilayer (Fig. 2).

2. 4.3 Interaction of PMAA with the lipid bilayer before and after NP exposure

The changes in Δf and ΔD observed from the end of stage (c) to the end of stage (d) in Fig. 1C and Fig. 1D represent the interactions of PMAA with the lipid bilayer, before the bilayer was exposed to NPs. For the 10 nm and 40 nm particles, these Δf and ΔD values are plotted in Fig. 4A and Fig. 4B, respectively. PMAA's interaction was unaffected by NP size, since all of this interaction occurred before the exposure of the bilayer to the NPs. The significant decrease in the frequency and small increase in the dissipation implied that there was significant

adsorption of PMAA on to the lipid bilayer, yet the basic structural organization and rigidity of the bilayer had not been affected.

For the 10 nm and 40 nm NPs, these Δf and ΔD values are plotted in Fig. 4C and Fig. 4D, respectively, and size affected these interactions. For the 10 nm NPs, there were no noticeable changes in frequency or dissipation and the bilayer was not affected by the exposure to the NPs (as discussed in Section 2.4.2). Further, subsequent contact with the PMAA did not result in any modifications to the bilayer. In contrast, for the 40 nm NPs, there was a significant frequency decrease, implying that mass was added to the bilayer. Exposure of the bilayer to the NPs caused appreciable mass loss in stage (d) to (e), but this mass loss was more than compensated by a mass increase in stage (e) to (f), implying that the PMAA adsorbed onto the bilayer and adsorbed to defect sites caused by lipid removal.

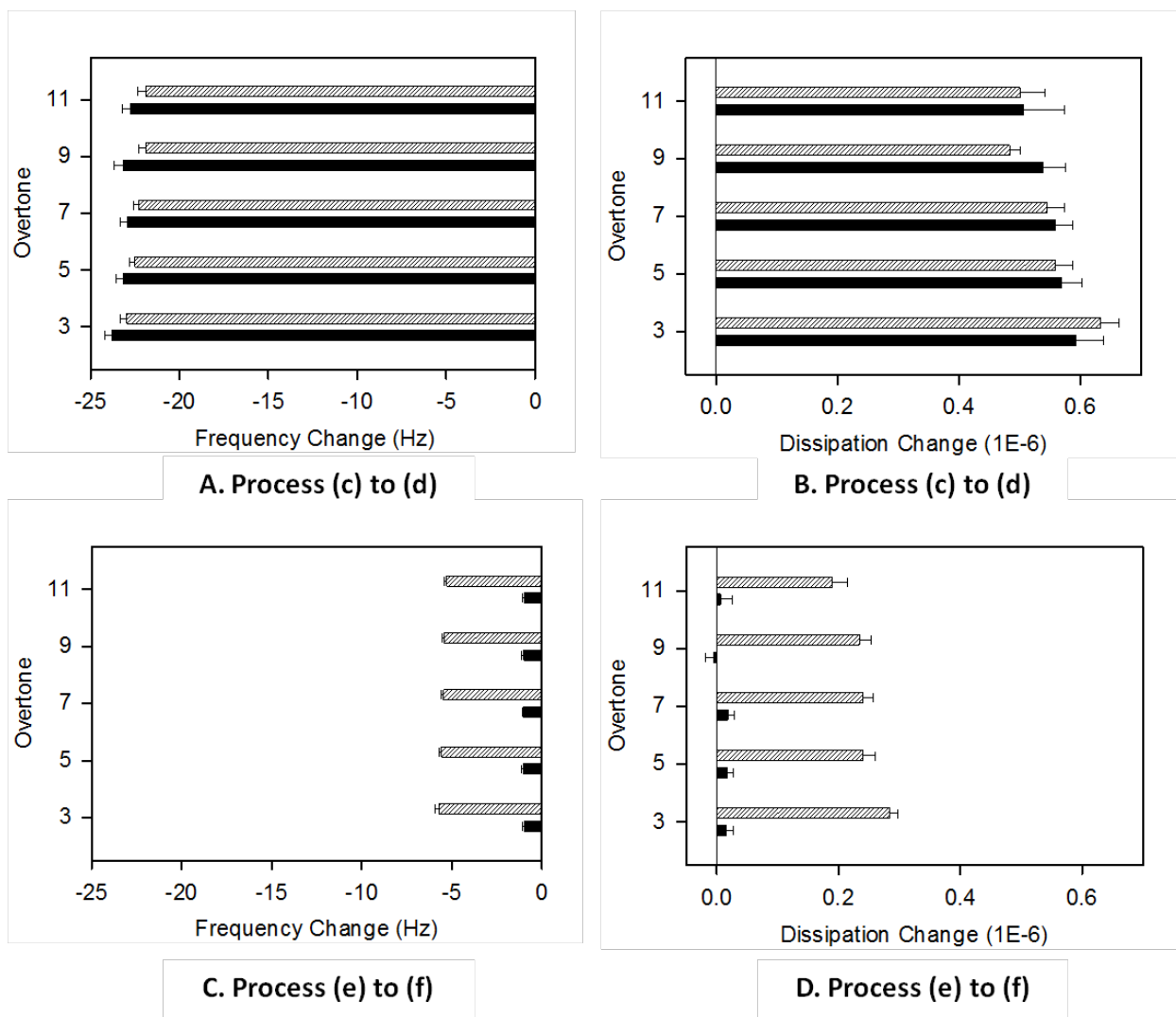


Figure 4. Frequency and dissipation changes associated with the PMAA-bilayer interactions both before (A and B) and after (C and D) the exposure of the bilayer to the nanoparticles. Patterned bars are for 10 nm particles and the filled bars are for the 40 nm particles. Note that (A) and (B) represent data before nanoparticle exposure occurred in QCM-D runs done with the specified nanoparticle sizes. Error bars show the standard error values. Each data point is based on at least 5 experimental samples at a constant concentration of 7.14×10^{10} particles/mL. Statistical analysis was performed with SigmaPlot 12.5 software at a 95% confidence interval ($\alpha=0.05$). The results of one-way analysis of variance (ANOVA) test showed that the results of different sizes have statistically significant difference ($P = <0.001$).

2.5. Discussion

2.5.1 Measured Δf and ΔD represent NP-bilayer interactions and not solvent effects

A fundamental question in QCM-D experiments is whether any of the measured frequency and dissipation changes could have originated from changes in the bulk properties of solvents. Significant changes in frequency and dissipation are possible even from what may be seen as small changes in solvent density and viscosity, according to the solvent dependent terms in Equation (2). In the present study, the question translates to the differences in the viscosities and densities of the solvent compared to the solvent containing NPs. In one case the solvent is water and in the other case it is a solution of PMAA in water. The larger NPs would make the most contributions to density and viscosity. Taking the most extreme case of the 40 nm NPs, viscosity (η) and density (ρ) changes due to the addition of NPs in the NP-free solvent can be written as

$$\frac{\eta_{w+NP}}{\eta_w} = \frac{\eta_{w+PMC+NP}}{\eta_{w+PMC}} = 1.000004,$$

and

$$\frac{\rho_{w+NP}}{\rho_w} = \frac{\rho_{w+PMC+NP}}{\rho_{w+PMC}} = 1.0000793$$
(5)

Corresponding to these bulk property changes, the changes in frequency and dissipation calculated from the solvent-dependent terms in Equation (2) are indeed entirely negligible and therefore, we can conclude that all changes we measured are solely due to the interaction of NPs with the bilayer membrane.

2.5.2 Estimating citric acid-stabilized gold NPs adsorption on bilayer

For the citric acid-stabilized gold NPs, we observed small mass losses for all four sizes of NPs. Mass increases were never observed, even though one might expect possible NP adsorption on the bilayer. We explored this by estimating the extent of NP adsorption on the bilayer by applying results reported by Hou et al., who studied the partitioning of tannic acid-stabilized gold NPs (size 5 to 100 nm) between the aqueous phase and the lipid bilayer [21]. They employed commercially available solid-supported lipid membranes (SSLMs), which are silica spheres with a non-covalent coating of egg PC lipid bilayers, and measured the lipid bilayer-water distribution coefficient K_{lipw} ($= C_{lip}/C_w$) to be 450 L/kg lipid. Here C_{lip} refers to the concentration of NPs in the lipid domain expressed as mass (or number) of lipid particles per kg of lipid and C_w is the concentration of NPs in water, expressed as mass (or number) of NPs per liter of the aqueous phase.

In our QCM-D experiments, we used a particle concentration of $C_w = 7.14 \times 10^{13}$ particles/L, for all sizes. Using the lipid bilayer-water distribution coefficient reported above, we found that the number concentration of NPs in the lipid bilayer would be $C_{lip} = 3.213 \times 10^{16}$ particles/kg of lipid. To calculate the number of NPs adsorbed on the bilayer, we have to determine the mass of lipid on the bilayer. The formation of the supported egg PC bilayer results in a frequency change of ~ 25 Hz which corresponds to a bilayer areal mass of 445 ng/cm^2 , based on the Sauerbrey constant ($C = 17.8 \text{ ng cm}^{-2} \text{ Hz}^{-1}$). This mass includes the mass of a layer of water between the quartz crystal and the supported lipid bilayer, which is $\sim 102 \text{ ng/cm}^2$ [22]. Correcting for this water mass, the areal mass of the lipid is 343 ng/cm^2 . Combining this with the estimate for C_{lip} , we find that the number of NPs associated with the bilayer is 1.1×10^7 particles/cm². Taking the mass of each NP using data provided by the manufacturer, we

calculated the total mass of NPs adsorbed on the bilayer per unit area and the corresponding frequency change on the quartz crystal (Table 2). All estimated frequency changes are negative since they correspond to mass addition resulting from the adsorption of NPs. The results clearly show that the adsorption of NPs on the lipid bilayer would not be detectable by the QCM-D for the 2, 5 and 10 nm particles and is very small but detectable, for the 40 nm particle.

Table 2. Estimation of expected frequency changes due to nanoparticle adsorption on bilayer

NP diameter (nm)	Mass of one NP based on manufacturer data (ng)	Predicted areal mass of adsorbed NP (ng/cm ²)	Expected frequency change due to NP adsorption (Hz)
2	6.67×10^{-10}	7.34×10^{-3}	$- 0.41 \times 10^{-3}$
5	2.0×10^{-9}	2.20×10^{-2}	$- 0.12 \times 10^{-2}$
10	1.75×10^{-8}	1.93×10^{-1}	$- 0.11 \times 10^{-1}$
40	11.11×10^{-7}	12.22	- 0.69

2.5.3 Citric acid stabilized gold NP adsorption on bilayer causes some lipid removal

The experimental QCM data for all four sizes of citric acid-stabilized gold NPs showed positive frequency changes, corresponding to net mass loss. The mass loss is quite small, in the range 0 to 6 ng, and must come from the removal of some lipid molecules from the bilayer. We propose that the NPs adsorb on the surface and the NP adsorption causes displacement of lipid head groups due to the surface insertion of the particle (Fig. 5). This affects the lipid conformation and the resulting membrane stresses are relieved by the escape of some lipid molecules from the bilayer. This is qualitatively similar to the suggestion made in the literature for α -helical peptides adsorbing on the lipid bilayer and the resulting membrane stress giving

rise to the formation of pores [23]. Only a small amount of lipid is removed consistent with the small amount of NP adsorption, and the lipid removal occurs leading to small pores or other forms of membrane defects that are not significant enough to perturb membrane stability.

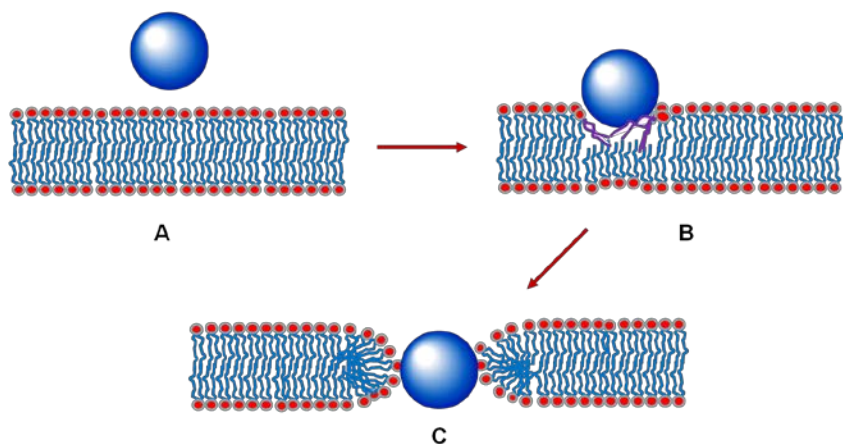


Figure 5. Schematic view of citric acid-stabilized gold nanoparticles interacting with the supported lipid bilayer. The nanoparticles adsorb on the surface displacing lipid head groups. This causes the lipids to change their conformation, making their energy states higher than that of the average lipid on the bilayer. The resulting stress on the bilayer is relieved by the removal of some lipid molecules from the bilayer. The lipid loss may create small pores in the bilayer. The mass loss from lipid removal outweighs the mass addition from the adsorbed nanoparticles and net mass loss is recorded by the QCM-D.

2.5.4 PMAA coated NPs adsorb more strongly to the bilayer

QCM-D measurements of gold NP-bilayer interactions were conducted in the presence of the weak polyelectrolyte poly(methacrylic acid). One expects the spontaneous adsorption of PMAA over the gold NPs and therefore these experiments could reveal the interactions between the polyelectrolyte coated gold NPs and the lipid bilayer that had been exposed to PMAA. For 2 nm and 5 nm NPs, a small negative frequency change (mass increase) was observed, while the dissipation change was negligible (Figs 2 and 3). For the 10 nm NPs, frequency and dissipation changes were both negligible, while for the 40 nm NPs there was a significant frequency increase

(mass loss) accompanied by a small increase in dissipation. Since NP adsorption can perturb the lipids and cause some lipid removal, evidently the adsorption of NPs in the presence of PMAA must be larger to compensate for the mass loss. For the 10 nm and 40 nm NPs, other mechanisms should be operative (discussed in the next section) to cause the mass loss observed.

Studies on the interactions of PMAA with gel and liquid crystalline states of DMPC bilayer have been presented in the literature by Xie and Granick [24]. They found that a large amount of PMAA adsorbed even at the earliest measurement times, and for very low solution concentrations of PMAA (0.1 and 1 mg/mL). This is similar to our QCM-D results where PMAA was found to adsorb on the PC bilayer from a 1 mg/mL solution of PMAA, giving rise to a frequency change of 24 Hz in about 2 minutes. Xie and Granick proposed that since the head groups of the DMPC were dipolar, being positive on the termini ($-N(CH_3)_3^+$) and negative a few angstroms underneath ($-PO_2^-$), the ions of PMAA would electrostatically interact with the dipoles of the lipid head groups, with PMAA lying on the bilayer surface in the lipid head group region. They also concluded (using infrared measurements of C-H vibration region) that the PMAA adsorption did not induce changes in the average area per phospholipid. The bilayer remained more or less unaffected. This is also consistent with the QCM-D observations where the observed dissipation changes remained very small, implying that the bilayer structure was not fundamentally affected. In the gel phase of the bilayer (not encountered in our QCM-D studies with PC) they found that defects exist (islands and patches of bilayer rather than homogeneous bilayer) and the PMAA adsorbs preferentially at the defect edges, thereby stabilizing the defects.

These observations suggest a simple interpretation for the small mass increase observed with the PMAA-coated 2 and 5-nm particles. The charge on the PMAA was small and the PMAA-coated nanoparticle had some hydrophobicity. As the PMAA adsorption on the bilayer

created interactions between the small number of charges on the PMAA and multiple dipoles of the lipid head groups causing head group tilts and creating space for the surface adsorption of the PMAA coated nanoparticles. After the initial surface adsorption, the hydrophobic PMAA-coated nanoparticles could even penetrate into the bilayer as has been reported for small hydrophobic NPs through molecular dynamics simulations. This could also be represented as a larger partition coefficient K_{lipw} compared to the partition coefficient measured for the citric acid stabilized-gold NPs. The mass increase due to adsorption remained slightly larger than any mass loss due to removal of stressed lipids. Also any defects in the bilayer associated with the lipid removal can be filled by PMAA similar to the observation of Xie and Granick of PMAA adsorbing on defect edges.

The penetration of the pores by hydrophobic nanoparticles has been observed in molecular dynamics simulations where the particle is engulfed within the hydrophobic domain of the bilayer. For example, Li et al. used coarse-grained molecular dynamics simulations to show that the hydrophobicity of the nanoparticle controls the interaction with the membrane [25]. For NPs interacting with a dipalmitoylphosphatidylcholine (DPPC) membrane, a zwitterionic membrane that is similar to PC, Li et al. showed that hydrophobic NPs would become included in bilayer, while semi-hydrophobic NPs adsorbed to the surface of the membrane [25]. When the simulation was allowed to progress for more time, deformations in the lipid bilayer were observed to be temporary, and rearrangement of lipid molecules could occur.

Experiments with lipid bilayers and vesicles have also shown relationships between NP physicochemical properties and interaction mechanisms with the lipid structure. For example, Bothun showed that hydrophobic 5.7 nm Ag nanoparticles, functionalized with decanethiol, became internalized in the hydrophobic lipid interior of a DPPC liposome [26]. The NP diameter

was near or exceeding the bilayer thickness, but due to the hydrophobic properties of the gold-decanethiol NPs, the particles could insert into the hydrophobic region of the bilayer. Other examples of gold and silver NPs treated with hydrocarbons to impart hydrophobicity have demonstrated NP insertion into vesicles and/or lipid bilayers [27–29]. In order to embed a nanoparticle into a hydrophobic membrane, the NP must be small and hydrophobic, with sizes estimated to be < 4-8 nm [26,30].

2.5.5 Size-dependent NP engulfment by bilayer causes lipid removal

For 40 nm NPs coated with PMAA, large mass losses were observed. We have attributed the mass increase observed for the 2 and 5 nm NPs to the stronger adhesion between the PMAA coated gold NPs and the bilayer. The question we need to answer is why such strong adhesion lead to mass loss in the case of the 40 nm NPs, but not for the smaller NPs. In addition, adhesion plays a different role in the behavior of the 40 nm NPs in water compared to with PMAA. We propose that the large PMAA-coated NP was engulfed by a fragment of the bilayer (Fig. 6) causing a significant amount of lipid to be removed from the bilayer (hence, the observed mass loss), and that this engulfment does not occur for the smaller PMAA-coated NPs and for the citric acid-stabilized 40 nm NPs in water.

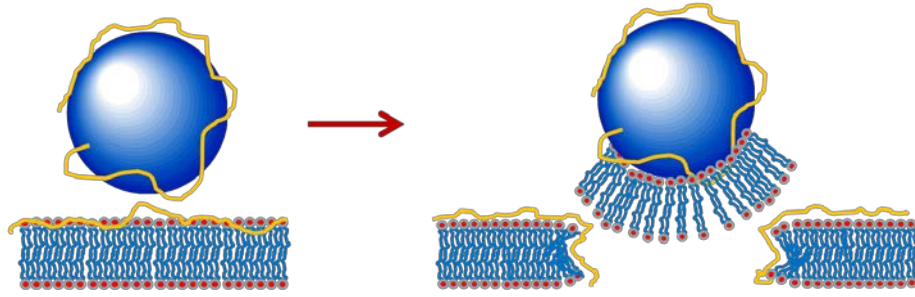


Figure 6. Schematic view of PMAA coated gold nanoparticles interacting with the supported lipid bilayer. For the 40 nm nanoparticle, the adhesive interaction of the nanoparticle with the bilayer allows a fragment of the bilayer to partially or completely engulf the nanoparticle and leave the supported bilayer. This appears as a significant mass loss recorded by the bilayer. For the 2, 5 and 10 nm PMAA-coated nanoparticles, such engulfment is not favored as discussed in detail in the text.

To determine the likelihood that the NP could be engulfed by the lipid bilayer, one has to consider the free energy change between the nanoparticle-engulfed state and the initial state of the planar bilayer coexisting with the spherical particle. This free energy change should be negative for this engulfment process to occur spontaneously. Taking a phenomenological view, three principal free energy contributions are to be considered. The first is the interaction of the NP with the bilayer in contact with it. Second, the lipid that was present in the planar bilayer is now present in a spherical bilayer. Finally, the removal of the lipid from the planar bilayer leaves behind a lipid interface in contact with the aqueous domain. We represent these three contributions through the simple expression

$$\Delta g = -4\pi R_p^2 \epsilon_{adh} + 8\pi\kappa + 2\pi R_p \delta \epsilon_{int} \quad (6)$$

where Δg is the free energy change expressed per nanoparticle, R_p is the radius of the nanoparticle, $-\epsilon_{adh}$ is the attractive adhesive interaction energy per unit area between the nanoparticle and the bilayer engulfing it, κ is the bending modulus of the bilayer, δ is the

thickness of the bilayer and ε_{int} is the positive interfacial energy per unit area. The first term represents the adhesion energy between the fully engulfed PMAA coated NP and the bilayer. We could instead have considered only partial engulfment, but the qualitative discussions and conclusions below are not affected by this choice. The second term represents the bending energy associated with the planar bilayer becoming a spherical bilayer. The third term represents the free energy of formation of the interface, or the edge energy. The interfacial area is taken as equal to $2\pi R_P \delta$. The condition $\Delta g < 0$ for the engulfment of the nanoparticle by the bilayer is satisfied if the NP size exceeds a critical radius R_{PC} obtained by equating Δg to zero.

$$R_{PC} = \delta \frac{\varepsilon_{int}}{\varepsilon_{adh}} + \left[\left(\delta \frac{\varepsilon_{int}}{\varepsilon_{adh}} \right)^2 + \frac{8\kappa}{\varepsilon_{adh}} \right]^{1/2} \quad (7)$$

The calculated critical radius is plotted (Fig. 7) for various values of the adhesion energy and interfacial energy. In all calculations, the bending modulus of the bilayer is taken equal to $20 kT$ as has been reported in the literature [31]. Obviously, the engulfment is more probable for larger NPs than smaller NPs, since the energy penalty associated with the bilayer bending decreases with increasing particle size. Further, if the adhesive energy ε_{adh} is large or if the interface energy ε_{int} is small, then the critical particle radius decreases, implying that smaller NPs could be engulfed by the bilayer decreases. Comparing the PMAA coated NPs of the smaller size against the 40 nm NPs, all of which have the same adhesion energy and interfacial energy, this model clearly suggests why the larger size particle allowed for engulfment and resulted in mass removal from the bilayer because of the bending energy contribution. Comparing the 40 nm citric acid-stabilized particle against the PMAA-coated NP, this model clearly suggests how the stronger adhesion in the latter case permits engulfment by the bilayer with resultant mass removal.

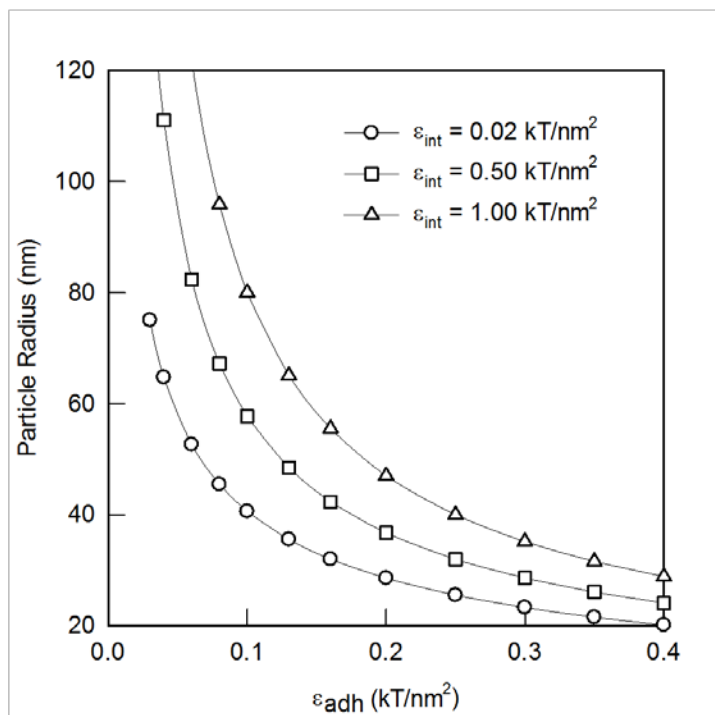


Figure 7. Calculated critical nanoparticle radius for engulfment by the lipid bilayer as a function of the adhesive interactions between the nanoparticle and the bilayer and the interfacial energy of the bilayer at the defect edge. The critical radius of the nanoparticle at which engulfment can occur becomes smaller with increasing adhesive energy and decreasing interfacial energy. The calculations are based on a phenomenological free energy model discussed in the text.

2.5.6 Delayed PMAA adsorption on bilayer defects

For the 40 nm PMAA coated particles, we observed a mass loss during the beginning of stage (e) followed by a mass increase during the beginning of stage (f). Since PMAA can adsorb on the defect sites, it is possible to interpret our results in terms of PMAA adsorption on the defect sites on the bilayer where the lipid had been removed. However, the adsorption of PMAA did not occur immediately following lipid removal early on in stage (e) even though the PMAA in the PMAA + NP + water solvent was available for adsorption. Instead, the PMAA adsorption process became possible only after the end of PMAA + NP + water solvent flow (stage e) and

when the flow of PMAA + water commenced (beginning of stage f). We speculate that this could be due to the diffusional barrier provided by the presence of NPs near the bilayer interface preventing the PMAA from reaching and adsorbing onto the bilayer and bilayer defects. Some support for such a speculation comes from a recent study that investigated the role of gravity force on spherical gold NPs, surface modified with 3-mercaptopropionic acid, interacting with lipid bilayer [32]. Zhu et al used the QCM-D with a closed flow chamber, positioning the supported lipid bilayer at the bottom and top of the liquid medium by adopting an upright and inverted configuration, respectively. On the upright crystal, the NP solution was above the bilayer while in the inverted crystal, the solution was below the bilayer. They found larger nanoparticle adsorption on the upright bilayer compared to the inverted bilayer. This could not be attributed to the gravity force since it is much smaller in magnitude compared to van der Waals forces and electrostatic forces governing adsorption. They argued that the gravity force causes a gradient in the NP distribution in the liquid in contact with the bilayer. For the upright bilayer, such gravity induced sedimentation causes a high local concentration of the NP near the bilayer and that is responsible for the increased adsorption. For the inverted crystal, the opposite situation prevails.

Based on this study, we speculate that a higher local concentration of the 40 nm gold NPs exists close to the bilayer surface preventing the PMAA from diffusing to and adsorbing on the bilayer during stage (e). Once the NP flow ends, this barrier is removed and even at the very beginning of stage (f) PMAA could immediately adsorb on the defect sites of the bilayer adding to the mass. Additional measurements and other experimental methods would be needed to confirm this speculative explanation.

2.6. Conclusions

Nanomaterials exhibit cytotoxicity through various mechanisms. All of the mechanisms except cell membrane disruption can also result from the molecular, atomic, or ionic species constituting the NP, without requiring the nanoparticulate nature of the material. Therefore, model membranes represent an attractive method to study membrane disruption, since there are no interfering factors such as would be the case if a biological cell is used. Supported lipid bilayers provide a powerful model membrane platform allowing for extraction of molecular scale information. In this work, QCM-D was employed to study the interactions of citric acid-stabilized gold NPs and gold NPs spontaneously coated by poly(methacrylic acid) with a zwitterionic egg PC bilayer. The results show that 2, 5, 10, and 40 nm diameter citric acid-stabilized gold NPs caused a small lipid loss from the bilayer. The dissipation changes were small enough to suggest that no significant perturbation of the membrane structure occurred. Since the lipid loss was quite small, it is possible that pores of a size sufficient to permeabilize the membrane were not generated, implying that the NPs need not be cytotoxic. NP adsorption appears to induce stress on the lipids, causing some lipid removal as the free energy lowering mechanism. When the NPs were coated with PMAA, the smaller NPs caused a mass increase on the bilayer. The increased adhesion between the NPs and the bilayer due to PMAA was responsible for increased NP adsorption overcompensating for the loss of some lipid molecules. We observed significant mass loss in the case of the 40 nm PMAA coated NP, and attributed this to the bilayer engulfing the NP and removing it from the crystal surface. We proposed a simple model to suggest that the competition between the particle-bilayer adhesion energy, the bilayer bending energy and the interfacial energy at bilayer defect edges allows the larger NPs and more adhesive NPs to be engulfed by the bilayer and leave the crystal surface causing mass loss. This

large mass change can be associated with membrane disruption and cytotoxicity. This suggests that even if gold NPs are intrinsically not cytotoxic, they can become cytotoxic in the presence of other organic additives through manipulation of their adhesive interactions with the bilayer.

2.7. Acknowledgments

This work was supported in part by the National Science Foundation (CBET 0966496). The authors thank Geoffrey Bothun at the University of Rhode Island for helpful discussions. In addition, Joseph Duffy, Christopher Lambert, Reeta Prusty Rao, and Hong Susan Zhou at Worcester Polytechnic Institute assisted with some use of lab equipment. Several WPI students assisted with preliminary experiments in this area: Andrew Carey, Houssam Lazkhani, Thomas Finelli, Yan Yan, and Sophia D'Angelo.

2.8. References

- [1] C.R. Thomas, S. George, A.M. Horst, Z. Ji, R.J. Miller, J.R. Peralta-Videa, T. Xia, S. Pokhrel, L. Mädler, J.L. Gardea-Torresdey, P. a Holden, A. A. Keller, H.S. Lenihan, A.E. Nel, J.I. Zink, Nanomaterials in the environment: from materials to high-throughput screening to organisms., *ACS Nano*. 5 (2011) 13–20. doi:10.1021/nn1034857.
- [2] N. Lewinski, V. Colvin, R. Drezek, Cytotoxicity of nanoparticles., *Small*. 4 (2008) 26–49. doi:10.1002/sml.200700595.
- [3] A. Nel, Toxic Potential of Materials at the Nanolevel, *Science*. 311 (2006) 622–627. doi:10.1126/science.1114397.
- [4] L.K. Limbach, P. Wick, P. Manser, R.N. Grass, A. Bruinink, W.J. Stark, Exposure of

- engineered nanoparticles to human lung epithelial cells: influence of chemical composition and catalytic activity on oxidative stress., *Environ. Sci. Technol.* 41 (2007) 4158–63.
- [5] L. Braydich-Stolle, S. Hussain, J.J. Schlager, M. C. Hofmann, In vitro cytotoxicity of nanoparticles in mammalian germline stem cells., *Toxicol. Sci.* 88 (2005) 412–9. doi:10.1093/toxsci/kfi256.
- [6] A. Nebbioso, A. Piccolo, Basis of a humeomics science: chemical fractionation and molecular characterization of humic biosuprastructures., *Biomacromolecules.* 12 (2011) 1187–99. doi:10.1021/bm101488e.
- [7] J. Gao, K. Powers, Y. Wang, H. Zhou, S.M. Roberts, B.M. Moudgil, B. Koopman, D.S. Barber, Influence of Suwannee River humic acid on particle properties and toxicity of silver nanoparticles., *Chemosphere.* 89 (2012) 96–101. doi:10.1016/j.chemosphere.2012.04.024.
- [8] R.F. Domingos, N. Tufenkji, K.I. Wilkinson, Aggregation of titanium dioxide nanoparticles: role of a fulvic acid., *Environ. Sci. Technol.* 43 (2009) 1282–6.
- [9] A. Czogalla, M. Grzybek, W. Jones, U. Coskun, Validity and applicability of membrane model systems for studying interactions of peripheral membrane proteins with lipids., *Biochim. Biophys. Acta.* 1841 (2014) 1049–1059. doi:10.1016/j.bbalip.2013.12.012.
- [10] H. Liu, D. Chen, L. Li, T. Liu, L. Tan, X. Wu, F. Tang, Multifunctional gold nanoshells on silica nanorattles: A platform for the combination of photothermal therapy and chemotherapy with low systemic toxicity, *Angew. Chemie - Int. Ed.* 50 (2011) 891–895.

doi:10.1002/anie.201002820.

- [11] A. Sharma, A. Tandon, J.C.K. Tovey, R. Gupta, J.D. Robertson, J.A. Fortune, A.M. Klibanov, J.W. Cowden, F.G. Rieger, R.R. Mohan, Polyethylenimine-conjugated gold nanoparticles: Gene transfer potential and low toxicity in the cornea, *Nanomedicine Nanotechnology, Biol. Med.* 7 (2011) 505–513. doi:10.1016/j.nano.2011.01.006.
- [12] M. Auffan, J. Rose, J.Y. Bottero, G. V. Lowry, J.P. Jolivet, M.R. Wiesner, Towards a definition of inorganic nanoparticles from an environmental, health and safety perspective, *Nat. Nanotechnol.* 4 (2009) 634–641. doi:10.1038/nnano.2009.242.
- [13] Y. Barenholz, D. Gibbes, B.J. Litman, J. Goll, T.E. Thompson, R.D. Carlson, A simple method for the preparation of homogeneous phospholipid vesicles., *Biochemistry.* 16 (1977) 2806–10.
- [14] C. A. Keller, K. Glasmästar, V.P. Zhdanov, B. Kasemo, Formation of supported membranes from vesicles., *Phys. Rev. Lett.* 84 (2000) 5443–6.
- [15] B.Y. Moghadam, W. C. Hou, C. Corredor, P. Westerhoff, J.D. Posner, Role of nanoparticle surface functionality in the disruption of model cell membranes., *Langmuir.* 28 (2012) 16318–26. doi:10.1021/la302654s.
- [16] A. Mechler, S. Praporski, K. Atmuri, M. Boland, F. Separovic, L.L. Martin, Specific and selective peptide-membrane interactions revealed using quartz crystal microbalance., *Biophys. J.* 93 (2007) 3907–16. doi:10.1529/biophysj.107.116525.
- [17] M. Rodahl, F. Höök, C. Fredriksson, C. A. Keller, A Krozer, P. Brzezinski, M. Voinova, B. Kasemo, Simultaneous frequency and dissipation factor QCM measurements of

- biomolecular adsorption and cell adhesion., *Faraday Discuss.* (1997) 229–46.
- [18] M. V Voinova, M. Jonson, B. Kasemo, “Missing mass ” effect in biosensor ’ s QCM applications, *Biosens. Bioelectron.* 17 (2002) 835–841.
- [19] K.F. Wang, R. Nagarajan, T.A. Camesano, Antimicrobial peptide alamethicin insertion into lipid bilayer: A QCM-D exploration, *Colloids Surfaces B Biointerfaces.* 116 (2014) 472–481. doi:10.1016/j.colsurfb.2014.01.036.
- [20] J.A. Gallego-Urrea, J. Tuoriniemi, M. Hassellöv, Applications of particle-tracking analysis to the determination of size distributions and concentrations of nanoparticles in environmental, biological and food samples, *Trends Anal. Chem.* 30 (2011) 473–483. doi:10.1016/j.trac.2011.01.005.
- [21] W. C. Hou, B.Y. Moghadam, C. Corredor, P. Westerhoff, J.D. Posner, Distribution of functionalized gold nanoparticles between water and lipid bilayers as model cell membranes., *Environ. Sci. Technol.* 46 (2012) 1869–76. doi:10.1021/es203661k.
- [22] T.J. Zwang, W.R. Fletcher, T.J. Lane, M.S. Johal, Quantification of the layer of hydration of a supported lipid bilayer, *Langmuir.* 26 (2010) 4598–4601. doi:10.1021/la100275v.
- [23] H.W. Huang, F.Y. Chen, M.T. Lee, Molecular mechanism of peptide-induced pores in membranes, *Phys. Rev. Lett.* 92 (2004) 198304–1. doi:10.1103/PhysRevLett.92.198304.
- [24] A.F. Xie, S. Granick, Phospholipid membranes as substrates for polymer adsorption., *Nat. Mater.* 1 (2002) 129–33. doi:10.1038/nmat738.
- [25] Y. Li, X. Chen, N. Gu, Computational investigation of interaction between nanoparticles and membranes: hydrophobic/hydrophilic effect., *J. Phys. Chem. B.* 112 (2008) 16647–

53. doi:10.1021/jp8051906.
- [26] G.D. Bothun, Hydrophobic silver nanoparticles trapped in lipid bilayers: Size distribution, bilayer phase behavior, and optical properties., *J. Nanobiotechnology*. 6 (2008) 13.
doi:10.1186/1477-3155-6-13.
- [27] S.H. Park, S.G. Oh, J.Y. Mun, S.S. Han, Effects of silver nanoparticles on the fluidity of bilayer in phospholipid liposome, *Colloids Surfaces B Biointerfaces*. 44 (2005) 117–122.
doi:10.1016/j.colsurfb.2005.06.002.
- [28] S. H. Park, S. G. Oh, J. Y. Mun, S. S. Han, Loading of gold nanoparticles inside the DPPC bilayers of liposome and their effects on membrane fluidities., *Colloids Surf. B. Biointerfaces*. 48 (2006) 112–8. doi:10.1016/j.colsurfb.2006.01.006.
- [29] H. Jang, L.E. Pell, B.A. Korgel, D.S. English, Photoluminescence quenching of silicon nanoparticles in phospholipid vesicle bilayers, *J. Photochem. Photobiol. A Chem.* 158 (2003) 111–117. doi:10.1016/S1010-6030(03)00024-8.
- [30] M. Schulz, A. Olubummo, W.H. Binder, Beyond the lipid-bilayer: interaction of polymers and nanoparticles with membranes, *Soft Matter*. 8 (2012) 4849-64.
doi:10.1039/c2sm06999g.
- [31] E. Evans, R. W., Entropy-driven tension and bending elasticity in condensed-fluid membranes, *Phys. Rev. Lett.* 39 (1977) 781–784.
- [32] T. Zhu, Z. Jiang, Y. Ma, Adsorption of nanoparticles and nanoparticle aggregates on membrane under gravity, *Appl. Phys. Lett.* 102 (2013) 2011–2014.
doi:10.1063/1.4802277.

Chapter 3

Nanoparticle Interactions with Model Membranes Modulated by Humic Substances

3.1 Abstract

One of the mechanisms of toxicity for engineered nanoparticles (NPs) originates from their ability to disrupt the integrity of cell membranes. In the natural environment, the interactions of NPs and cell membranes also depend on other components present in the media, such as humic substances. The goal of this study was to characterize how the presence of humic substances changes the mechanism of NP–membrane interactions. The interactions of the NPs and supported lipid bilayers in the presence of four humic substances were measured with quartz crystal microbalance with dissipation (QCM-D). Using gold NPs with various functionalizations (i.e. anionic, cationic and non-ionic ligands) led to an increased understanding of the mechanisms of NP–membrane interactions. Fulvic and humic acids extracted from Suwannee River (SRFA and SRHA), which had relatively lower molecular weights, adsorbed to the bilayer, while higher molecular weight components, commercial humic acid (HA) and the humic acid extracted from Elliott soil (ESHA), did not induce any changes to the bilayers. In addition, the NPs in SRFA and SRHA increased the mass of the bilayer by 20–30 ng, while the NPs in HA and ESHA changed the mass of the bilayer by < 10 ng. Control experiments were designed to test the effect of NPs in the absence of humic substances (i.e. the NPs were dissolved in water). In these cases, regardless of the type of NP functionalization, no substantial bilayer mass changes were observed. This suggests that the charge and chemistry of the ligands had a minor effect on NP–membrane interactions. Furthermore, in both the control and humic acid experiments, there were small dissipation changes (less than 1 unit) indicating that the overall membrane structure was not perturbed. These results show that the presence of humic substances as well as their physical and chemical properties exert a direct impact on the interactions between cell membrane and the nanoparticles.

3.2 Introduction

Regulatory agencies in the U.S and Europe have recognized the potential risks of engineered nanoparticles by commissioning scientific societies to identify the health, safety, and environmental impacts of nanoscience and nanotechnology [1]. Gold nanoparticles (NPs) are especially interesting for toxicity studies due to their wide range of applications in diagnostics and therapeutics, with estimates that the global market of gold NPs will approach 5 billion USD by 2020 [2]. Over the last few decades, researchers have studied the toxicity of gold NPs by multiple techniques, such as viability assays on mammalian cells or bacteria with respect to NP applications in medicine [3,4]. One of the mechanisms by which NPs cause cell death is disruption of cell membrane integrity by forming holes or membrane thinning [4–6]. Both computational [7–13] and experimental [5,14] techniques, including atomic force microscopy (AFM), have confirmed that NPs can penetrate and translocate through cell membranes and potentially form pores. Previous studies have investigated the roles of several parameters such as nanoparticle size, shape, concentration, core material, and NP capping agents on NP–cells interactions [15]. However, there are still unanswered questions about the effects of these properties on cell membrane integrity [5].

Due to the possibility of NPs being released into the natural environment during their life cycle [16], it is necessary to investigate the effects of NPs at the nano–bio interface, where there are other complex chemical species present, such as natural organic material (NOM). NOM represents heterogeneous mixtures of polydispersed materials in soils and natural waters, mainly composed of humic substances (e.g. humic and fulvic acids) and other organic materials, such as polysaccharides, proteins, lipids etc. Both humic acids (HAs) and fulvic acids (FAs) possess negative charge due to the abundance of carboxylic and phenolic groups [17], and this can affect

the toxicity of NPs as they alter the adsorption, aggregation/stabilization, dissolution and surface transformation of the nanoparticles. It is not clear if the presence of NOM affects NP disruption of cell membranes. Prior studies were conducted on the toxicity of NPs in the presence of the NOM, as reviewed by Wang et al. and Grillo et al. [17,18]. Many prior studies used microorganisms, and showed that in the presence of NOMs, NPs' toxicity either increased, decreased or remain unchanged depending on type of NOMs and the particles. The controversial data imply that the role of NOM in nanotoxicity is complicated and needs to be further investigated. The complexity is even greater when microorganisms are used for toxicity studies. For instance, dissolved organic matter is reported to decrease the toxicity of Ag on *Daphnia magna* by forming complexes with the metal ions and decreasing the availability of Ag⁺ [19]. In contrast, another study with AgNPs reported that terrestrial HA enhanced the toxicity of NPs on bacteria as the NOM induced generation of reactive oxygen species [20]. In the present study, we focused on one mechanism of toxicity, cell membrane disruption. Our goal in the present research was to characterize how NOM affects membrane interaction of NPs, and how these effects are dependent on the nature of the humic substance.

We hypothesized that the presence and nature of humic acids would change the mechanism of NP–membrane interactions. Interactions between gold NPs and supported lipid bilayers were measured via quartz crystal microbalance with dissipation (QCM-D) in the presence of different humic substances. Gold NPs with a diameter of 10-12 nm treated with different capping agents forming particles with different surface charges; (11-Mercaptoundecyl)-N,N,N-trimethylammonium bromide (MUTAB), and 2-aminoethanethiol as the cationic ligands, 3-mercaptopropionic acid and citrate coating as the anionic ligands and 2-mercaptoethanol and 1-propanethiol as the nonionic ligands.

To isolate membrane disruption from other possible toxicity mechanisms, we utilized supported lipid bilayers (SLBs) as a model of a cell membrane. SLBs and vesicles are two common forms of model membranes that have been successfully used in NP toxicity studies to show the formation of pores in lipid membranes [21–25]. For instance, vesicles have been used to model cell membranes in dye leakage assays performed in parallel to cell viability assays, which showed that cell death was the result of gold NP damage to the cell membrane [4]. SLBs are especially good candidates to represent cell membranes due to their simplicity and reproducibility of formation, as well as possibility of surface characterization by various techniques such as AFM and QCM-D [25,26].

QCM-D was used to detect the formation and structural change of SLBs as it is a powerful real-time technique to quantify the amount of adsorbed mass. Changes in the frequency and dissipation of energy during cycles of oscillation caused by applying AC voltage to the sensor are measured with this technique. The data can be used to interpret changes in mass and rigidity of the layer, as decreases in frequency correspond to addition of mass, while decreases in dissipation of energy correspond to film rigidity.

In order to mimic the natural environment, four humic substances were examined; commercially available humic acid provided by Sigma-Aldrich (HA), humic acid extracted from Elliott soil (ESHA), humic acid extracted from the Suwannee River (SRHA), and fulvic acid extracted from the Suwannee River (SRFA). Our results showed that the molecular weight of the humic substance was critical in determining the nature of the interactions with SLBs.

3.3 Materials and methods

3.3.1 Gold nanoparticles

Spherical, gold nanoparticles with diameters of 10-12 nm were purchased (Nanopartz Inc.; Loveland, CO) with different functionalizations, which were 1-propanethiol, 2-mercaptoethanol, 2-aminoethanethiol, 3-mercaptopropionic acid, and (11-Mercaptoundecyl)-N,N,N-trimethylammonium bromide. According to the manufacturer, the thickness of the capping agent is less than the variability of size of the NPs themselves, which means the ligands did not change the size of the NPs significantly. The size standard deviations (20%) were measured by dynamic light scattering (DLS) and Transmission Electron Microscopy (TEM) by the manufacturer when in their purchased concentration of 10^{14} particles/mL. All particles studied were hydrophilic with 1-propanethiol adding a slightly more hydrophobic characteristic. The original stock solutions were dispersed in de-ionized water and stored at 7 °C in a light impenetrable container. The concentrated NP solutions were diluted with ultrapure water (Milli Q) or humic/fulvic acid solution to a concentration of 3.119×10^{12} particles/mL and 7.14×10^{12} particles/mL, depending on the experiment. Zeta potentials were determined using a Malvern Instrument and Zetasizer software.

3.3.2 Vesicle preparation

L- α -phosphatidylcholine (egg, chicken) (PC) with purity > 99% was purchased (Avanti Polar Lipids). All other chemicals were purchased from Sigma-Aldrich (St. Louis, MO), unless stated. Lipid vesicles were prepared according to published procedures [27,28]. Briefly, 0.15 mL of 100 mg/mL egg PC in ethanol solution was dried with nitrogen gas and desiccated for 24 h.

The egg PC solution was then rehydrated using 6 mL of a buffer solution containing 10 mM Tris (hydrozymethyl) aminomethane and 100 mM sodium chloride, pH 7.8. The solution was vortexed for 15 s followed by 5 freeze-thaw-vortex cycles. An ultrasonic dismembrator (Model 150T, Fisher Scientific, Waltham, MA) was used to form small unilamellar lipid vesicles by sonicating the egg PC solution for 30 min. in pulse mode with a 30% duty cycle (3-second pulse at an amplitude of 60%, followed by a 7-second pause), while in a glass tube immersed in an ice bath [27,28]. After centrifugation (Eppendorf Centrifuge 5415 D) at $16000 \times g$ for 10 min, the supernatant was decanted from the pellet and stored under nitrogen gas at 7°C for up to one month. The average size of the vesicles was 125 nm as measured by dynamic light scattering (DLS) using a Malvern Instrument. Size stability of the vesicle solution was confirmed by DLS measurements over 30 days (data not shown). All solutions were vortexed for 15 s before use. Prior to use, lipid vesicle suspensions were diluted to 0.1 mg/mL using Tris–NaCl buffer.

3.3.3 Humic substances

Commercial humic acid (HA) was purchased from Aldrich (St. Louis, MO). Suwannee River Fulvic Acid Standard II (SRFA), Suwannee River Humic Acid Standard II (SRHA), and Elliott Soil Humic Acid (ESHA) were purchased from the International Humic Substances Society (IHSS). Humic solutions with concentration of 100 mg/L were prepared by adding the powder to ultrapure water and stirring for one hour at 30 °C. The solution was then sonicated for 1 h in a water bath ultrasonicator and stored at 7 °C at dark to preserve integrity. Before each experiment, the solution was placed on a stir plate at 600 rpm for one hour and filtered twice through a 0.2 µm syringe filter. The pH of

SRFA, SRHA, and ESHA was 4 and the pH of HA was 7. The properties of the NOMs are obtained from the manufacturer and listed in Table 1.

Table 1. Properties of the NOMs.

NOM	Molecular weight (g/mol)	Amino acid content($\mu\text{mol/g}$)
ESHA	12700 [29]	777
SRHA	1066 [30]	89
SRFA	711 [30]	24
HA	20000-50000	N/A

3.3.4 Quartz crystal microbalance with dissipation (QCM-D) monitoring for bilayer formation and NPs interaction

QCM-D measurements were performed with a Q-Sense E4 (Biolin Scientific, Sweden). QCM-D sensor crystals (5 Hz), reactively sputter-coated with silicon dioxide, were purchased from Biolin Scientific (Gothenburg, Sweden). The QCM-D recorded measurements of frequency (mass changes) and dissipation (surface rigidity) at five different harmonics. Overtones 3, 5, 7, 9, and 11 of the sensor crystal's natural frequency (5 MHz) were measured and normalized automatically to each overtone (f/n , where f is frequency and n is the harmonic number) by the Q-Sense software. These overtones allow for comparison throughout the bilayer depth, where the third overtone is closest to the bilayer surface, and the eleventh overtone is closest to the silica substrate. The fundamental frequency was not analysed because of its sensitivity to changes in the

solvent flow. Typical sensitivities for all other overtones in liquids are ~ 0.1 Hz for frequency (~ 1.7 ng/cm²) and $\sim 0.1 \times 10^6$ for dissipation. Before each experiment, the crystals were cleaned using modified Q-Sense protocols which include sequential rinses with ethanol, ultrapure water, 2% sodium dodecyl sulfate, and ultrapure water. After drying the crystal under nitrogen flow, any other organic contaminants were removed by two cycles of oxygen plasma cleaning using Plasma Prep II (SPI Supplies, West Chester, PA) for 45 seconds/cycle.

The bilayer was formed as reported previously [27,28,31,32]. After establishing a baseline with buffer, PC vesicles were flowed over SiO₂ crystal at 0.15 mL/min. A stable lipid bilayer was formed within 8 minutes. The SLB was then rinsed for 6 minutes to remove un-ruptured vesicles. Ultrapure water was then administered to the system to establish the viscosity change due to water prior to NPs administration. Functionalized gold NPs diluted in ultrapure water interacted with the bilayer for 10 minutes (Fig. 1 part B).

Experiments were also performed in the presence of humic substances. The gold NPs were suspended in the humic or fulvic acid solution, and to establish a viscosity baseline, humic or fulvic acid was introduced 8 minutes before and post introduction of gold NPs. At least five replicates were performed for each type of gold NP. Statistical analysis to compare the mass changes observed for each type of NP was performed using SigmaPlot 12.5 by a one-way analysis of variance test (ANOVA), using all pairwise comparisons.

3.3.5 Relating changes in frequency to mass changes using Sauerbrey relation

The Sauerbrey equation for rigid films describes the inverse relationship between frequency change (Δf) and mass adsorption (Δm) [33] :

$$\Delta m = -\frac{C \cdot \Delta f}{n}$$

Where C is the mass sensitivity constant ($C = 17.7 \text{ ng} \cdot \text{cm}^{-2} \cdot \text{Hz}^{-1}$) and n is the overtone number. For the analysis, Δf data for overtones 3, 5, 7, 9, and 11 were measured. To ensure the validity of the Sauerbrey model, the system must be rigid which would be indicated by a low dissipation value. Also, the mass adsorbed must be small relative to the quartz crystal and must be evenly distributed over the area of the crystal to ensure the validity of using the Sauerbrey relationship [34]. The Sauerbrey relationship may underestimate the mass for soft films that do not couple completely to the sensor crystal, but it gives us a close approximation of the mass changes on a rigid surface [35,36].

3.4 Results

3.4.1 Effect of humic substance on zeta potential of NPs

The surface charge modification of the NPs was characterized via zeta potential. The NPs became more electrostatically negative when in the presence of humic acids (Table 2). Due to the charge of the different ligands, nanoparticles had different zeta potentials in water, but in each NOM, particles with different coatings showed similar zeta potentials.

Table 2. Zeta potential values for the different NPs in water and with NOM.

Particle Functionalization	Media	NPs Zeta Potential (mV)
1-propanethiol-functionalized	water	-19.3 ± 8.1
	HA	-41.0 ± 7.1
2-mercaptoethanol-functionalized	water	-29.5 ± 7.2
	HA	-44.5 ± 8.0
2-aminoethanethiol-functionalized	water	-50.5 ± 10.7
	HA	-43.9 ± 10.0
3-mercaptopropionic acid-functionalized	water	-45.4 ± 9.3
	HA	-46.6 ± 9.0
Citric acid-stabilized	water	-29.1 ± 7.6
	HA	-41.8 ± 12.7
	SRHA	-32.7 ± 7.5
	SRFA	-28.6 ± 12.5
	ESHA	-37.0 ± 2.1
MUTAB-functionalized	water	- 9.9 ± 3.0
	SRHA	-30.4 ± 1.84
	SRFA	-29.3 ± 9.89
	ESHA	- 37.05 ± 1.76

3.4.2 Formation of SLB monitored by QCM-D

QCM-D was used to verify real-time SLB formation on the crystals. First, water-filled lipid vesicles adsorb on the silica crystals, as observed by a decrease in frequency (labeled as 1 on Fig. 1 part A) and increase of dissipation of energy (3). When the vesicles reached critical surface coverage, they ruptured, releasing their interior liquid and causing the frequency to increase as mass is lost (2). Bilayer formation is characterized by a decrease in energy dissipation (4), and the final values for Δf and ΔD were -25 Hz and 0.2×10^6 , respectively [37], and these values were very reproducible.

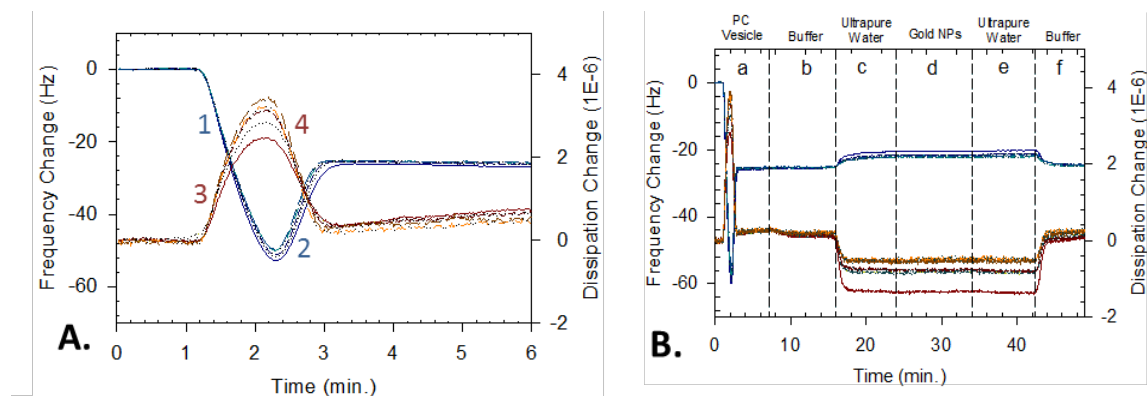


Figure 1. Representative plots showing QCM-D frequency and dissipation changes as a function of time. The blue lines represent frequency changes, and the red lines represent dissipation. Overtones 3, 5, 7, 9, and 11 are shown. (A) The first 6 minutes demonstrate bilayer formation. The formation is numbered 1-4 to indicate the different aspects of formation: 1) a drop in frequency corresponds to mass deposition; 2) subsequent rise in frequency corresponds to the release of fluid from ruptured vesicles; 3) a rise in dissipation is due to the presence of fluid in vesicles attached to the surface; 4) a decrease in dissipation change is due to the release of fluid and increased rigidity of mass. (B) 1-propanethiol-functionalized gold NPs in water.

3.4.3 Monitoring the interactions of NPs with SLBs in the presence of humic substances

Before flowing the NP solution on SLB, the bilayer surface was exposed to a humic substance with each of the humic substances having a characteristic way of interacting with the SLB. In the case of SRFA and SRHA (circled on Fig. 2 parts C and D), the frequency decreased after the humic substance was introduced indicating the adsorption of the humic substance to the bilayer. However, the other two humic acids, HA and ESHA, did not change the frequency (Fig. 2, parts A and B). The changes of the bilayer interacting with citrate-stabilized NPs and MUTAB-functionalized NPs were examined in ESHA, SRHA, SRFA and water. In order to detect any mass and viscoelastic changes of the bilayer, the frequency and dissipation values were read at two time points: one minute before NP flow started, and one minute before the second humic acid flow ended. The dissipation changes were negligible for all of the humic substances (Fig. 3) indicating that the bilayer remained rigid and the Sauerbrey model could be used to estimate the mass change of the bilayer.

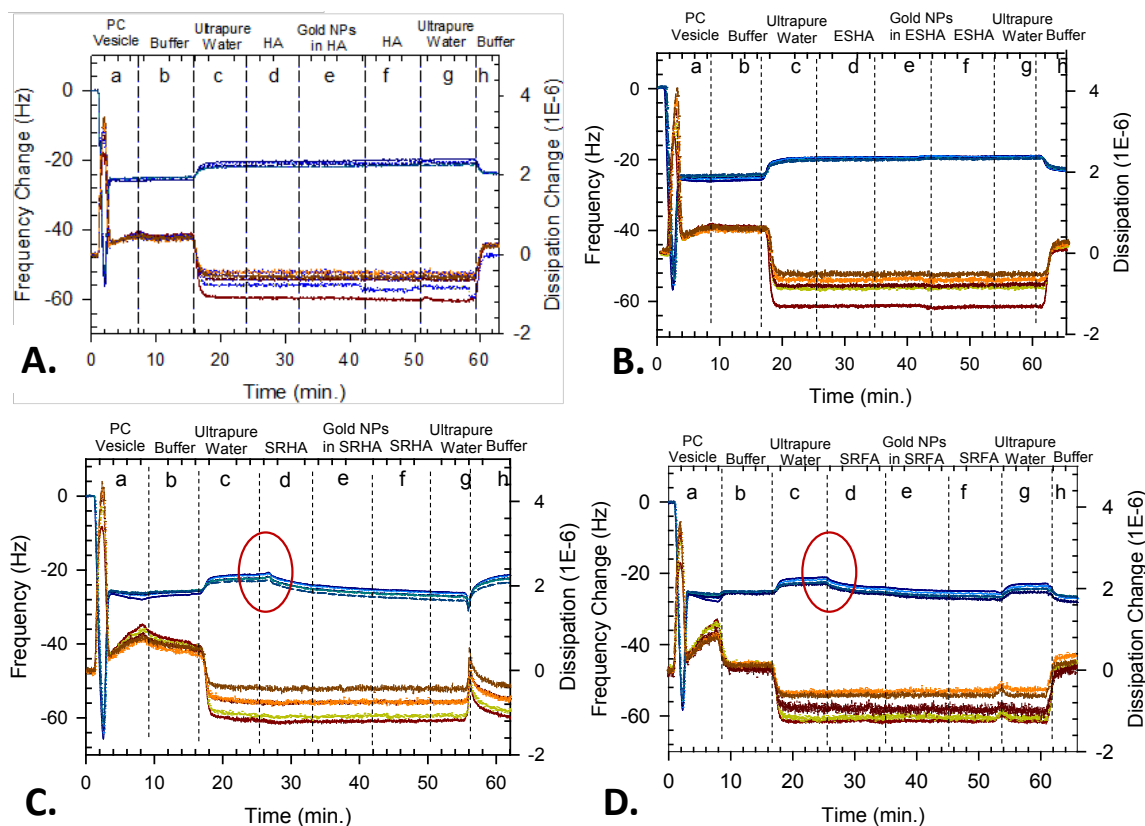


Figure 2. Representative plots showing QCM-D frequency and dissipation changes as a function of time. The blue lines represent frequency changes, and the red lines represent dissipation. Overtones 3, 5, 7, 9, and 11 are shown. (A) Citrate-stabilized gold NPs in HA (B) Citrate-stabilized gold NPs in ESHA. (C) Citrate-stabilized gold NPs in SRHA. (D) Citrate-stabilized gold NPs in SRFA. The circled areas show the bilayer changes resulting from interactions with the humic substances.

The mass changes calculated by the Sauerbrey equation showed that in the presence of water and ESHA, the bilayer changed similarly: Citrate-stabilized NPs decreased the bilayer mass by ~5 ng (Fig. 4 parts C and D) where the MUTAB-functionalized NPs added < 5 ng to the mass (Fig. 4. parts G and H). In the presence of SRHA and SRFA, the NPs had the same effect on the SLBs, with both showing mass addition for both citrate-stabilized and MUTAB-

functionalized gold NPs. In both SRHA and SRFA, the mass addition was slightly larger for anionic citrate-stabilized particles compared to cationic particles with MUTAB ligand.

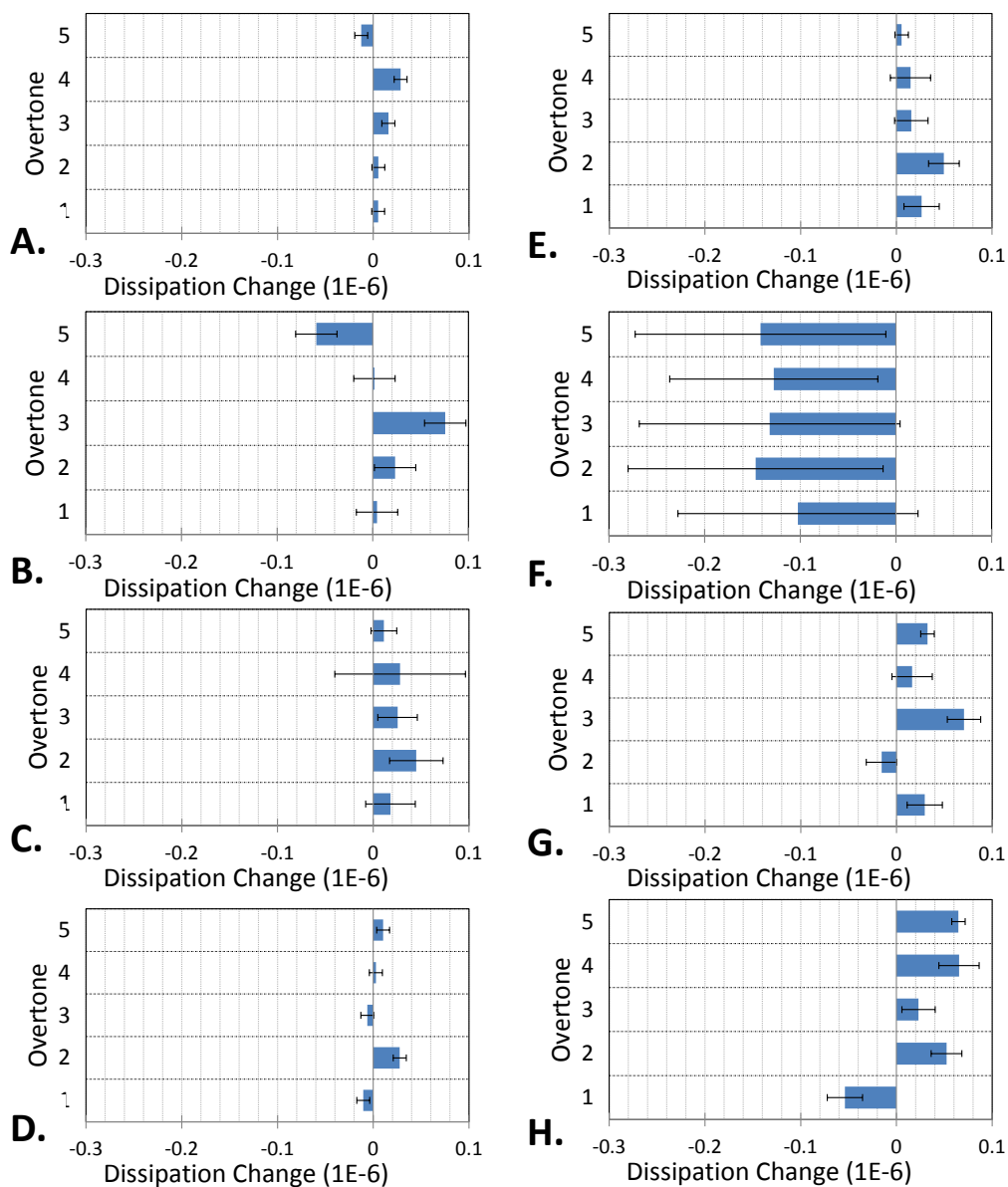


Figure 3. Change in dissipation of energy for interactions between SLB and citrate-stabilized gold nanoparticles in (a) SRFA, (b) SRHA, (c) ESHA, and (d) water; and interactions between SLB and MUTAB-functionalized gold nanoparticles in (e) SRFA, (f) SRHA, (g) ESHA, and (h) water. Each dissipation change graph is based on at least 5 experimental replicates.

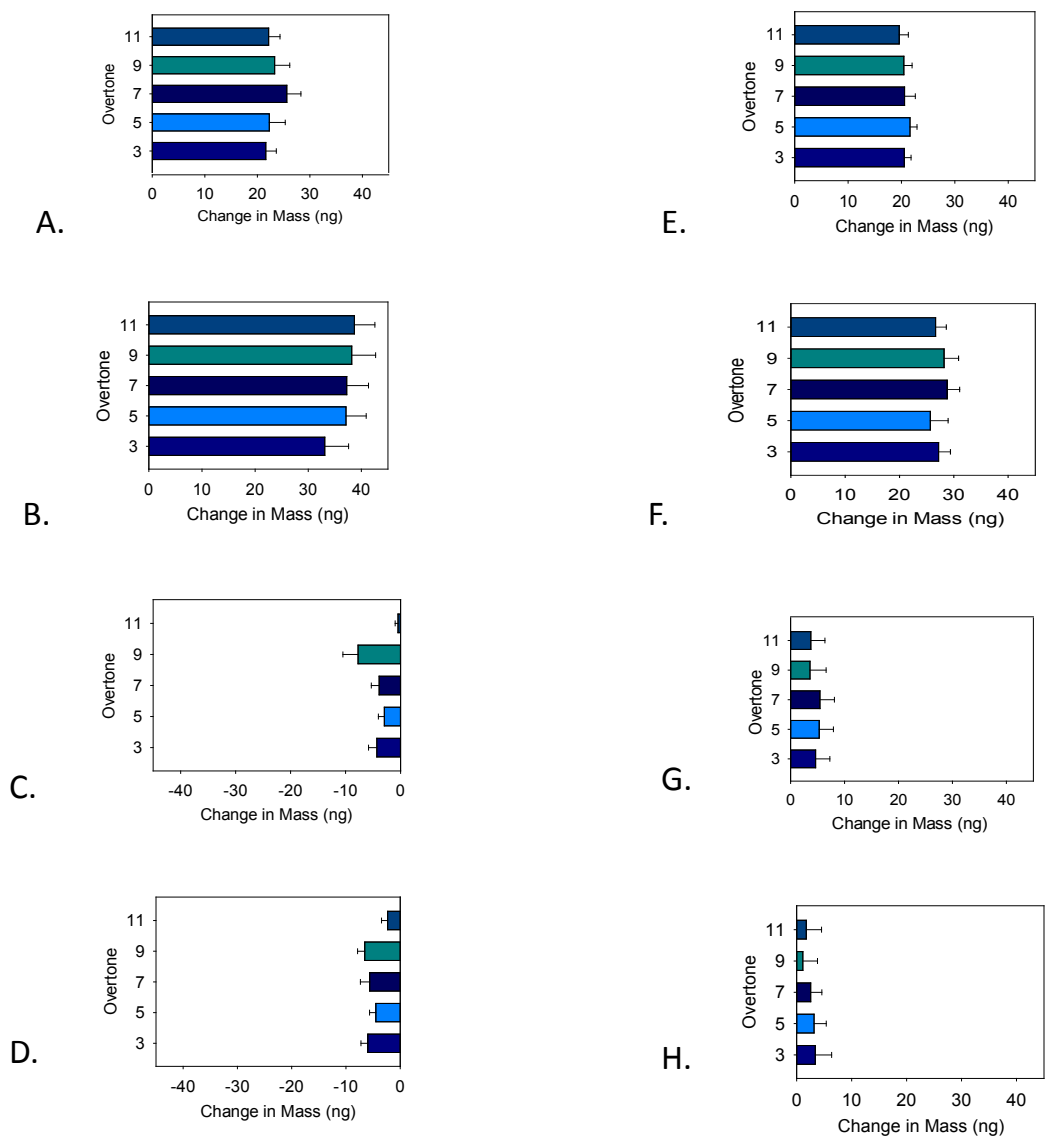


Figure 4. Calculated mass changes (using the Sauerbrey equation) for interactions between SLB and citrate-stabilized gold nanoparticles in (A) SRFA, (B) SRHA, (C) ESHA, and (D) water; and interactions between SLB and MUTAB-functionalized gold nanoparticles in (E) SRFA, (F) SRHA, (G) ESHA, and (H) water. Each calculation is based on at least 5 experimental replicates at a constant concentration of 7.14×10^{12} particles/mL. Statistical analysis was performed with SigmaPlot 12.5 software at a 95% confidence interval ($\alpha=0.05$). The results of one-way analysis of variance (ANOVA) test showed that the results of different functionalized NPs have statistically significant difference in the presence of humic acids as well as water ($P < 0.001$). The mass calculated is per 1 cm^2 of crystal area.

3.4.3 Mass change of bilayer as the result of interactions with different functionalized gold NPs in water and HA

When NPs functionalized with the different ligands interacted with the bilayer, the bilayer's integrity remained constant with little dissipation changes observed (Fig. 5) indicating the validity of Sauerbrey equation in estimating the mass change. All functionalized NPs in water had a similar trend of mass removal from the bilayer ranging from 5 to 15 ng. Also, for each type of NPs, the change of frequency had similar values for all overtones (Figs. 5 and 6) indicating similar changes for every depth of the bilayer. In HA, all of the NPs caused some mass removal except the particles with anionic 3-mercaptopropionic acid ligands, which added ~ 8 ng to the mass of the bilayer. For the other four NPs, the mass loss was less significant in the presence of the HA.

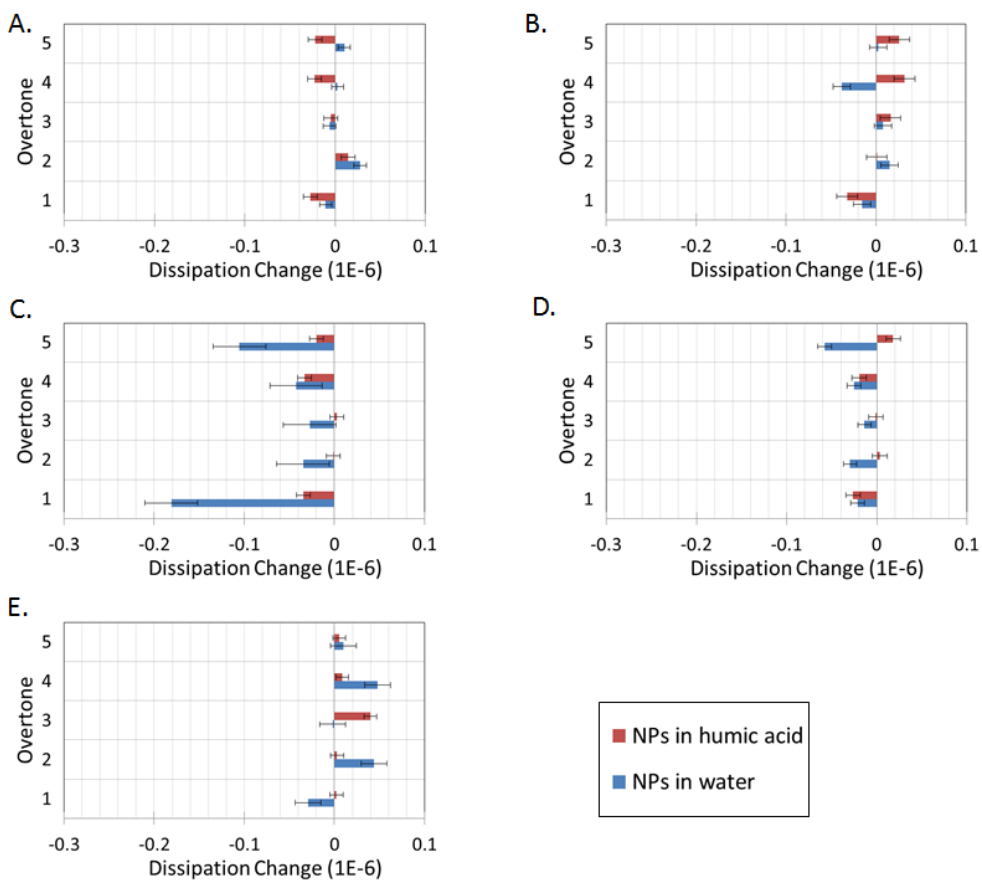


Figure 5. Dissipation change graphs for 10-12 nm gold NPs with (A) citrate ligands, (B) 1-propanethiol (C) 2-mercaptoethanol, (D) 2-aminoethanethiol, and (E) 3-mercaptopropionic . Blue bars are for NPs in water and red bars represent NPs in humic acid. Each dissipation change graph is based on at least 5 experimental replicates.

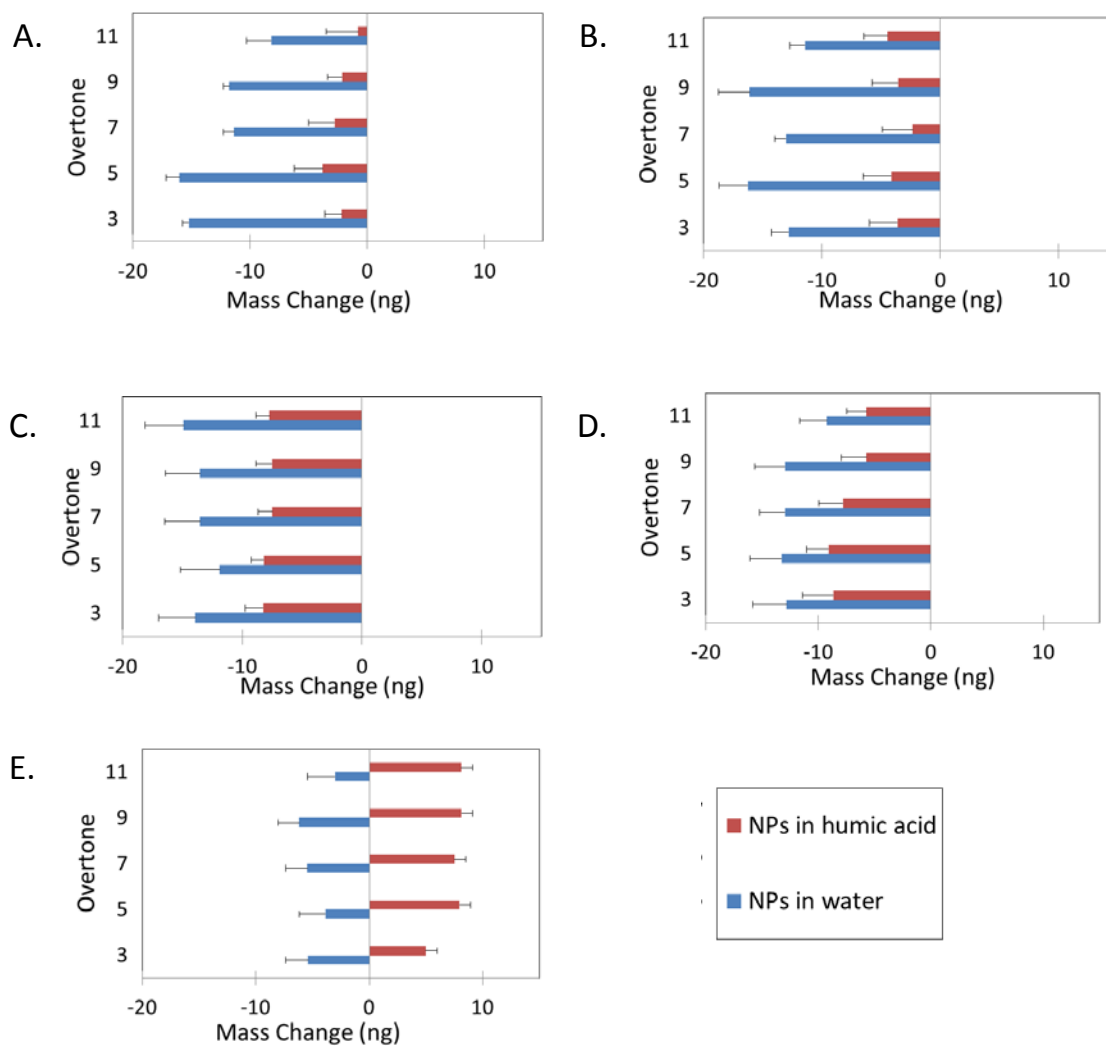


Figure 6. Calculated mass changes based on Sauerbrey relationship for interactions of gold NPs with PC bilayer for 10-12 nm gold NPs with (A) citrate ligands, (B) 1-propanethiol, (C) 2-mercaptoethanol, (D) 2-aminoethanethiol, and (E) 3-mercaptopropionic acid. Blue bars are for NPs in water and red bars are for NPs in HA. Error bars show the standard error values. Each functionalization calculation is based on at least 5 experimental samples at a constant concentration of 3.119×10^{12} particles/mL. A one-way analysis of variance (ANOVA) test at a 95% confidence interval ($\alpha=0.05$) showed that the mass changes for different functionalized NPs were significantly different, when comparing values in water with HA ($P < 0.001$). The mass calculated is per 1 cm^2 of crystal area.

3.5 Discussion

Engineered nanoparticles can change the structure of cell membranes and induce toxicity to living organisms in the environment. In order to better understand how compounds present in the natural environment alter NP-membrane interactions, we chose a variety of humic substances for investigation, and examined gold NPs with several chemical functionalizations (Fig. 7).

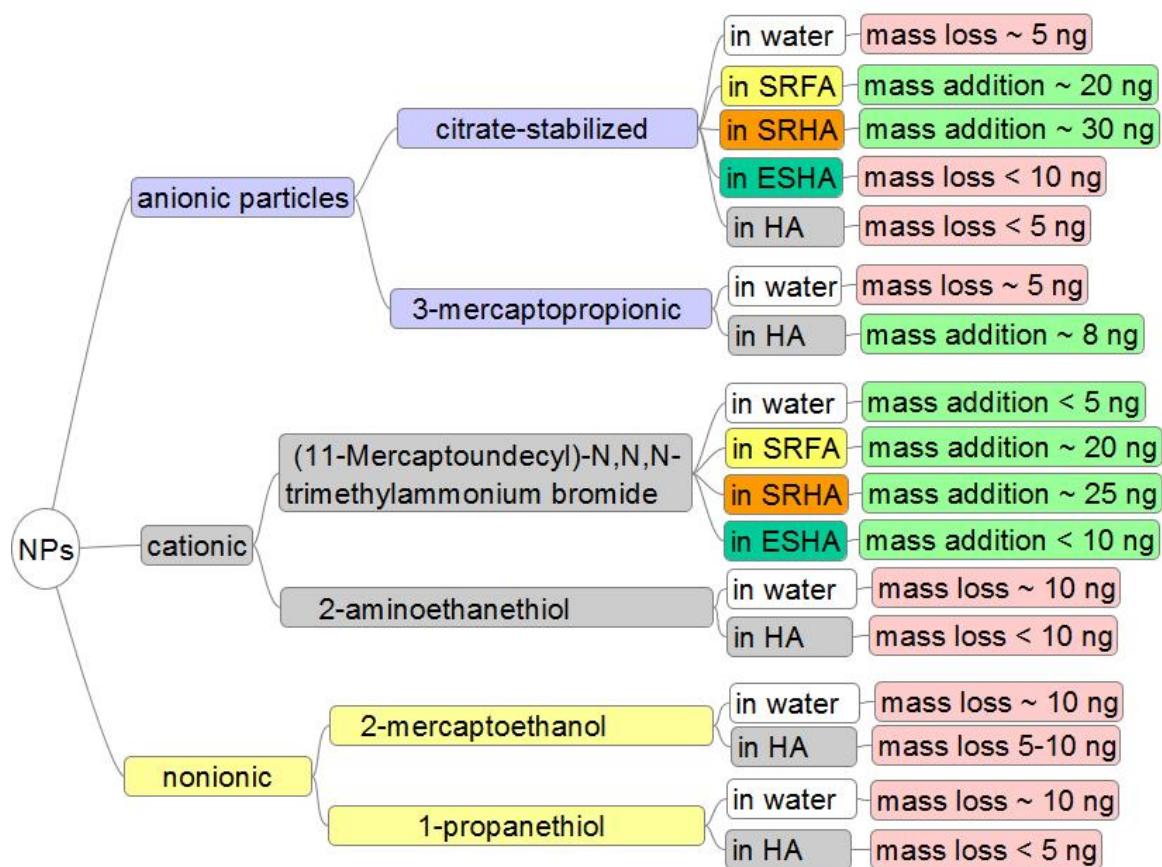


Figure 7. Comparing the bilayer mass changes resulting from NPs–SLB interactions in the presence of humic substances.

3.5.1 Humic acids coated the nanoparticles, masking surface charges

When NPs were exposed to humic substances, the zeta potential values were more negative compared to when they were dissolved in water, indicating that the humic substances

coated the surface of the NPs (Table 2). Coating of NPs with natural organic matter was previously shown for different types of nanoparticles as the negative surface charge of metal oxide NPs (e.g. TiO₂, ZnO, Fe₂O₃, and NiO) increased significantly when they were dissolved in the natural organic matter extracted from the Suwannee River (SRNOM) [38]. Similarly, Stankus et al. showed that SRHA coated the surface of gold NPs functionalized with different capping agents (e.g. anionic (citrate and tannic acid), neutral (2,2,2-[mercaptoethoxy(ethoxy)]ethanol and polyvinylpyrrolidone), and cationic (mercaptopentyl(trimethylammonium)) [39]. In addition, the electrophoretic mobility of SRHA molecules was more negative in the presence of gold NPs with these different ligands showing that SRHA coated the nanoparticles regardless of the capping agent [39]. Coating of nanoparticles with NOMs leads to increased stability of NPs as reported in NP aggregation kinetic studies [38,40–45]. The NPs, regardless of their ligands, possessed the same zeta potentials when they were dissolved in the humic substances suggesting that the charge of humic substances suppressed the charge of NP ligands.

3.5.2 Interactions between humic substances and a bilayer are affected by the molecular size and structure of the humic substances

The adsorption of HA on the surface of a bilayer is controlled by hydrogen bridging with the electronegative functional groups in the HA and on the lipid head groups and hydrophobic bonds between the HA and SLB.[46,47] QCM-D data showed that the mass of the bilayer increased after interacting with SRFA and SRHA, while the mass remained unchanged with HA and ESHA. This is supported by previous studies reporting that the effect of a humic substance on a bilayer depends on the molecular properties of the humic substance [46,47]. For example,

Ojwang et al. studied the perturbation of 1-palmitoyl-2-oleoyl- Sn-glycero-3-phosphocholine (POPC) membrane by using fluorescence dye leakage from the vesicles interacting with four different NOMs. They observed that the kinetics of bilayer–HA interactions depend on the environmental conditions (e.g. pH, HA concentration, and temperature) as well as chemical characteristics of the NOMs, such as density of polar functional groups [46].

In order to interpret our results, we employ the previous model of NOM–membrane proposed by Ojwang and Cook to explain the two step process of adsorption/absorption of humic substances to the lipid bilayer [46,47]. Based on this model, HA–bilayer interactions take place with a two–step mechanism starting from an initial adsorption induced by hydrogen bridging and electrostatic interactions between the lipid polar head groups and the NOM functional groups. The next step is the absorption of the humic substance into the membrane, governed by hydrophobic forces between the membrane and hydrophobic fragments of the NOM. Any perturbation or structural change to the bilayer occurs in the absorption step, where the fragments of humic substance become located in the lipid structural lattice. The adsorption/absorption model suggests that in order to initiate the adsorption, the HA moieties should have enough charge density to support the initial hydrogen bridging. This explains the importance of pH conditions as well as the presence of high density polar groups, functionalized aromatic and alkyl moieties of humic substance in initial adsorption of HAs on the bilayer. As a further extension of this model, we propose that rigidity and conformation of humic substances is another important factor in the initiation of the adsorption process.

According to our results, SRHA and SRFA went through both adsorption and absorption steps as the frequency decreases after addition of SRHA and SRFA indicating the mass addition to the bilayer (Fig. 2, parts E and F). This indicates that SRHA and SRFA have sufficient charge

density to initiate hydrogen bridging as well as hydrophobic attractions with the membrane, allowing them to insert into the lipid lattice structure. In our study, HA and ESHA did not induce any mass change to the bilayer indicating the lack of attractive forces for these species to undergo the adsorption and/or absorption steps. This could be explained by considering the role of pH conditions in the adsorption/absorption model as well as the molecular conformation of the humic substances. Previous studies have indicated the importance of pH when studying the interactions between model membrane systems and surface charge particles as lower pH provides more electrostatic attractions and hydrogen bridging for the initial adsorption [46–48]. Campbell et al. concluded the importance of pH on the accumulation of NOM (a soil-derived fulvic acid and Suwannee River HA) with phytoplankton and fish gill surfaces at a pH range of 4-7 [48].

The organic matter was more conducive to accumulation on the biological surfaces at more acidic pH than the neutral pH. In our experiments, the bilayer interactions with commercially available HA, which had a pH of 7, did not cause a change in the frequency/mass of the bilayer as the neutral pH makes it less likely that the HA can accumulate on the SLB. Instead, we suggest that the commercially available HA was more likely to coexist with the bilayer (Fig. 2, part A).

However, ESHA does not adsorb to the membrane although the ESHA solution was used at a pH of 4, which would lead to the expectation of having an adequate electrostatic attraction for the adsorption. The lack of adsorption of ESHA to the membrane could be explained by considering the conformational properties of the humic substance. It has been previously proposed that biopolymers with molar mass of higher than 10^4 g/mol possess rigid structures resulting from their associations into double or triple helices aggregating together.⁴⁹ The AFM

and TEM images of these rigid biopolymers show that their length is larger than 1 μm and they have the capacity to form gels. Both ESHA and HA fit into this category and are expected to be rigid coils or of similar nature (Table 1). Considering the abovementioned points, we propose the following mechanism for the interactions of the NOM with the bilayer. SRFA and SRHA have lower molecular weights than the other two humic acids; therefore, hydrophobic interactions can provide the driving force for their adsorption to the lipid membrane incorporating some NOM particles between the lipid molecules. In contrast, ESHA and HA have higher molecular weights and more rigid structures, and therefore cannot fit into the small space between the lipid molecules. In ESHA and HA, the hydrophobic groups cannot provide enough attractive forces for adsorption, at least not at neutral pH.

3.5.3 Mechanism of interactions between NPs and a bilayer are affected by the properties of the humic substances that are present in the media

The QCM-D results confirm that the presence of humic substances changes the mechanism of NP–membrane interactions. The results show that the change of the dissipation of energy was insignificant for all types of NP and the media, indicating that interactions with the NPs did not disrupt the membrane (Fig. 2 and Fig. 4). However, application of the Sauerbrey model shows that depending on the media, the interaction of the bilayer with NPs led to different mass changes. In the absence of humic substance, the NPs that were dissolved in water either did not change the mass of the bilayer or decreased the mass by a very small amount (~ 10 ng). For all types of particles with different functional groups, the bilayer mass remained unchanged after interacting with NPs dissolved in water, implying that the interactions are most likely due to non-

electrostatic forces. Small mass loss from the bilayer was previously reported for 2, 5, 10 and 40 nm citrate-stabilized NPs [26]. These findings showed that the surface binding of NPs to the bilayer leads to rearrangement of the lipid molecules and induces some internal stress on the bilayer. In response to this stress, some lipid molecules detach from the membrane to lower the free energy of the system. Here, the adsorption of the NPs is not significant enough to cause any large pore formation or lead to lysis of the membrane.

In contrast, the bilayer interactions with the NOM-coated NPs caused significant mass addition due to adsorption on the bilayer. The interactions of NPs-SLB in SRFA and SRHA led to 20-30 ng of mass addition while the mass change in ESHA and HA was not significant (<10 ng). Therefore, the media in which NPs interact with the bilayer had a major effect on the mechanism of interaction. This was previously observed for citrate-stabilized gold NPs interacting with bilayer in the presence of PMAA [26]. In order to mimic the organic matter in the environment, Bailey et al. used PMMA in the media, and concluded that upon the adsorption of hydrophobic PMMA-coated particles to the bilayer the lipid head group tilts and creates some space for the partial insertion of 2 and 5 nm NPs. Here, the adsorption of NPs coated with SRFA and SRHA is qualitatively similar to previously reported adsorption of NPs coated with PMAA due to the prompted adhesion in the presence of the polymer [26]. Since all NPs complex with the fulvic and humic acids, the driving force for the adsorption is likely to be hydrophobic attractions. It has been previously reported that hydrophobic nanoparticles can insert into the hydrophobic region of the bilayer [26,50-52]. In this case, the mass addition as the result of NP adsorption is higher than the small mass loss caused by removal of stressed lipids. In addition, it has been previously proposed that SRHA has a higher adsorption capacity for citrate-stabilized NPs than SRFA [45].

In the presence of HA and ESHA, the NPs do not change the mass of the bilayer because when NPs complex with these humic acids, they are not available at a sufficient concentration to adsorb onto the bilayer. The conformation of the NP–NOM complex is different in ESHA and HA compared to SRFA and SRHA. The difference between the conformation of higher molecular weight and lower molecular weight NOM is schematically illustrated in Fig. 8. ESHA and HA are macromolecules with less flexibility, which do not wrap around the NPs. The NPs in ESHA and HA become trapped in a loose network of the humic substances and so there is less opportunity for the NPs to have contact with the bilayer surface. This is similar to the mechanism of bridging of multiple NPs by stiff polysaccharides reported previously [43]

3.6 Summary and conclusions

This study provided a mechanistic approach to understanding the interaction of functionalized gold NPs with a SLB, and the role of humic substances during these interactions. In water, NPs interacted similarly with the SLB regardless of functionalization. Due to the neutral pH or the rigidity of the structure, the HA did not readily adsorb to the SLB. Similarly, ESHA with a high molecular weight and rigid structure did not adsorb to the SLB. In contrast, SRHA and SRFA adsorbed to the bilayer starting from initial electrostatic attractions followed by hydrophobic driving force. In the presence of SRHA and SRFA, the bilayer mass increased as the result of interaction with NPs coated with different ligands. While surface charge does have minor effects as observed with small mass changes, it was concluded that the presence of SRFA and SRHA provided the driving forces for the interaction mechanisms observed for significant mass additions to the lipid bilayer surface. In HA and ESHA, there was a lack of driving force for adsorption of NPs to the bilayer as the particles were trapped in the gel-like structure of the rigid humic superstructure. This study demonstrates the importance of investigating both

functionalized NPs and NOM together with a supported lipid bilayer system to gain knowledge relevant to environmental exposure.

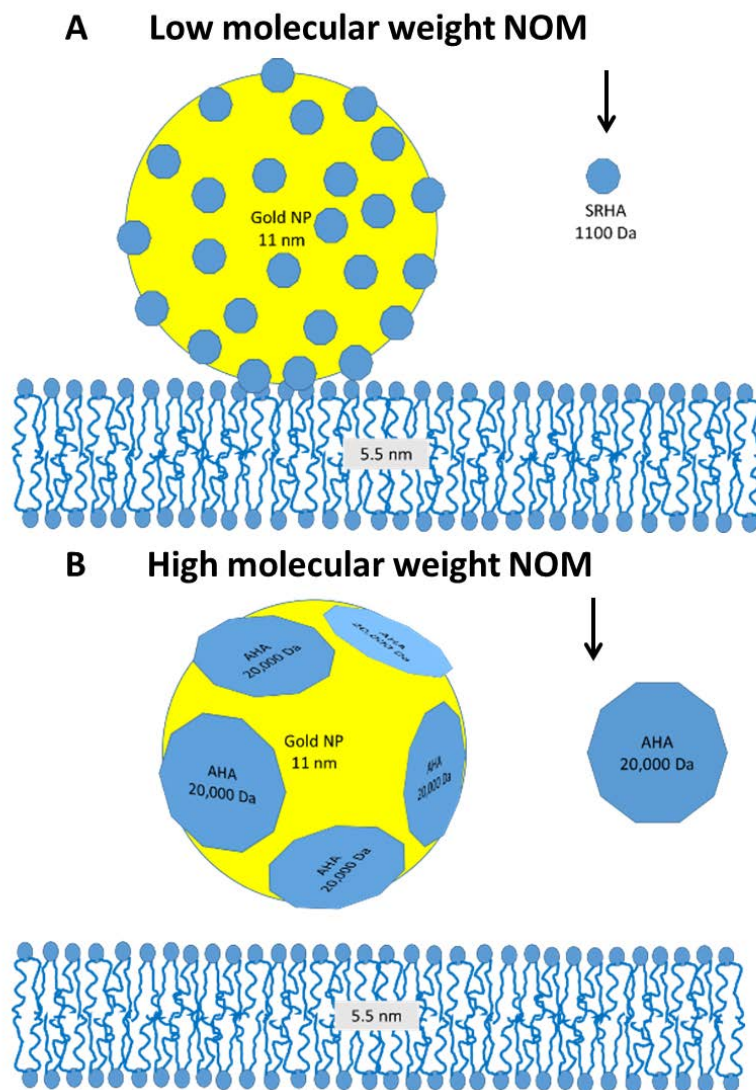


Figure 8. Schematic of the mechanism of bilayer interaction with NPs in humic substances. (A) Humic and fulvic acids with low molecular weights (e.g. SRFA and SRHA) coat NPs and adsorb to the bilayer by the hydrophobic attractions. (B) The humic substances with high molecular weights and more rigid structures (e.g. ESHA and HA) trap NPs in a mesh or gel and prevent NP adsorption to the bilayer.

3.7 Acknowledgments

This work was supported in part by the National Science Foundation (CBET 0966496). This work presents the combined data obtained by the main author and Christina M. Bailey. The author would like to thank Dr. Joseph Duffy, Dr. Christopher Lambert, Dr. Reeta Prusty Rao, and Dr. Arne Gericke at Worcester Polytechnic Institute who assisted with some use of lab equipment. Several WPI students assisted with preliminary experiments in this area: Kellie L. Waterman, Theresa Logan, Michelle Ly, Kathleen F. Wang.

3.8 References

- [1] A. Dowling, R. Clift, N. Grobert, D. Hutton, R. Oliver, O. O’neill, J. Pethica, N. Pidgeon, J. Porritt, J. Ryan, Et Al., Nanoscience and nanotechnologies : opportunities and uncertainties, London R. Soc. R. Acad. Eng. Rep. 46 (2004) 618–618.
doi:10.1007/s00234-004-1255-6.
- [2] Grand View Research, Inc.: San Francisco, CA, USA, Gold Nanoparticles Market Analysis by End-Use (Medical & Dentistry, Electronics, Catalysis) and Segment Forecasts to 2020, (2015). <http://www.grandviewresearch.com/industry-analysis/gold-nanoparticles-industry>.
- [3] C.J. Murphy, A.M. Gole, J.W. Stone, P.N. Sisco, A.M. Alkilany, E.C. Goldsmith, S.C. Baxter, Gold Nanoparticles in Biology: Beyond Toxicity\to Cellular Imaging, Acc. Chem. Res. 41 (2008) 1721-1730.
- [4] C.M. Goodman, C.D. McCusker, T. Yilmaz, V.M. Rotello, Toxicity of gold nanoparticles

- functionalized with cationic and anionic side chains., *Bioconjug. Chem.* 15 (2004) 897–900. doi:10.1021/bc049951i.
- [5] P.R. Leroueil, S. A. Berry, K. Duthie, G. Han, V.M. Rotello, D.Q. McNerny, J.R. Baker, B.G. Orr, M.M.B. Holl, Wide varieties of cationic nanoparticles induce defects in supported lipid bilayers., *Nano Lett.* 8 (2008) 420–4. doi:10.1021/nl0722929.
- [6] S. Hong, J. A. Hessler, M.M. Banaszak Holl, P. Leroueil, A. Mecke, B.G. Orr, Physical interactions of nanoparticles with biological membranes: The observation of nanoscale hole formation, *J. Chem. Heal. Saf.* 13 (2006) 16–20. doi:10.1016/j.chs.2005.09.004.
- [7] J.Q. Lin, Y.G. Zheng, H. W. Zhang, Z. Chen, A simulation study on nanoscale holes generated by gold nanoparticles on negative lipid bilayers., *Langmuir.* 27 (2011) 8323–32. doi:10.1021/la201086u.
- [8] R.C. Van Lehn, A. Alexander-Katz, Penetration of lipid bilayers by nanoparticles with environmentally-responsive surfaces: simulations and theory, *Soft Matter.* 7 (2011) 11392. doi:10.1039/c1sm06405c.
- [9] R. Qiao, A.P. Roberts, A.S. Mount, S.J. Klaine, P.C. Ke, Translocation of C60 and its derivatives across a lipid bilayer., *Nano Lett.* 7 (2007) 614–9. doi:10.1021/nl062515f.
- [10] S. Nangia, R. Sureshkumar, Effects of Nanoparticle Charge and Shape Anisotropy on Translocation through Cell Membranes, (2012) 17666-71.
- [11] L. Livadaru, A. Kovalenko, Fundamental mechanism of translocation across liquidlike membranes: toward control over nanoparticle behavior., *Nano Lett.* 6 (2006) 78–83. doi:10.1021/nl052073s.
- [12] K. Yang, Y.Q. Ma, Computer simulation of the translocation of nanoparticles with different shapes across a lipid bilayer., *Nat. Nanotechnol.* 5 (2010) 579–83.

- doi:10.1038/nano.2010.141.
- [13] J. Lin, H. Zhang, Z. Chen, Y. Zheng, Penetration of Lipid Membranes by Gold Nanoparticles : Insights into Cellular, 4 (2010) 5421–5429.
- [14] Y. Roiter, M. Ornatska, A.R. Rammohan, J. Balakrishnan, D.R. Heine, S. Minko, Interaction of nanoparticles with lipid membrane., Nano Lett. 8 (2008) 941–4. doi:10.1021/nl080080l.
- [15] A. Verma, F. Stellacci, Effect of surface properties on nanoparticle-cell interactions., Small. 6 (2010) 12–21. doi:10.1002/sml.200901158.
- [16] A.E. Nel, L. Mädler, D. Velegol, T. Xia, E.M. V Hoek, P. Somasundaran, F. Klaessig, V. Castranova, M. Thompson, Understanding biophysicochemical interactions at the nano-bio interface., Nat. Mater. 8 (2009) 543–57. doi:10.1038/nmat2442.
- [17] Z. Wang, L. Zhang, J. Zhao, B. Xing, Environmental processes and toxicity of metallic nanoparticles in aquatic systems as affected by natural organic matter, Environ. Sci. Nano. 3 (2016) 240–255. doi:10.1039/C5EN00230C.
- [18] R. Grillo, A.H. Rosa, L.F. Fraceto, Engineered nanoparticles and organic matter: A review of the state-of-the-art., Chemosphere. 119C (2014) 608–619. doi:10.1016/j.chemosphere.2014.07.049.
- [19] F. Seitz, R.R. Rosenfeldt, K. Storm, G. Metreveli, G.E. Schaumann, R. Schulz, M. Bundschuh, Ecotoxicology and Environmental Safety Effects of silver nanoparticle properties , media pH and dissolved organic matter on toxicity to *Daphnia magna*, Ecotoxicol. Environ. Saf. 111 (2015) 263–270. doi:10.1016/j.ecoenv.2014.09.031.
- [20] D. Cupi, N. B.Hartmann, A. Baun, The influence of natural organic matter and aging on suspension stability in guideline toxicity testing of silver , zinc oxide , and titanium

- dioxide nanoparticles with daphnia magna, *Environmental Tech. and Chem.* 34 (2015) 497–506. doi:10.1002/etc.2855.
- [21] A. Mecke, S. Uppuluri, T.M. Sassanella, D. K. Lee, A. Ramamoorthy, J.R. Baker, B.G. Orr, M.M. Banaszak Holl, Direct observation of lipid bilayer disruption by poly(amidoamine) dendrimers., *Chem. Phys. Lipids.* 132 (2004) 3–14. doi:10.1016/j.chemphyslip.2004.09.001.
- [22] T.A. Spurlin, A. Gewirth, Poly-L-lysine-induced morphology changes in mixed anionic/zwitterionic and neat zwitterionic-supported phospholipid bilayers., *Biophys. J.* 91 (2006) 2919–27. doi:10.1529/biophysj.106.082479.
- [23] S. Hong, P.R. Leroueil, E.K. Janus, J.L. Peters, M. M. Kober, M.T. Islam, B.G. Orr, J.R. Baker, M.M. Banaszak Holl, Interaction of polycationic polymers with supported lipid bilayers and cells: nanoscale hole formation and enhanced membrane permeability., *Bioconjug. Chem.* 17 (2006) 728–34. doi:10.1021/bc060077y.
- [24] A. Mecke, D. K. Lee, A. Ramamoorthy, B.G. Orr, M.M. Banaszak Holl, Membrane thinning due to antimicrobial peptide binding: an atomic force microscopy study of MSI-78 in lipid bilayers., *Biophys. J.* 89 (2005) 4043–50. doi:10.1529/biophysj.105.062596.
- [25] A. Mecke, I.J. Majoros, A.K. Patri, J.R. Baker, M.M.B. Holl, B.G. Orr, Lipid bilayer disruption by polycationic polymers: the roles of size and chemical functional group., *Langmuir.* 21 (2005) 10348–54. doi:10.1021/la050629l.
- [26] C.M. Bailey, E. Kamaloo, K.L. Waterman, K.F. Wang, R. Nagarajan, T.A. Camesano, Size dependence of gold nanoparticle interactions with a supported lipid bilayer: A QCM-D study., *Biophys. Chem.* 203–204 (2015) 51–61. doi:10.1016/j.bpc.2015.05.006.
- [27] Y. Barenholz, D. Gibbes, B.J. Litman, J. Goll, T.E. Thompson, R.D. Carlson, A simple

- method for the preparation of homogeneous phospholipid vesicles., *Biochemistry*. 16 (1977) 2806–10.
- [28] C. A. Keller, K. Glasmästar, V.P. Zhdanov, B. Kasemo, Formation of supported membranes from vesicles., *Phys. Rev. Lett.* 84 (2000) 5443–6.
- [29] T.S. Cdoj, S. Mitsuhiro, Y.J. Tatsuaki, Molecular Weight Characterization of Humic Substances by MALDI-TOF-MS, 52 (2004) 29–32.
- [30] R. C. Averett, J. A. Leenheer, D. M. Mcknight, and K. A. Thornu. Humic Substances in the Suwannee River, Georgia: Interactions, Properties, and Proposed Structures., United States Geological Survey Water-Supply Paper 2373 (1994).
- [31] P.S. Cremer, S.G. Boxer, Formation and spreading of lipid bilayers on planar glass supports, 291 (1999) 2554–2559.
- [32] R.P. Richter, A.R. Brisson, Following the Formation of Supported Lipid Bilayers on Mica : A Study, 88 (2005) 3422–3433. doi:10.1529/biophys.
- [33] G. Sauerbrey, Verwendung von Schwingquarzen zur Wagungdiinner Schichten und zur Mikrowagung, *Zeitschrift Fur Phys.* 155 (1959) 206–222. doi:10.1007/BF01337937.
- [34] M.C. Dixon, Quartz crystal microbalance with dissipation monitoring : enabling real-time characterization of biological materials and their interactions, *Journal of Biomolecular Techniques* 19 (2008) 151–158.
- [35] O. Furman, S. Usenko, B.L.T. Lau, Relative importance of the humic and fulvic fractions of natural organic matter in the aggregation and deposition of silver nanoparticles., *Environ. Sci. Technol.* 47 (2013) 1349–56. doi:10.1021/es303275g.
- [36] B.D. Vogt, E.K. Lin, W. Wu, C.C. White, Effect of film thickness on the validity of the Sauerbrey equation for hydrated polyelectrolyte films, *J. Phys. Chem. B* (2004) 12685–

12690.

- [37] N.J. Cho, C.W. Frank, B. Kasemo, F. Höök, Quartz crystal microbalance with dissipation monitoring of supported lipid bilayers on various substrates., *Nat. Protoc.* 5 (2010) 1096–106. doi:10.1038/nprot.2010.65.
- [38] Y. Zhang, Y. Chen, P. Westerhoff, J. Crittenden, Impact of natural organic matter and divalent cations on the stability of aqueous nanoparticles., *Water Res.* 43 (2009) 4249–57. doi:10.1016/j.watres.2009.06.005.
- [39] D.P. Stankus, S.E. Lohse, J.E. Hutchison, J. a Nason, Interactions between natural organic matter and gold nanoparticles stabilized with different organic capping agents., *Environ. Sci. Technol.* 45 (2011) 3238–44. doi:10.1021/es102603p.
- [40] J. Liu, S. Legros, F. von der Kammer, T. Hofmann, Natural organic matter concentration and hydrochemistry influence aggregation kinetics of functionalized engineered nanoparticles., *Environ. Sci. Technol.* 47 (2013) 4113–20. doi:10.1021/es302447g.
- [41] Z. Li, K. Greden, P.J.J. Alvarez, K.B. Gregory, G. V Lowry, Adsorbed polymer and NOM limits adhesion and toxicity of nano scale zerovalent iron to *E. coli.*, *Environ. Sci. Technol.* 44 (2010) 3462–7. doi:10.1021/es9031198.
- [42] J. Gao, K. Powers, Y. Wang, H. Zhou, S.M. Roberts, B.M. Moudgil, B. Koopman, D.S. Barber, Influence of Suwannee River humic acid on particle properties and toxicity of silver nanoparticles., *Chemosphere.* 89 (2012) 96–101. doi:10.1016/j.chemosphere.2012.04.024.
- [43] S.M. Louie, R.D. Tilton, G. V. Lowry, Critical review: impacts of macromolecular coatings on critical physicochemical processes controlling environmental fate of nanomaterials, *Environ. Sci. Nano.* 3 (2016) 283–310. doi:10.1039/C5EN00104H.

- [44] J. Liu, S. Legros, G. Ma, J.G.C. Veinot, F. von der Kammer, T. Hofmann, Influence of surface functionalization and particle size on the aggregation kinetics of engineered nanoparticles., *Chemosphere*. 87 (2012) 918–24. doi:10.1016/j.chemosphere.2012.01.045.
- [45] J.A. Nason, S. A. McDowell, T.W. Callahan, Effects of natural organic matter type and concentration on the aggregation of citrate-stabilized gold nanoparticles., *J. Environ. Monit.* 14 (2012) 1885–92. doi:10.1039/c2em00005a.
- [46] L.M. Ojwang', R.L. Cook, Environmental conditions that influence the ability of humic acids to induce permeability in model biomembranes, *Environ. Sci. Technol.* 47 (2013) 8280–8287. doi:10.1021/es4004922.
- [47] N.M. Elayan, W.D. Treleaven, R.L. Cook, Monitoring the effect of three humic acids on a model membrane system using ³¹P NMR, *Environ. Sci. Technol.* 42 (2008) 1531–1536. doi:10.1021/es7024142.
- [48] P.G.C. Campbell, M.R. Twiss, K.J. Wilkinson, Accumulation of natural organic matter on the surfaces of living cells: implication of toxic solutes with aquatic biota., *Can. J. Fish. Aquat. Sci.* 54 (1997) 2543–2554.
- [49] J. Buffle, K.J. Wilkinson, S. Stoll, M. Filella, J. Zhang, A generalized description of aquatic colloidal interactions: The three- colloidal component approach, *Environ. Sci. Technol.* 32 (1998) 2887–2899. doi:10.1021/es980217h.
- [50] G.D. Bothun, Hydrophobic silver nanoparticles trapped in lipid bilayers: Size distribution, bilayer phase behavior, and optical properties., *J. Nanobiotechnology.* 6 (2008) 13. doi:10.1186/1477-3155-6-13.
- [51] S.H. Park, S. G. Oh, J. Y. Mun, S. S. Han, Loading of gold nanoparticles inside the DPPC bilayers of liposome and their effects on membrane fluidities., *Colloids Surf. B.*

Biointerfaces. 48 (2006) 112–8. doi:10.1016/j.colsurfb.2006.01.006.

- [52] Y. Li, X. Chen, N. Gu, Computational investigation of interaction between nanoparticles and membranes: hydrophobic/hydrophilic effect., J. Phys. Chem. B. 112 (2008) 16647–53. doi:10.1021/jp8051906.

Chapter 4

Formation of raft-containing supported lipid bilayers:

A qualitative study by quartz crystal microbalance

4.1 Abstract

Supported lipid bilayers (SLBs) are important platforms to study the biophysical properties of lipid membranes and protein-lipid interactions. Cellular lipid membranes are lateral heterogeneous structures including highly liquid-ordered domains enriched with cholesterol and sphingomyelin referred as “lipid rafts”. Since these membrane microdomains are responsible for a variety of biological functions such as association of some membrane proteins and cellular signaling, formation of lipid bilayers containing lipid rafts is important for *in vitro* studies of cell biology. However, the presence of lipid raft components such as sphingomyelin and cholesterol makes the formation of the bilayer more challenging which leads to adsorption of intact vesicles on the substrate without formation of the bilayer. Quartz crystal microbalance (QCM-D) provides real-time data on the formation of SLBs. In this study, the formation of lipid bilayer composed of 1,2-Dioleoyl-sn-glycero-3-phosphocholine (DOPC), 1,2-dioleoyl- sn-glycero-3-phospho-L-serine (DOPS), cholesterol (Chol), sphingomyelin (SM), and ganglioside (GM) was investigated using QCM-D. A challenge was that the raft-containing vesicles remained intact on the SiO₂ crystal. Therefore, different experimental conditions were tested to induce vesicle fusion, such as pH, temperature, osmotic pressure, and vesicle size. The key parameter in forming the bilayer was found to be applying osmotic pressure to the vesicles by having the vesicles exterior concentration of NaCl higher than interior concentration. When this concentration gradient was applied to the vesicles before flowing them on the substrate, vesicle rupture was favored and formation of a complete bilayer could occur. Here, we report the effects of each tested variable on the adsorption and fusion of the raft-containing vesicles, and the results are discussed based on the mechanisms of vesicle-vesicle and vesicle-substrate interactions.

4.2 Introduction

Supported lipid bilayers (SLBs) serve as pivotal models to mimic biological cell membranes as they provide several advantages such as simplicity, reproducibility and capability of being characterized by different experimental techniques [1]. Most of the SLBs that are commonly used to study biophysical properties of lipid membrane are composed of single or binary lipid systems while biological membranes typically contain hundreds of lipid components and proteins providing different functionalities to living cells [2]. Complex biological membranes are composed of lipids with different chain lengths and different saturation states that are organized in the form of microdomains, causing lateral heterogeneity in lipid bilayers [3]. Recent advances in characterization techniques, such as fluorescence recovery after photo bleaching, single-particle tracking and mass spectrometry imaging, have been capable of detecting lateral microdomains enriched with cholesterol and sphingolipids in lipid bilayers [4–7]. When sphingomyelin with long saturated hydrocarbon chain is combined with cholesterol they produce a special phase called liquid ordered (L_o). These so-called “lipid rafts” have less fluidity than the liquid disordered phase (L_d) composed of glycerophospholipids with unsaturated hydrocarbon chains [3]. In general, the lipid rafts are thicker than the bulk membrane and they provide a biological platform for placement of certain lipid-anchored proteins with functionality of signaling and trafficking [3]. Due to the profound biological implications, the attempt to form more complex lipid bilayers containing lipid rafts is increasingly appreciated as a means to better understand membrane structural biology.

The most common method for formation of SLBs is vesicle fusion, which is a spontaneous self-assembly of bilayers from vesicles adsorbed on a surface. Due to its simplicity and reproducibility, vesicle fusion method is often preferred as it consists of adsorption of

vesicles on a surface followed by rupture and fusion of the vesicles to form an extended, uniform bilayer. When the lipid system is composed of one or two lipid components, vesicle fusion has been a successful approach to form a bilayer, as monitored by different techniques such as surface plasmon resonance, ellipsometry, and QCM-D [8–10]. However, formation of multi-component lipid bilayers with lipid rafts is potentially challenging as vesicle fusion does not always occur spontaneously. In this study we report our QCM-D data to address this challenge and provide a practical approach to form SLBs containing lipid-raft components (e.g. cholesterol, sphingomyelin and ganglioside).

In addition to zwitterionic (DOPC), negatively charged (DOPS) lipids, our lipid system contained 25 % cholesterol, 25 % sphingomyelin and a small fraction of ganglioside. Previous studies showed that the structure of vesicles containing more than 15 % of cholesterol and sphingomyelin is composed of both L_o and L_d domains [3,5,11]. Therefore our main challenge was that the vesicles containing raft domains did not spontaneously go through fusion to form a complete SLB. In order to understand the root cause of this challenge and overcome that, one can look at the vesicle fusion as the combination of two processes of vesicle adsorption on the substrate and vesicle rupture. Therefore, facilitating each of these processes leads to formation of complete SLB containing raft domains. Vesicle adsorption is influenced by vesicle-substrate and vesicle-vesicle interactions which can be manipulated by changing solution properties such as solvent composition, pH, ionic strength, etc. Vesicle rupture has been proven to be a response to release the high curvature energy of vesicles. Models for rupture of single vesicle introduced two factors influencing the pore formation in the vesicle which leads to vesicle rupture [12]. According to these models, two scenarios are considered for rupture. It occurs either near the rim of vesicle-substrate contact area where membrane bending is significant or rupture can happen at

any arbitrary point on the vesicle as a result of distributed tension over the whole vesicle membrane. Parameters such as vesicle size, osmotic stress and ionic concentration can influence the rupture since they directly affect the bending energy of the vesicles and the vesicle tension at the substrate-vesicle contact area. Previous studies on simple zwitterionic bilayers, have investigated the influence of different experimental conditions (e.g. PH, applying osmotic stress, solvent composition, vesicle size, and temperature) on vesicle fusion [13–21]. Here we used the same approach to optimize the experimental conditions to induce fusion in the vesicles that contain liquid ordered raft domains.

QCM-D is a powerful analytical tool to characterize the mass change (as a frequency shift) and viscoelastic properties (as a change in dissipation of energy) of a film. It has been previously used to study the details of vesicle to bilayer transition[15,16,20,21] , such as rate of vesicle binding and critical coverage of vesicles on the surface, as well as the interactions between different biomacromolecules and SLBs. A robust protocol for formation of zwitterionic SLBs on silicon oxide substrate has been already established and widely used to study vesicle fusion via QCM-D. In the process of following the previously published basic protocol to form bilayers containing lipid – raft components [22,23], we noticed that the protocol was very sensitive to small perturbations. The fusion of the vesicles containing lipid raft components (e.g. cholesterol, ganglioside and sphingomyelin) did not happen spontaneously, as the vesicles adsorbed on SiO₂ substrate but often remained unruptured or partially ruptured. In order to increase the robustness of the protocol, we modified the conventional QCM-D protocol by optimization of different experimental parameters. Among all of the tested parameters, applying the osmotic pressure on the vesicles before running them through QCM-D chamber was the

necessary change to the protocol. The final protocol was very robust which led to complete rupture of vesicles and formation of bilayer, reproducibly.

4.3 Methods and materials

4.3.1 Vesicle preparation

1,2-Dioleoyl-sn-glycero-3-phosphocholine (DOPC), 1,2-dioleoyl-sn-glycero-3-phospho-L-serine (DOPS), Sphingomyelin (SM; egg, chicken), Cholesterol (Chol; ovine wool), and monosialoganglioside (GM1; brain, ovine-ammonium salt) were purchased from Avanti Polar Lipids, Inc. (Alabaster, AL). According to the vendor, the transition temperatures of DOPS, DOPC were -11°C and -17 °C, respectively. Egg sphingomyelin was mostly 16:0 sphingomyelin with a small percentage of 18:0 and 22:0 sphingomyelin. The transition temperatures for SM 16:00, 18:00 and 22:00 were reported by the vendor to be 40.5 °C, 45 °C and below 47.5 °C, respectively.

DOPC, DOPS, SM, and Chol were dissolved in chloroform to a concentration of 10 mM, and GM1 was dissolved in methanol to a concentration of 0.63 mM. The lipids were mixed with the molar ratio of DOPC/DOPS/SM/Chol/GM1; 0.4/0.1/0.25/0.25/0.03. After evaporation of organic solvents under a stream of nitrogen, the dried film was kept in vacuum desiccator for at least 4 hours to remove any residual solvents. The film was hydrated in the buffer solution at 56 °C to yield a total lipid concentration of 0.3 mM. After five freeze-thaw cycles, the large multilamellar vesicles were formed. In order to reduce the size of vesicles extrusion or sonication or/and combination of the two techniques were applied as rotational and translational diffusion studies of the vesicles did not show any difference between the vesicles prepared by sonication

and the ones prepared by extrusion [24]. For extrusion, the lipid suspension was extruded 21 times through a polycarbonate filter (pore size, 50 nm) using a mini-extruder (Avanti Polar Lipids, Inc.) just before use. For sonication, an ultrasonic dismembrator (Model 150T, Thermo Fisher Scientific, Waltham, MA) was used in pulsed mode for 45 minutes at 56 °C. A 30% duty cycle was used for sonication (pulse on for 3 s, followed by a pause for 7 s) at an amplitude of 60. After sonication, the vesicle solution was centrifuged at 16000 rcf for 10 minutes remove the TiO₂ particles from the ultrasonic dismembrator probe (J2-MI Centrifuge, Beckman Coulter, Brea, CA). [25] The supernatant containing SUVs was collected and stored at 4°C under nitrogen and they were stable for two to three weeks. In order to determine the size of the vesicles, dynamic light scattering (DLS) were performed (Zetasizer Nano ZS, Malvern, Worcestershire, UK). The stock solution was diluted to the desired concentration before each QCM-D experiment.

4.3.2 Quartz crystal microbalance with dissipation monitoring (QCM-D)

QCM-D data was obtained by a Q-Sense E4 series (Q-Sense AB, Sweden) instrument with silicon dioxide – coated crystals (5 Hz) purchased from Biolin Scientific (Gothenburg, Sweden). In the cleaning step, the crystals were rinsed with sequential flows of ethanol, de-ionized water, and 2% sodium dodecyl sulfate and de-ionized water each for 5 minutes. After that, crystals were thoroughly dried with nitrogen gas and etched with two cycles of 45 s oxygen plasma cleaning using Plasma Prep II (SPI Supplies, West Chester, PA). The experimental procedure began with setting a baseline in buffer. To form a stable SLB on a crystal, the lipid solution is injected into the QCM-D chamber at 0.15 mL/min to allow vesicles to attach to the silica-coated crystal surface. After the vesicles ruptured to form a stable bilayer, the crystal was

rinsed with buffer to remove unattached particles [9,25–27]. In order to have two different buffers across vesicle membrane, the vesicles first made in the desired interior buffer with the concentration of 0.3 mM and they were diluted with the secondary buffer to obtain the desired exterior buffer with vesicle concentration of 0.1 mM. In these cases, the vesicles were diluted in the secondary buffer just before the QCM-D lipid flow to keep the osmotic stress exposure time consistent.

4.3.3 Statistical analysis and mathematical modeling

All the experiments were performed in at least triplicates (except for the cases that are specified in the text to have been done in duplicates). Quantitative data are reported as mean \pm standard deviation and statistical significance was calculated based on one-way analysis of variance (ANOVA; $\alpha = 0.05$ and $p < 0.05$ was considered statistically significant). Qsense Dfind analysis software was used to determine the mass and thickness of the adsorbed layer using F and D values of different overtones.

4.4 Results and discussion

4.4.1 Vesicle containing cholesterol, sphingomyelin, and ganglioside remained unruptured on the surface.

QCM-D data indicated that kinetics of vesicle adsorption for the binary lipid system of DOPS/DOPC (1:4) was different from multi-component lipid system containing raft component. The data confirmed that when the common protocol for formation of zwitterionic bilayers was applied for the complex lipid system; the lipid-raft containing vesicles did not rupture to form the

bilayer. QCM-D characterizes the self-assembly of supported lipid bilayers by detecting the mass and structural changes of the surface. QCM-D data for the binary system of DOPS/DOPS (1:4 molar ratio) is shown as the representative of complete bilayer formation (Fig 1. A), which was what we ideally expected to observe as the proof of complete rupture of vesicles. Typically, formation of a continuous, defect-free bilayer composed of single zwitterionic lipid is characterized by the final Δf and ΔD values of -25 Hz and 0.2×10^6 , respectively [28]. Briefly, vesicles adsorb on the surface without rupturing until reaching a critical coverage (θ^*), and then the vesicles start to rupture to form a complete supported bilayer. Decrease in frequency indicates the adsorption of vesicles on the substrate. Increase in frequency corresponds to rupture of vesicles causing release of the trapped buffer inside the vesicles. In this process, the minimum in frequency (maximum in dissipation) is when the rate of mass loss due to release of water exceeds the rate of mass addition due to continuing vesicle adsorption. Another approach to check the formation of complete bilayer is to plot ΔD versus Δf values (so-called “D/f plot”). D/f plot is used as a QCM-D fingerprint of a kinetic pathway. A typical D/f plot of bilayer formation is shown in Fig. 1 B.

QCM-D data showed that when there were lipid-raft components (chol, GM1 and SM) in the lipid system, different types of adsorption behaviors were observed (Fig 1. C, D, and E). The absolute final values for Δf and ΔD were higher than -25 Hz and 0.2×10^6 , respectively, confirming that either all of the intact vesicles or part of them adhere to the surface and remained unruptured. In addition to the high final f and D values, the existence of soft, water-containing and dissipative vesicles is proved by spreading of f and D values for different overtones. From our experiment, three main pathways of vesicle deposition were observed for incomplete rupture of vesicles. In one scenario, as shown in Fig. 1 C, the f and D values changed monotonically

indicating the adsorption of vesicles to the surface until reaching surface saturation from which, the F and D values remained stable. In this case, no vesicle rupture was observed whereas in Fig. 1 D, some portion of vesicles ruptured after reaching a critical coverage. This case has a similar trend as the typical signal for formation of bilayer, except that the magnitude of final values for F and D are higher than the expected values of complete rigid bilayer. The third kinetic pathway which also corresponds to unruptured vesicles is shown in Fig. 1 E. where D increased and F decreased to reach the peaks as we would expect for the critical coverage however after a very small increase in frequency, the F signal stabilized indicating that the vesicles remained intact on the surface (Fig. 1 part b) The frequency increase indicates the release of the trapped buffer from some of the vesicles. Since not all of the vesicles ruptured to form a rigid bilayer, the released buffer from ruptured vesicles remained in between the unruptured vesicles leading to formation of more dissipative hydrated film or possibly the restructuring of the lipids within the film. The increase of dissipation as the result of lipid restructuring has been previously reported for DOPC/DOPS (molar ratio of 1:1) bilayer on SiO₂ surface where the formed bilayer was rinsed with Mg²⁺ solution in the absence of vesicles. Because the signal change was not induced by adsorption of vesicles, it was concluded that restructuring happened by association of water at the active bilayer edges [8].

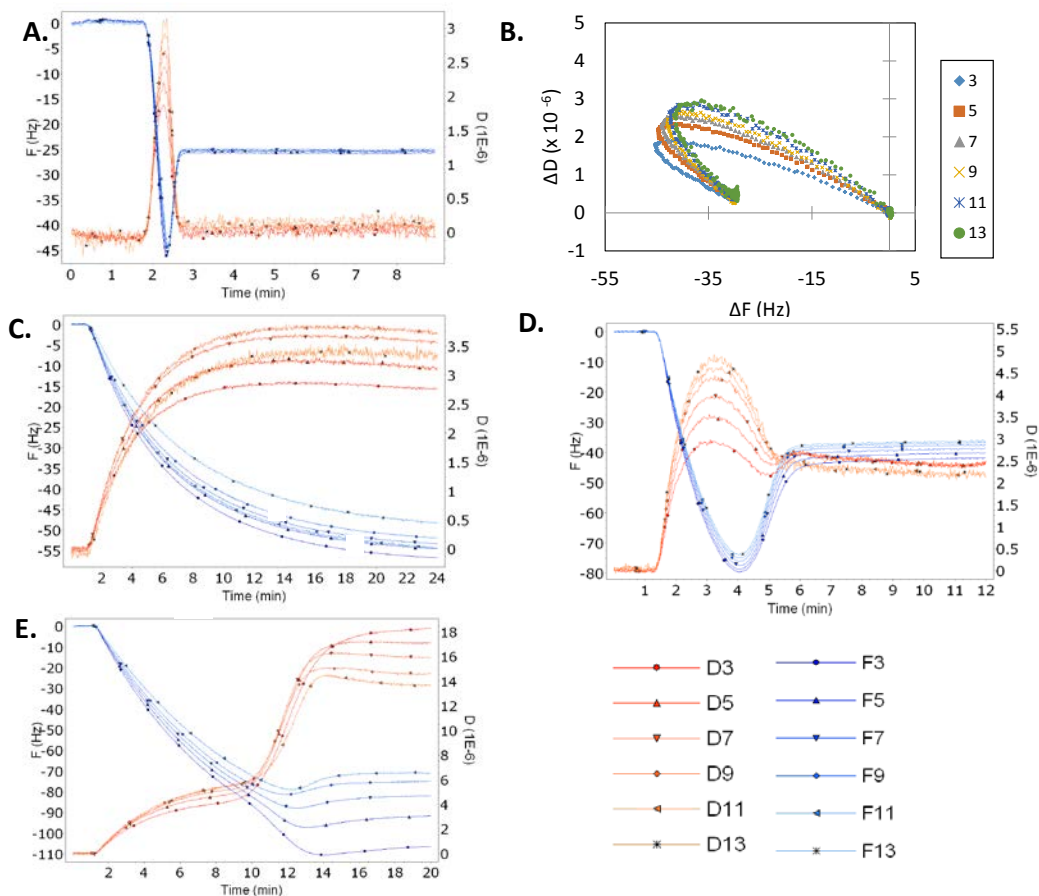


Figure 1. Representative plots showing QCM-D frequency and dissipation changes as a function of time. The blue lines represent frequency changes, and the red lines represent dissipation. (A) A typical QCM-D plot of complete bilayer formation starting from adsorption of DOPC/DOPS (with molar ratio of 1:4) vesicles on the crystal followed by complete rupture of the vesicles. (B) D/F plot as the fingerprint of DOPC/DOPS (with molar ratio of 1:4) bilayer formation (C) QCM-D plot of an unsuccessful lipid formation. Lipid raft-containing vesicles adsorbed on the surface and remained unruptured. (D) A representative QCM-D plot for an unsuccessful lipid formation with partial rupture of lipid raft-containing vesicles. Vesicle adsorbed on the surface and after reaching a critical surface coverage, most of the vesicles ruptured, but the final film contained some unruptured vesicles. (E) A representative QCM-D plot for an unsuccessful lipid formation with partial rupture of lipid raft-containing vesicles. Vesicle adsorbed on the surface and after reaching a critical surface coverage, few vesicles ruptured, but the released interior buffer remained trapped between the unruptured vesicles leading to increase of dissipation and restructuring of lipid film.

4.4.2 Effect of experimental parameters on vesicle fusion

Effect of experimental conditions on the process of vesicle fusion can be understood from the energy perspective where a combination of different favorable and unfavorable terms is influencing the process. SLB formation takes place as the result of two processes; vesicle adsorption and vesicle rupture. Vesicle fusion can potentially happen in a bulk solution and as the result of contact between floating vesicles; however, adsorption of vesicle to the surface can lead to the release of adhesion energy in favor of the fusion process. Vesicle adsorption on the other hand is hindered by any repulsive interactions between neighboring vesicles or between the vesicles and the substrate. Therefore adjusting the experimental conditions (such as solution chemistry, ionic strength and pH) can promote the vesicle adsorption and consequently the vesicle fusion [20,21]. The second process in SLB formation is vesicle rupture which leads to release of the tension on the vesicles (bending energy). Therefore, increasing the vesicle curvature and deformation promotes the rupture and the vesicle fusion. Vesicle size and osmotic stress are two of the experimental conditions that influence the level of vesicle deformation and consequently the vesicle fusion [14–19]

. Previously, different adsorption behaviors were reported by Reimhult et. al when different substrates were used to understand the effect of surface chemistry on Egg PC vesicle adsorption [29]. On Si_3N_4 and SiO_2 surfaces, the adsorption behavior was similar for what we observed for raft-free vesicles (Fig. 1, A), while adsorption of vesicles on TiO_2 and oxidized Pt surfaces followed the same pathway as we observed for the non-ruptured vesicles on the surface (Fig. 1, B) [29]. In addition to the surface chemistry, other experimental conditions, such as

temperature and vesicle size have been previously reported to influence the adsorption kinetics. In the following sections, we discuss our results on the effect of each parameter, in detail.

4.4.3 Effect of vesicle size

Since vesicle size can affect both the bending energy of the vesicles and the level of deformation after vesicle adsorption, we examined the size of the vesicle as a rupture-inducing parameter. Our QCM-D data indicated that decreasing the size of the vesicle did not lead to complete rupture of vesicles and formation of SLB. The result for vesicle sizes of 80 and 110 nm are compared with each other in Fig. 2. Our QCM-D data indicate that the adsorption kinetics is the same for the vesicles with different sizes. This is consistent with a previous study on fusion of PC vesicles on SiO₂, SiN₄, Au, Pt and TiO₂ substrates where variation of vesicle size did not change the qualitative behavior of vesicle adsorption [15]. The data (Fig. 2) indicates that the final values of F and D are larger than of what we expect for a complete bilayer. In addition, the signals for different overtones are spread out indicating that the final adsorbed film is soft and dissipative. In order to compare the adsorption kinetics of the different size vesicles, the D/F plots are compared (Fig 2. C and D) with the QCM-D fingerprint of bilayer formation (Fig. 1 B). The D/F plots show that the adsorption kinetic for both sized are qualitatively similar indicating the occurrence of a two-step process. The first process, in which the adsorption of intact vesicles is the dominant process, is similar to the first step in the bilayer formation fingerprint (Fig. 1 B). However, the second step is different from the bilayer formation fingerprint as it shows an increase of the softness of the layer. This can be indicative of a partial rupture of the vesicles which leads to the hydration and restructuring of the lipid film. For both cases, the adsorption duration was about 10 minutes; however, the absolute values of F and D at the critical coverage

are lower for smaller vesicles. The change of F and D in the first adsorption process is more significant for larger vesicles indicating adsorption of more mass on the crystal.

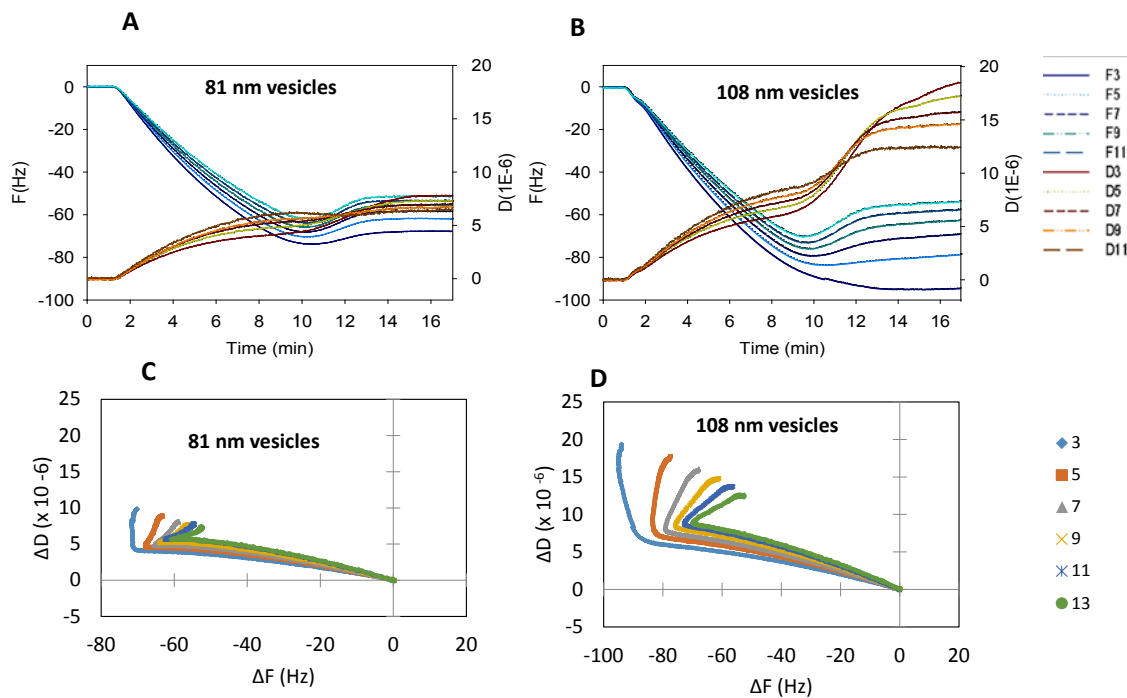


Figure 2. Effect of vesicle size on the rupture of vesicles. The experiment were performed in triplicates at 23 °C , with buffer of 10 mM Tris+ 150 mM NaCl + 2 mM CaCl₂ (pH of 7.40) and lipid concentration of 0.1 mM.

As mentioned before, the data confirms that the lipid film is soft and dissipative. In the case of soft film, the F and D values are overtone-dependent which means the Sauerbrey would not be applicable to for estimation of mass and thickness. In order to better understand vesicle adsorption on the QCM-D crystal, we used viscoelastic Voigt model to fit the ΔF and ΔD output and calculate the thickness of the bilayer.

According to the Voigt model, the frequency and dissipation of energy are related to the properties of the viscoelastic film submerged in a Newtonian liquid by

$$\Delta f = -\frac{1}{n} \frac{\eta_L}{2\pi\delta_L m_q} - f_o \frac{m_f}{m_q} \left[1 - \frac{2}{\rho_f} \left(\frac{\eta_L}{\delta_L} \right)^2 \frac{G''}{G'^2 + G''^2} \right], \quad (1)$$

$$\Delta D = \frac{\eta_L}{n\pi f_o \delta_L m_q} + \frac{m_f}{m_q} \left[\frac{4}{\rho_f} \left(\frac{\eta_L}{\delta_L} \right)^2 \frac{G'}{G'^2 + G''^2} \right]$$

where η_L is the viscosity of the liquid medium and δ_L is the decay length of the acoustic wave in the liquid medium, ρ_f is the density of the film on the crystal and G'' and G' are the loss modulus and the storage modulus connected to the dissipation, $D = G''/(2\pi G')$.

By assuming the film density to be 1000 kg m^{-3} and the viscosity of the bulk solution to be 0.001 Ps s^{-1} [30], the thickness of the adsorbed layer for vesicles of 80 nm and 110 nm were $17 \pm 1 \text{ nm}$ and $25 \pm 0.1 \text{ nm}$, respectively. These results show the possibility of monolayer or multilayer of unruptured vesicles on the surface. In addition, since the thickness of the film is much smaller than the diameter of the vesicles, it confirms that vesicles are deformed as the result of adsorption. It has been previously proposed in other literature that vesicles on the surface possess a pancake-like shape [18,31] which is schematically shown in Fig. 3. In order to check the quality of the fit, we checked the overlap of curve and the measured data (Fig. 4).

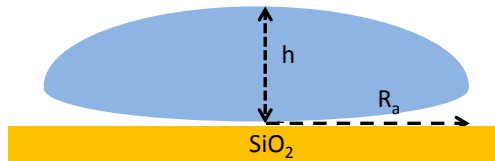


Figure 3. Adsorbed vesicle with a pancake-like shape

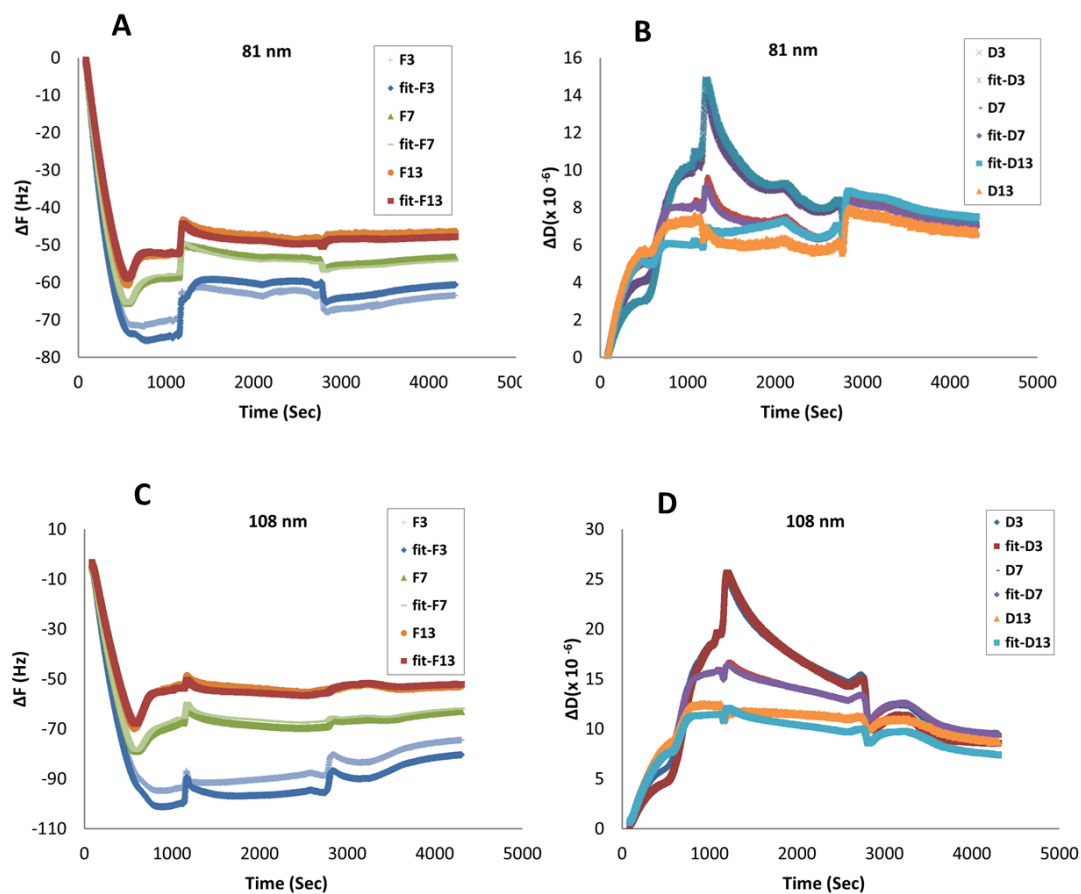


Figure 4. Comparing the measured values of ΔF and ΔD with the fitted values obtained from Voigt model for 3rd, 7th and 13th overtones. (A) and (B) ΔF and ΔD vesicles with diameter of 81 nm, (C) and (D) ΔF and ΔD vesicles with the diameter of 108 nm. The data was obtained from the experiment were performed in triplicates at 23 °C , with buffer of 10 mM Tris+ 150 mM NaCl + 2 mM CaCl₂ (pH of 7.40) and lipid concentration of 0.1 mM. A and B

Effects of vesicle size on vesicle fusion has been studied previously and the effect of vesicle size on the rupture has been discussed [29,32]. Reducing the size of vesicle can affect the vesicle rupture in two opposite ways. As mentioned before, vesicle rupture can happens as a

response to high membrane bending energy. Therefore, using smaller vesicles with higher curvature energy increases the vesicle membrane tension and promotes rupture of adsorbed vesicles to release the bending energy. On the other hand, adsorption of vesicle on a substrate leads to vesicle deformation which is critical in vesicle rupture [12] as it is shown that greater deformation leads to more favorable rupture. It has been previously reported that vesicle with larger size deforms to greater extent [18] which means reducing the size of the vesicles can lead to less rupture. However, we showed that changing the vesicle size from 81 nm to 108 nm did not change the amount of vesicle rupture, significantly. Therefore, more optimization of experimental conditions was required to induce the rupture.

4.4.4 Effect of Temperature Change

Since the multicomponent vesicles contained SM with transition temperature of greater than 40°C, we expected to see a different kinetic pathway by increasing the temperature and making the vesicles more fluidic. The data confirmed that the kinetic pathway was temperature-dependent, but increasing the temperature of QCM-D experiment from 23 °C to 50 °C did not lead to complete rupture of vesicles (Fig 5). For all of the temperatures, the absolute final values of final D and F are higher than what we expect for a complete bilayer indicating the existence of non-ruptured vesicles in the film. At 23°C the vesicles adsorbed on the surface to reach a critical coverage from where only few vesicles ruptured as there was no significant increase in frequency. The further increase in dissipation corresponds to restructuration of the lipid structure. Increasing the temperature to 35 °C led to more rupture of vesicles as the frequency increased more significantly after reaching the critical coverage. However, the rupture of vesicles did not form a more rigid lipid structure. The increase of dissipation after the critical coverage indicated

the hydration and restructuration of the film. When the temperature increased to 50 °C, more rupture took place and the kinetic pathway was more similar to the bilayer formation since after reaching the critical coverage, the dissipation decreased aligned with formation of more rigid lipid bilayer. The final D value of 2.5×10^6 indicated the presence of some unruptured vesicles in the bilayer structure.

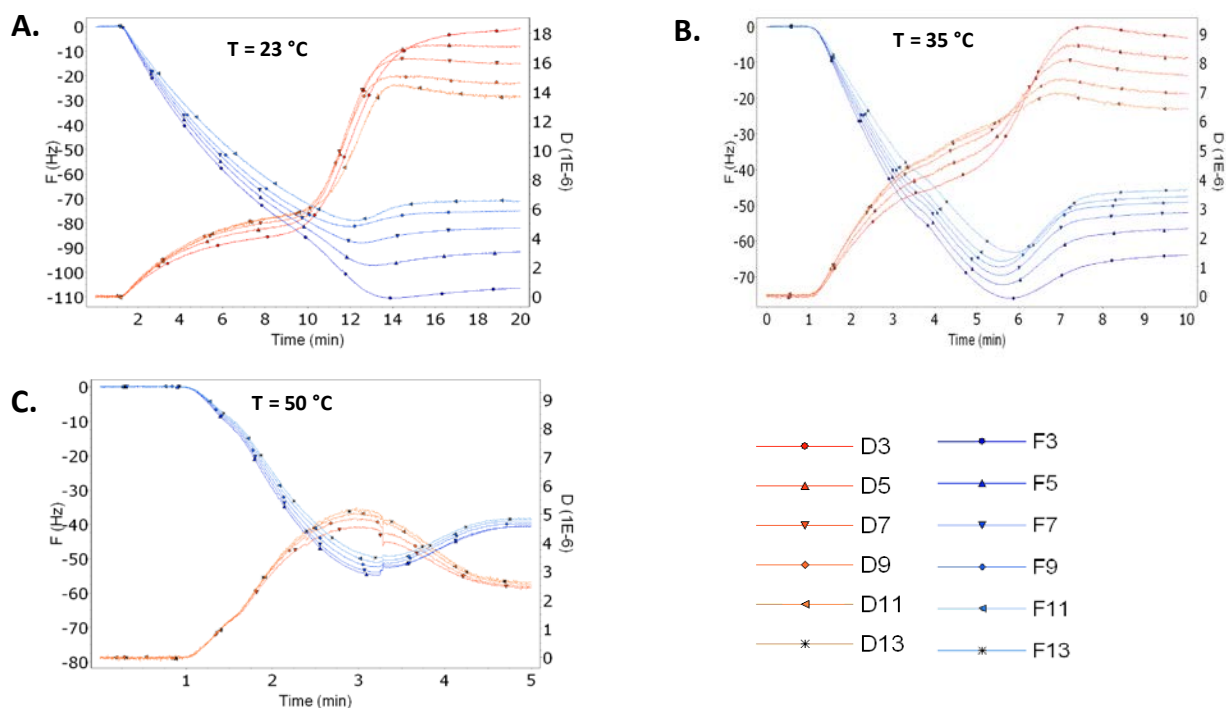


Figure 5. Effect of temperature increase on vesicle rupture. All reported cases were performed with buffer of 10 mM Tris+ 150 mM NaCl + 2 mM CaCl_2 with pH of 7.40 and lipid concentration of 0.1 mM. Vesicle size was determined as 114 nm. Experiments were performed in duplicates.

In the literature it has been shown that vesicle spreading and fusion is temperature dependent as increasing the temperature leads to greater vesicle – vesicle interactions which is in favor of vesicle fusion [20]. SLB formation has been generally observed at temperatures above

the transition temperature (T_m) of the lipid species and a recommended strategy to form a SLB is to perform the experiment at approximately 15 °C above the highest T_m of the lipid components [33]. However, raising the temperature up to 60 °C (data not shown) did not lead to the complete rupture of vesicles indicating the temperature is not the dominant effective parameter in the rupture. This was previously reported in a study on adsorption kinetics of DPPC vesicles on SiO₂ [34]. In that study, performing QCM-D experiment at the temperature above DPPC transition temperature did not always led to vesicle rupture. The small DPPC vesicles of 90 nm diameter formed a complete SLB at the temperatures about T_m , but larger vesicles with the diameter of 160 nm did not rupture at the same condition. It was concluded that other parameters such as vesicle size and vesicle surface coverage are important factors in formation of SLB [34].

In addition, our data showed that the peak values of F and D decreased by increasing the temperature, which means there was a less vesicle coverage on the surface. The dependence of vesicle coverage on temperature was previously observed in a QCM-D study of DPPC liposome on SiO₂ surface [34]. Increase in temperature leads to higher vesicle-vesicle interactions and as the result, a lower critical coverage of adhered vesicles is required for vesicle fusion. Our data also indicates that increasing the temperature decreased the time of the critical coverage from about 11 minutes (Fig. 5 A) to 3 minutes (Fig. 5 C). It has been previously observed in the literature and the it was qualitatively explained that increasing the temperature makes the lipid structure more fluidic and leads to faster transformation of vesicles to a SLB [15]. Here, we explain these results according to diffusivity of the vesicles since until reaching the critical coverage, the adsorption of vesicles to the support takes place through diffusion of the vesicles [31,35]. Based on the Stokes-Einstein equation for a sphere, diffusivity is defined,

$$D = \frac{k_B T}{6\pi\eta R_s} \quad (2)$$

Where k_B is the Boltzmann constant, T is the temperature, η is the viscosity, and R_s is the vesicle radius in the bulk solution. From Equation (1) one can see that the diffusivity which is unit of cm^2/s is temperature dependent and it increases by raising the temperature which means at higher temperature the adsorption duration is shorter.

4.4.5 Effect of buffer composition and osmotic pressure

The final modification that successfully led to formation of complete bilayer formation was performed by preparing the vesicles in 20 mM phosphate buffer (pH 7) with the concentration of 0.3 mM and then diluted to obtain the exterior buffer of 20 mM phosphate (pH 7) and 100 mM NaCl. This modification was promising, as it led to formation of complete bilayer in every replicate (tested more than 20 times). As QCM-D plot indicates (Fig. 6), the final F and D values were -30.0 ± 0.1 Hz and $0.50 \pm 0.01 \times 10^{-6}$, respectively, slightly higher than what we obtained for bilayer of DOPC/DOPC (4:1). These values are comparable with previously reported F and D values of -27.8 Hz and 0.43×10^{-6} for bilayer of DOPC/chol/SM (0.5: 0.25: 0.25) where Melby et al. reported the final values increased by adding more chol and SM to the lipid content [3]. In addition, the F and D signal of different overtones overlapped which indicates the formation of rigid bilayer. Therefore, Sauerbrey equation can be applied to calculate the mass and thickness of the film.

$$\Delta m = -C\Delta F \quad (3)$$

Here, $C = 17.8 \text{ ng cm}^{-2} \text{ Hz}^{-1}$ is the Sauerbrey mass sensitivity constant of the crystal at its fundamental frequency (5 Hz). From Eq. 15 we calculated the mass of the film

to be 534 ng. This includes the mass of lipid bilayer and the hydration layer between the substrate and the bilayer. The mass and thickness of the hydration layer have previously reported to be 102 ng/cm² and ~1 nm, respectively [31,36]. By assuming the density of film to be 1 g/cm³ [18], the thickness of the bilayer is calculated as 4.5 nm. Our estimate is close the previous reports for SLBs of DOPC/DOPS (1:4) (~4.1 nm thickness[8,37], Egg PC (4.5 nm) [31]. In addition, An et al. used AFM to study the SLB composed of DOPC/DOPS/chol/SM (1:1:2:2 molar ratio) on mica and showed that the thickness of lipid raft domain and liquid-disordered domain were ~4.8 nm and ~5.4 nm, respectively [37].

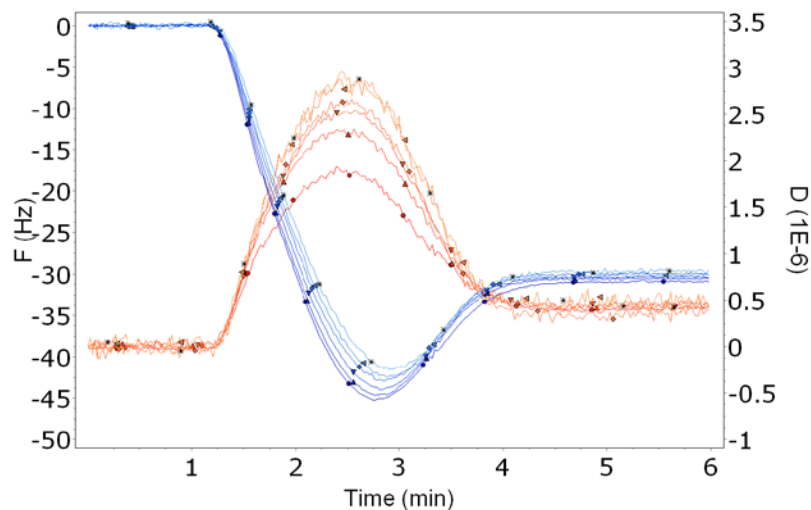


Figure 6. Formation of bilayer composed of DOPC/DOPS/SM/Chol/SM (0.4: 0.1: 0.25: 0.25 with 0.03% GM1) at 23°C. The vesicle interior buffer was 20 mM phosphate (pH = 7) and the exterior buffer contained 20 mM phosphate buffer (pH= 7) + 100 mM NaCl. Vesicle diameter was estimated as 65 ± 0.0 nm. The experiment was performed in 12 replicates.

During the rupture process, the energy related to vesicle curvature and deformation is released, therefore having higher bending energy (smaller vesicles) or increasing the vesicle deformation would be in favor of vesicle rupture. Vesicle deformation which is denoted by height to width ratio of an adsorbed vesicle (h/R_a in Fig. 3) is critical in vesicle fusion on a

substrate. Adsorption-induced rupture is known to start at the rim of vesicle-substrate contact area as the membrane stress caused by deformation is the highest at that region [12]. Deformation can happen for different reasons such as vesicle flattening of on the surface [18], the contact with neighboring vesicles [30], and osmotic stress [19]. When the deformation reaches a critical value, the rupture releases the excessive curvature energy [8].

Osmotic stress which is caused by having a concentration gradient across vesicle membrane can be positive (hyperosmosis) or negative (hypoosmosis) by having higher osmolyte concentration in the vesicle exterior or interior buffer, respectively [14,19]. In order to induce osmotic stress on the unruptured vesicle on QCM-D crystal, it is suggested to either flow buffer with different osmolyte concentration on the adsorbed vesicles or dilute the prepared vesicles with a buffer containing different osmolyte concentration [28]. We examined both cases by applying hyperosmotic stress on the vesicles with different NaCl as the osmolyte. At isosmotic condition, where both the internal and external buffers had 100 mM NaCl (Fig. 7 A), the final D and F values indicated the presence of unruptured vesicles on the surface. In order to apply the osmotic pressure on the vesicles which were adsorbed on the surface and remained intact, we flew buffer containing 250 mM NaCl for about 10 minutes and returned to the initial buffer to see if the final F and D values got closer to the bilayer final values (Fig. 7 B). The result showed that the final F and D values did not improve as they were still about -40 Hz and 2.5×10^{-6} and they were spread out across the different overtones which means rinsing the vesicles under hyperosmotic condition did not induce vesicle rupture. This is consistent with the study of Zhu et al. where they showed the osmotic pressure actually does not have any effect on fusion kinetics [19]. In contrast, there are studies reporting improved vesicle fusion as the result of concentration gradient across the vesicle membrane. We also observed that when we applied the hyperosmotic

condition to the vesicles just before starting the QCM-D run, we could successfully form the complete bilayer (Fig. 7 parts C to G).

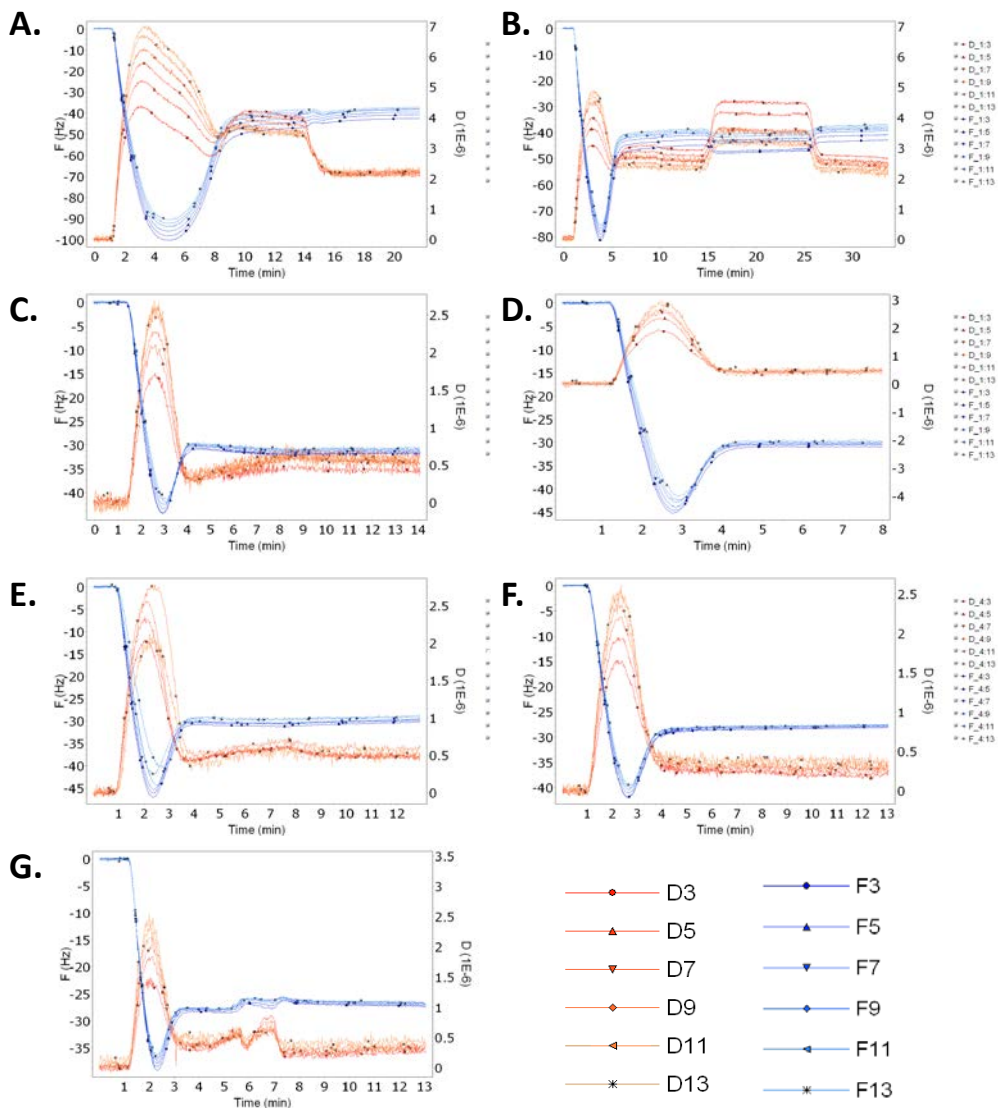


Figure 7. Effect of osmotic pressure and buffer composition on the rupture of vesicles. (A) Isosmotic condition (20 mM phosphate + 100 mM NaCl, pH=7, vesicle diameter=55 nm, lipid flow: 0-13 minutes, buffer rinse: 13 minutes to the end); (B) Vesicle adsorption happened at isosmotic condition, then the film was rinsed with high-NaCl buffer to apply hyperosmotic condition (pH=7, vesicle diameter 58 nm, Interior buffer: 20 mM phosphate+ 100 mM NaCl; Exterior buffer: 20 mM phosphate + 100 mM NaCl + 2.5 mM $MgCl_2$; Rinsing buffer: 20 mM phosphate + 250 mM NaCl, lipid flow: 0-8 minutes, low-NaCl buffer rinse: 8-13 minutes, high-NaCl: 13-23

minutes, low-NaCl buffer rinse: 23 minutes to the end); (C) Hyperosmotic condition (pH = 7, vesicle diameter 63 nm, Interior buffer: 20 mM phosphate, Exterior buffer: 20 mM phosphate + 100 mM NaCl + 2.5 mM MgCl₂, lipid flow: 0-9 minutes, buffer rinse: 9 minutes to the end) ; (D) Hyperosmotic condition (pH = 7, vesicle diameter 65 nm, Interior buffer: 20 mM phosphate + 100 mM NaCl, Exterior buffer: 20 mM phosphate + 250 mM NaCl + 2.5 mM MgCl₂, lipid flow: 0-7 minutes, buffer rinse: 7 minutes to the end) ; (E) Hyperosmotic condition (pH=7, vesicle diameter 81 nm, Interior buffer: 20 mM phosphate, Exterior buffer: 20 mM phosphate + 100 mM NaCl, lipid flow: 0-6.5 minutes, buffer rinse: 6.5 minutes to the end); (F) Hyperosmotic condition (pH = 7, vesicle diameter 62 nm, Interior buffer: 20 mM phosphate, Exterior buffer: 20 mM phosphate + 100 mM NaCl, lipid flow: 0-6 minutes, buffer rinse: 6 minutes to the end); (G) Hyperosmotic condition (pH = 7, vesicle diameter 74 nm, Interior buffer: 20 mM phosphate, Exterior buffer: 20 mM phosphate + 100 mM NaCl, lipid flow: 0-6 minutes, buffer rinse: 6 minutes to the end). All of the experiments were performed in minimum four replicates. The lipid concentration was 0.1 mM for all of the cases.

In order to understand the effect of osmotic stress on vesicle fusion, we consider its effect of both of vesicle adsorption and vesicle rupture processes. Regarding the rupture process, the osmotic imbalance across the vesicle membrane causes water flow across the membrane resulting in shrinking at hyperosmosis conditions and volume increase in hypoosmosis conditions. Change of vesicle size leads to change in bending energy. However, from an energy perspective, it has been proven that the deformation induced by osmotic pressure is much less than the deformation resulted from adsorption of vesicles. Previous studies indicated that osmotic stress does not change the level of vesicle deformation [19] to the enough extend that leads to the rupture.

In terms of vesicle adsorption, having different concentrations of osmolyte in the external buffer can also affect the vesicle-vesicle and vesicle-substrate contact. As mentioned earlier, reducing the repulsive vesicle-vesicle and vesicle-substrate interactions can promote the vesicle fusion. Most of the previous studies on the osmotic stress used NaCl as the osmolyte and showed

that hyperosmotic condition facilitates the vesicle fusion [12,14,20,28,34]. This can be due to electrostatic effects rather than osmotic stress effect as higher concentration of NaCl facilitates the vesicle fusion by screening the repulsive electrostatic interactions between negatively charged surface and the vesicles [19]. Effect of lipid charge on SLB formation has been previously studied for lipid systems with different ratios of DOPC to DOPS which are zwitterionic and negatively-charged, respectively. It has been shown that the presence of Mg^{+2} ions reduces the repulsive interactions between the carboxylate groups in DOPS and the phosphate groups of DOPS and DOPC [8]. This is similar to the previous studies where using the buffers with high ionic strength or low pH was suggested to screen the repulsive forces and facilitate the vesicle fusion [13,20,21,28].

In order to isolate the effect of osmotic stress from other variables (e.g. ionic strength) Zhu et al. compared the vesicle fusion at osmotic gradients induced by using NaCl and sucrose. Concentration gradient of sucrose across the vesicle membrane did not influence the vesicle fusion [19]. In addition, at identical external NaCl concentrations, the osmotic stress induced by various internal NaCl concentrations did not influence the vesicle fusion. These two observations, Zhu et al. confirmed that osmotic stress does not change the fusion kinetics [19]. This is to some extent in agreement with our observation as the NaCl gradient was only effective when it was applied to vesicles before adsorption. When the vesicles adsorbed on the surface, flowing the buffer with higher NaCl concentration did not induce the rupture. From here, we propose that applying the NaCl gradient across the vesicle membrane induced the rupture by changing the electrostatic interactions between the vesicles and/or vesicle and the substrate rather than applying vesicle-membrane tension by osmotic stress. Further investigation is required for extended clarification.

4.5 Summary

Supported lipid bilayers (SLBs) have become important model systems to study the biophysical properties of lipid membranes as well as the interactions of various biomolecules with the membranes. The robust formation of SLBs have been demonstrated mostly for systems with one or two lipid components and QCM-D has become a convenient tool to monitor the formation of the SLB. However, the experimental conditions to form a SLB with a given phospholipid do not translate well to other lipid choices as well as compositions. In this study, we explained the challenge of forming SLBs with lateral heterogeneous structures including domains enriched with cholesterol and sphingomyelin referred as “lipid rafts”. This type of membrane is especially important for studies of A β peptide interactions with bilayers to assess the influence of lipid components of neuronal membrane in Alzheimer’s disease.

By optimizing different experimental conditions (e.g. pH, temperature, osmotic pressure, and vesicle size), we were able to induce vesicle fusion, The key parameter in forming the bilayer was found to be applying osmotic pressure to the vesicles by having the concentration of NaCl in the vesicles exterior higher than that inside the vesicles. When this concentration difference was applied to the vesicles before flowing them on the substrate, vesicle rupture was favored and the reproducible formation of a complete bilayer could occur. Here, we report the effects of all variables investigated on the adsorption and fusion of the vesicles, and the results are discussed based on the mechanisms of vesicle-vesicle and vesicle-substrate interactions.

4.6 Acknowledgement

The authors thank Joseph Duffy, Christopher Lambert, Reeta Prusty Rao, and Arne Gericke at Worcester Polytechnic Institute assisted with some use of lab equipment. We would

also thank Cynthia A. Bukowski, Martin Burkardt for assisting with the experiments in this study.

4.7 References

- [1] N.J. Cho, C.W. Frank, B. Kasemo, F. Hook, Quartz crystal microbalance with dissipation monitoring of supported lipid bilayers on various substrates, *Nat. Protoc.* 5 (2010) 1096–1106. doi:Doi 10.1038/Nprot.2010.65.
- [2] T. Weimbs, S.H. Low, S.J. Chapin, K.E. Mostov, Apical targeting in polarized epithelial cells: There's more afloat than rafts, *Trends Cell Biol.* 7 (1997) 393–399.
doi:10.1016/S0962-8924(97)01130-6.
- [3] E.S. Melby, A.C. Mensch, S.E. Lohse, D. Hu, G. Orr, C.J. Murphy, R.J. Hamers, J.A. Pedersen, Formation of supported lipid bilayers containing phase-segregated domains and their interaction with gold nanoparticles, *Environ. Sci. Nano.* 3 (2016) 45–55.
doi:10.1039/C5EN00098J.
- [4] M. Sundh, S. Svedhem, D.S. Sutherland, Influence of phase separating lipids on supported lipid bilayer formation at SiO₂ surfaces, *Phys. Chem. Chem. Phys.* 12 (2010) 453–460.
doi:10.1039/B912598A.
- [5] A. V. Samsonov, I. Mihalyov, F.S. Cohen, Characterization of cholesterol-sphingomyelin domains and their dynamics in bilayer membranes, *Biophys. J.* 81 (2001) 1486–1500.
doi:10.1016/S0006-3495(01)75803-1.
- [6] C. Yuan, J. Furlong, P. Burgos, L.J. Johnston, The size of lipid rafts: an atomic force microscopy study of ganglioside GM1 domains in sphingomyelin/DOPC/cholesterol

- membranes., *Biophys. J.* 82 (2002) 2526–35. doi:10.1016/S0006-3495(02)75596-3.
- [7] C. Dietrich, L.A. Bagatolli, Z.N. Volovyk, N.L. Thompson, M. Levi, K. Jacobson, E. Gratton, Lipid rafts reconstituted in model membranes, *Biophys. J.* 80 (2001) 1417–1428. doi:10.1016/S0006-3495(01)76114-0.
- [8] R. Richter, A. Mukhopadhyay, A. Brisson, Pathways of lipid vesicle deposition on solid surfaces: a combined QCM-D and AFM study., *Biophys. J.* 85 (2003) 3035–47. doi:10.1016/S0006-3495(03)74722-5.
- [9] R.P. Richter, A.R. Brisson, Following the formation of supported lipid bilayers on mica: a study combining AFM, QCM-D, and ellipsometry., *Biophys. J.* 88 (2005) 3422–33. doi:10.1529/biophysj.104.053728.
- [10] C. A. Keller, K. Glasmästar, V.P. Zhdanov, B. Kasemo, Formation of supported membranes from vesicles., *Phys. Rev. Lett.* 84 (2000) 5443–6.
- [11] N. Kahya, D. Scherfeld, K. Bacia, B. Poolman, P. Schwille, Probing lipid mobility of raft-exhibiting model membranes by fluorescence correlation spectroscopy, *J. Biol. Chem.* 278 (2003) 28109–28115. doi:10.1074/jbc.M302969200.
- [12] V.P. Zhdanov, Mechanism of rupture of single adsorbed vesicles, *Chem. Phys. Lett.* 641 (2015) 20–22. doi:10.1016/j.cplett.2015.10.053.
- [13] P.S. Cremer, S.G. Boxer, Formation and spreading of lipid bilayers on planar glass supports, *J. Phys. Chem. B.* 103 (1999) 2554–2559. doi:10.1021/jp983996x.
- [14] J. A Jackman, J. Choi, V.P. Zhdanov, N. Cho, Influence of osmotic pressure on adhesion of lipid vesicles to solid supports, *Langmuir*, 29 (2013), 11375–11384

- [15] E. Reimhult, F. Ho, B. Kasemo, Intact vesicle adsorption and supported biomembrane formation from vesicles in solution : Influence of surface chemistry , vesicle size , temperature , and osmotic pressure, (2003) 1681–1691.
- [16] N. Hain, M. Gallego, I. Reviakine, Unraveling supported lipid bilayer formation kinetics: Osmotic effects, *Langmuir*. 29 (2013) 2282–2288. doi:10.1021/la304197m.
- [17] U. Seifert, Configurations of fluid membranes and vesicles, *Adv. Phys.* 46 (1997) 13–137. doi:10.1080/00018739700101488.
- [18] I. Reviakine, M. Gallego, D. Johannsmann, E. Tellechea, Adsorbed liposome deformation studied with quartz crystal microbalance, *J. Chem. Phys.* 136 (2012). doi:10.1063/1.3687351.
- [19] T. Zhu, Z. Jiang, E.M.R. Nurlybaeva, J. Sheng, Y. Ma, Effect of osmotic stress on membrane fusion on solid substrate, *Langmuir*. 29 (2013) 6377–6385. doi:10.1021/la401054g.
- [20] S. Boudard, B. Seantier, C. Breffa, G. Decher, O. Félix, Controlling the pathway of formation of supported lipid bilayers of DMPC by varying the sodium chloride concentration, *Thin Solid Films*. 495 (2006) 246–251. doi:10.1016/j.tsf.2005.08.184.
- [21] B. Seantier, C. Breffa, O. Felix, G. Decher, Dissipation-enhanced quartz crystal microbalance studies on the experimental parameters controlling the formation of supported lipid bilayers, *J. Phys. Chem. B*. 109 (2005) 21755–21765. doi:10.1021/jp053482f.
- [22] K. Sasahara, K. Morigaki, K. Shinya, Effects of membrane interaction and aggregation of

- amyloid β -peptide on lipid mobility and membrane domain structure., *Phys. Chem. Chem. Phys.* 15 (2013) 8929–39. doi:10.1039/c3cp44517h.
- [23] K. Sasahara, K. Morigaki, K. Shinya, Amyloid aggregation and deposition of human islet amyloid polypeptide at membrane interfaces., *FEBS J.* 281 (2014) 2597–612. doi:10.1111/febs.12807.
- [24] M.M. Lapinski, A. Castro-forero, A.J. Greiner, R.Y. Ofoli, G.J. Blanchard, Comparison of Liposomes Formed by Sonication and Extrusion : Rotational and Translational Diffusion of an Embedded Chromophore, (2007) 11677–11683. doi:10.1021/la7020963.
- [25] Y. Barenholz, D. Gibbes, B.J. Litman, J. Goll, T.E. Thompson, R.D. Carlson, A simple method for the preparation of homogeneous phospholipid vesicles., *Biochemistry.* 16 (1977) 2806–10.
- [26] P.S. Cremer, S.G. Boxer, Formation and Spreading of Lipid Bilayers on Planar Glass Supports, 291 (1999) 2554–2559.
- [27] A. Mechler, S. Praporski, K. Atmuri, M. Boland, F. Separovic, L.L. Martin, Specific and selective peptide-membrane interactions revealed using quartz crystal microbalance., *Biophys. J.* 93 (2007) 3907–16. doi:10.1529/biophysj.107.116525.
- [28] N. J. Cho, C.W. Frank, B. Kasemo, F. Höök, Quartz crystal microbalance with dissipation monitoring of supported lipid bilayers on various substrates., *Nat. Protoc.* 5 (2010) 1096–106. doi:10.1038/nprot.2010.65.
- [29] E. Reimhult, F. Ho, B. Kasemo, Intact Vesicle Adsorption and Supported Biomembrane Formation from Vesicles in Solution : Influence of Surface Chemistry , Vesicle Size ,

- Temperature , and Osmotic Pressure †, (2003) 1681–1691.
- [30] A.R. Ferhan, J.A. Jackman, N. Cho, Investigating how vesicle size influences vesicle adsorption on titanium oxide : A competition between steric packing and shape deformation †, *Phys. Chem. Chem. Phys.* 19 (2017) 2131–2139.
doi:10.1039/C6CP07930J.
- [31] C.M. Bailey, A. Tripathi, A. Shukla, Effects of Flow and Bulk Vesicle Concentration on Supported Lipid Bilayer Formation, *Langmuir*. (2017) acs.langmuir.7b02764.
doi:10.1021/acs.langmuir.7b02764.
- [32] E. Reimhult, F. Höök, B. Kasemo, Vesicle adsorption on SiO₂ and TiO₂: Dependence on vesicle size, *J. Chem. Phys.* 117 (2002) 7401. doi:10.1063/1.1515320.
- [33] A. Manuscript, *NIH Public Access*, 18 (2014) 448–458.
doi:10.1016/j.cocis.2013.06.004.Model.
- [34] Y. Jing, H. Trefna, M. Persson, B. Kasemo, S. Svedhem, Formation of supported lipid bilayers on silica: relation to lipid phase transition temperature and liposome size., *Soft Matter*. 10 (2014) 187–95. doi:10.1039/c3sm50947h.
- [35] J.A. Jackman, M.C. Kim, V.P. Zhdanov, N. J. Cho, Relationship between vesicle size and steric hindrance influences vesicle rupture on solid supports, *Phys. Chem. Chem. Phys.* 18 (2016) 3065–3072. doi:10.1039/C5CP06786C.
- [36] P.S. Cremer, S.G. Boxer, Formation and Spreading of Lipid Bilayers on Planar Glass Supports, 291 (1999) 2554–2559.
- [37] H. An, M.R. Nussio, M.G. Huson, N.H. Voelcker, J.G. Shapter, Material properties of

lipid microdomains: Force-volume imaging study of the effect of cholesterol on lipid microdomain rigidity, *Biophys. J.* 99 (2010) 834–844. doi:10.1016/j.bpj.2010.04.072.

Chapter 5

A QCM-D based mechanistic study of Alzheimer's disease

5.1 Abstract

The structural transition of amyloid β peptide ($A\beta$) into the β -sheet state followed by amyloid fibril formation is the cause of a significant step in the pathogenesis of Alzheimer's disease (AD). Numerous studies have demonstrated that lipid membrane surfaces promote the conversion of amyloidogenic proteins into misfolded toxic aggregates, and eventually these aggregates destabilize the structural integrity of the cell membrane. As the result, the main objective of this research is to quantitatively study amyloid peptide–membrane interactions. Moreover, both the aggregation process and the membrane destabilization process will be studied. An important membrane model is the supported lipid bilayer (SLB). It enables us to use surface-sensitive imaging techniques that can detect interfacial events. Such a model can be conveniently probed using the quartz crystal microbalance with dissipation (QCM-D) technique. Here we propose using the QCM-D technique to understand the fibril formation process and the consequent structural change of the membrane. In this QCM-D measurement, a supported lipid bilayer (SLB) will be deposited on the surface of an SiO_2 -coated quartz crystal, and $A\beta$ aggregation intermediates will be introduced in the bulk solution above the crystal to initiate the interaction between the SLB and the protein. This research helps us to study the formation of amyloids and their related toxicity, which will further our understanding of the onset and progression of the neurodegenerative diseases. The cause of most neurodegenerative diseases, such as Alzheimer's disease, has been poorly understood. Understanding the cause of this disease would be the first step in developing therapeutics.

5.2 Introduction

The structural transformation of protein to abnormal aggregated species (amyloid) is the hallmark of neurodegenerative diseases such as prion disease, Alzheimer's disease, and Parkinson's disease [1][2] Better understanding of amyloid formation and its related toxicity would be the first step in developing effective therapeutics to prevent the onset and progression of neurodegenerative diseases. Alzheimer's disease (AD) was first described as a disease marked by extracellular amyloid beta ($A\beta$) plaques deposited on the brain tissue of patients [3]. The major components of these senile plaques are $A\beta$ (1-40) and $A\beta$ (1-42) peptides with 40 and 42 amino acid residues, respectively, while $A\beta$ (1-42) peptide is the predominant component of diffuse plaques [4]. $A\beta$ (1-42) is typically more neurotoxic than $A\beta$ (1-40) [5]. $A\beta$ peptide is produced by sequential cleavage of transmembrane amyloid precursor protein (APP) by β - and γ -secretase [6]. Based on the well-known amyloid cascade hypothesis, $A\beta$ fibrillation starts by formation of soluble monomers [7], the accumulation of which leads to peptide misfolding and formation of lower-molecular-weight soluble oligomers (such as dimers and trimers) with β sheet structure. According to this hypothesis, fibrillation is a nucleation-dependent process, which means that the addition of more monomers to the oligomers leads and the formation of higher-molecular-weight protofibrillar oligomers and eventually amyloid fibrils [8]. It has been reported that among all these species, from monomers to mature fibrils, small oligomers are the species most toxic to cells [9].

The transformation of $A\beta$ peptide from monomers to aggregates has been studied in solution, as well as in the presence of lipid membrane, via different techniques such as transmission electron microscopy (TEM), fluorescence spectroscopic assays (Thioflavin T, Congo red), fluorescence microscopy, Nuclear magnetic resonance spectroscopy (NMR), Fourier

transform infrared (FTIR) spectroscopy, and circular dichroism (CD) spectroscopy [10–12]. In the earlier studies, the aggregate species (e.g., monomers, oligomers, fibrils) were formed in solution and then added to the membrane for toxicity studies via a variety of assays such as cell culture assay and vesicle leakage assay [8,13–16]. Later studies introduced membranes as a template for misfolding and ordering of amyloidogenic proteins into fibrils [10,12,17,18]. Soluble proteins bind to the membrane surface and go through a conformational shift from a random coil free in solution to a membrane-bound α -helix structure. The increase of proteins on the surface of the membrane causes their conformational change into β -sheet aggregates [19,20]. Physicochemical interactions of amyloid β -peptide with lipid bilayers were discussed in a review article by K. Matsuzaki [21], and a novel model was proposed for A β -membrane interactions with regard to different membrane components [22]. The brain lipids are composed of three main categories: glycerophospholipids, sphingolipids, and cholesterol [23]. Sphingolipids and cholesterol self-aggregate into specific domains called lipid rafts. These lipid rafts are sphingolipid-cholesterol-enriched domains in a liquid-ordered (L_o) phase floating in the more liquid glycerophospholipid-rich and cholesterol-poor bulk (L_d phase). Based on Matsuzaki's model, enzymatic cleavage of APP, and therefore A β generation, takes place in lipid rafts which are composed of sphingolipids and cholesterol. On the other hand, the presence of cholesterol helps the generation of ganglioside clusters. Generated A β that has an unordered structure in soluble form binds to the ganglioside clusters forming an α -helix-rich structure at lower peptide-to-ganglioside ratios. By increasing the ratio, the peptide changes its conformation to a β -sheet form which facilitates the aggregation (fibrillization) of A β , leading to toxicity [22]. From this model, it is clear that toxicity of A β needs to be studied with systems containing all of the aforementioned lipid components (i.e., cholesterol, galglioside, and sphingomyelin).

Among all aggregate species (from monomers to mature fibrils), small oligomers showed the greatest toxicity [1,9,19], but the mechanism of toxicity is not fully understood yet. It is generally proposed that the toxicity of amyloid oligomers is the result of their direct interactions with cell membrane (citations to be added), which led to loss of membrane structural integrity and cell death [20]. Suggested mechanisms of membrane disruption include three main categories: pore formation, peptide behaving as a detergent, and formation of peptide-rich microdomains inside the bilayer [1,24]. Small oligomers containing 4 to 6 monomers have shown the ability to form pores through the membrane and consequent calcium ion imbalance across the membrane which causes cell apoptosis [25]. Previous research on interactions of antimicrobial peptides with egg PC supported lipid bilayer (SLB) characterized four different states of peptide–membrane interactions including insertion of a single peptide or peptide clusters, formation of pores, and adsorption of peptides on the surface [26]. These different modes of membrane destabilization can be monitored by QCM-D, which is a sensitive, real-time, and label-free technique for probing the mass and viscoelasticity change of surface-bound materials.

QCM-D is a great tool in studying peptide aggregation because it is a label-free technique. One of the challenges in the field of membrane–amyloid peptide interaction is that the process of A β aggregation is very complicated and very sensitive to experimental conditions such as peptide concentration [25], initial state of the peptide [27], peptide stock preparation [28], source of the peptide, and batch to batch variability of the peptide [29]. Therefore, not only is any attempt to gather more data significantly appreciated in this field, but also special attention should be given to designing experimental assays that limit the variability of the resulting data. For instance, labeling the peptide with a fluorescent agent, which is required for some of the

imaging assays, might perturb the peptide structure; therefore, it is crucial to compare the properties of the label-free peptide with the labeled one [25]. Here, we propose using the quartz crystal microbalance with dissipation (QCM-D) technique to probe the fibril formation process and the consequent structural change of the membrane. In this QCM-D measurement, a SLB will be deposited on the surface of a SiO₂-coated quartz crystal, and a solution of A β monomers and small oligomers is introduced in the bulk solution above the crystal to initiate an interaction between the SLB and the protein. The lipid composition is a combination of 1,2-dioleoyl-sn-glycero-3-phosphocholine (DOPC), 1,2-dioleoyl-sn-glycero-3-phospho-L-serine (DOPS), sphingomyelin (SM), cholesterol (Chol), and ganglioside (GM1).

5.3 Methods and materials

5.3.1 Small unilamellar vesicles (SUVs)

1,2-Dioleoyl-sn-glycero-3-phosphocholine (DOPC), 1,2-dioleoyl-sn-glycero-3-phospho-L-serine (DOPS), sphingomyelin (SM; egg, chicken), cholesterol (Chol; ovine wool), and monosialoganglioside (GM1; brain, ovine-ammonium salt) were purchased from Avanti Polar Lipids, Inc. (Alabaster, AL). The molecular weights of the lipids are listed in Table 1. DOPC, DOPS, SM, and Chol were dissolved in chloroform to a concentration of 10 mM, and GM1 was dissolved in methanol to a concentration of 0.63 mM. The lipids were mixed with the molar ratio of DOPC/DOPS/SM/Chol/GM1 of 0.4/0.1/0.25/0.25/0.03. After the evaporation of the organic solvents under a stream of nitrogen, the dried film was kept in vacuum desiccator for at least 4 hours to remove any residual solvents. The film was hydrated in the buffer solution at 56 °C to

yield a total lipid concentration of 0.3 mM. After five freeze–thaw cycles, large multilamellar vesicles were formed. In order to reduce the size of vesicles, an ultrasonic dismembrator (Model 150T, Thermo Fisher Scientific, Waltham, MA) was used in pulse mode for 45 minutes at 56 °C. A 30% duty cycle was used for sonication (pulse on for 3 s, followed by a pause for 7 s) at an amplitude of 60. After sonication, the vesicle solution was centrifuged at 16,000 rcf for 10 minutes remove the TiO₂ particles from the ultrasonic dismembrator probe (J2-MI Centrifuge, Beckman Coulter, Brea, CA). [30] The supernatant containing SUVs was collected and stored at 4°C under nitrogen, and it was stable for two to three weeks. In order to determine the size of the vesicles, dynamic light scattering (DLS) was performed (Zetasizer Nano ZS, Malvern, Worcestershire, UK). The stock solution was diluted to the desired concentration before each QCM-D experiment.

Table1. Molecular weights of lipids

lipid	Molecular weight
DOPC	786.15 ¹
DOPS	810.03 ¹
SM	703.03 ¹
Chol	386.66 ¹
GM1	1568.81 ¹

¹ The values are provided by the vendor (Avanti Polar Lipids, Inc.).

5.3.2 Quartz crystal microbalance with dissipation.

QCM-D data was obtained by a Q-Sense E4 series (Q-Sense AB, Sweden) instrument with silicon dioxide-coated crystals (5 Hz) purchased from Biolin Scientific (Gothenburg, Sweden). In the cleaning step, the crystals were rinsed with sequential flows of ethanol, deionized water, and 2% sodium dodecyl sulfate and deionized water for 5 minutes each. After that, the crystals were thoroughly dried with nitrogen gas and etched with two cycles of 45 s oxygen plasma cleaning using Plasma Prep II (SPI Supplies, West Chester, PA). The experimental procedure began with setting a baseline in buffer. To form a stable SLB on a crystal, the lipid solution is injected into the QCM-D chamber at 0.15 mL/min to allow vesicles to attach to the silica-coated crystal surface. After the vesicles ruptured to form a stable bilayer, the crystal was rinsed with buffer to remove unattached particles [30–33].

5.3.3 A β

Because the initial conformation of the peptide can influence the subsequent lipid-peptide interactions [21], the highly purified peptide (free of metal trace) was carefully chosen to prevent batch-to-batch variabilities. Lyophilized white powder of A β (1-42) (AggreSure™ β Amyloid, Human) was purchased from Anaspec (San Jose, CA). According to the manufacturer the purity of the peptide was >95%, and the peptide was pretreated to be in monomeric state. The peptide was reconstituted in 50mM Tris/150mM NaCl (pH 7.2) to a final concentration of 47 μ M followed by 3 minutes of bath sonication at 4 °C. The peptide was then centrifuged at 10,000 rpm for 5 minutes at 4 °C to remove any precipitated material. The peptide reconstitution was performed just before running the QCM-D. In order to keep the experimental conditions consistent through all of the experiment, special attention was given to the timing of peptide

stock preparation so that the period between the addition of the buffer to the lyophilized powder and the time of peptide introduction to the QCM-D crystal was kept to 15 min.

5.3.4 Thioflavin T (Th-T) assay

Aggregation of A β was monitored by the Th-T assay at 37 °C. Fluorescence was measured on a Victor 3 Wallac instrument (PerkinElmer, Waltham, MA). The Th-T was dissolved in 50mM Tris/150mM NaCl (pH 7.2) to a final concentration of 200 μ M in each well, and the peptide was reconstituted in 50mM Tris/150mM NaCl (pH 7.2) and added to each well to a final concentration of 47 μ M. The fluorescence was read every 5 min, with 15 s of shaking in between. The excitation and emission wavelengths were 440 nm and 480 nm, respectively. A reading from the blank control wells containing only buffer was used to measure background fluorescence, which was subtracted from the readings of the other wells. All fluorescence readings were expressed in relative fluorescence units (RFU).

5.4 Results and discussion

A β in vivo is normally very low ($<10^{-8}$ M) [19]; however, under pathological conditions peptide accumulation leads to a series of conformational changes to the peptide structure and the consequent cell death. Here, in order to elucidate the mechanism of toxicity, we focused on the interactions of lipid membrane with A β peptide. A β has an unordered structure in solution, but it transforms to an α -helical structure upon adsorption to the membrane. Increasing the peptide density leads to further transformation of its structure to β -sheet form. Lipid membranes play a catalytic role in the process of amyloid peptide aggregation [19–21] because adsorption of

peptide on the lipid membrane leads to peptide accumulation on the surface. Moreover, the oligomers that are formed in the presence of a lipid membrane take on a different structure than the oligomers that are formed in solution. Therefore, studying the oligomerization in the presence of lipid membrane provides better insight into what happens in the pathological process. As mentioned before, brain cell membrane contains liquid-ordered microdomains (the so-called lipid rafts) that are rich in sphingomyelin and cholesterol. The adsorption of A β peptide is known to take place in these domains and, more specifically, on ganglioside clusters of the lipid rafts [20,19,34]. In two review papers by Kotler et al. and R. Murphy, previous studies on aggregation of A β in the presence of lipid membrane are summarized [16][8]. As listed in these review papers, there is still some lack of understanding about how aggregation of monomer and small oligomers leads to membrane disruption. Previous research studies on A β fibrillation in the presence of membrane either started with already aggregated species as the polymerization seeds or used lipid components that are not biologically relevant to brain cell lipid membranes. In addition, the focus of these studies is on answering the question of how membrane affects the adsorption of A β and catalyze the aggregation process. To our knowledge this is study is one of the first studies on characterization of a raft-containing membrane during the aggregation process starting from the earlier even which is transformation of monomers and small oligomers to mature fibrils. Here, we extended the focus of study one step further to characterize both of the aggregation and the membrane disruption that potentially take place simultaneously.

5.4.1 Kinetics of peptide aggregation characterized by ThT assay

As previously mentioned, aggregation of A β peptide is significantly influenced by the source of the peptide and the experimental conditions. In order to confirm that our peptide was capable of undergoing fibrillation in these experimental conditions, we utilized the fluorescence spectroscopy assay, known as the ThT assay.

The ThT assay, one of the most common assays used to characterize the formation of β sheet-rich species, quantifies peptide aggregation kinetics [35]. ThT is a fluorescent probe that binds to β -sheet amyloid species and causes the absorption maximum and fluorescence spectrum to go through a red shift. In other words, when excited at 440 nm, the fluorescence emission at 480 nm increases proportionally to the concentration of β -sheet species [35]. The kinetics of peptide aggregation is known to follow the common crystallization pathway, which includes nucleation, elongation, secondary nucleation, and polymorphism [36]. The initial nucleation happens when monomers attach to each other and form small oligomers (e.g., dimers and trimers). Small oligomers with fewer monomers possess an α -helical structure, which subsequently transforms into a β -sheet form as more monomers are added to the oligomer. The secondary nucleation of A β is defined as the aggregation of small oligomers or protofibrils resulting in formation of spherulites (spherical species) [36]. Mature fibrils of A β have a diameter of about 10 nm and a length of several micrometers [37].

As the results show (Fig. 1), the peptide was following a sigmoidal kinetic pathway. During the short lag time, the fibril seeds are formed. This is the time in which the structure of small oligomers transforms to misfolded β sheets. Seed formation is followed by fast growth to form elongated fibrils. The last plateau phase corresponded to the saturation state, where there were no more β -sheet species added to

the fibrils. The ThT data were consistent with previous reports [11,35,38] and indicated that it took less than 7 hours for our peptide to transform from monomers to mature fibrils.

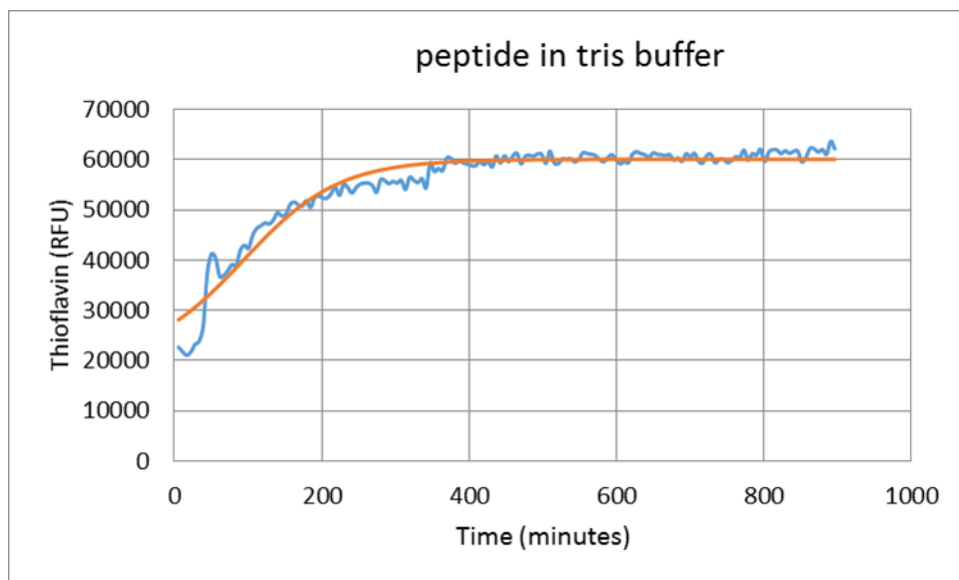


Figure 1. Kinetics of A β peptide aggregation in solution. Peptide was reconstituted in 50mM Tris buffer and 150mM NaCl (pH 7.2). The experiment was performed in triplicate.

5.4.2 Peptide–membrane interactions characterized by QCM-D

In order to understand the mechanism of peptide–membrane interactions, we used QCM-D to elucidate the aggregation of the peptide as well as the consequent change of bilayer structure. In their review article, Butterfield and Lashuel schematically plotted the different possible mechanisms of interactions between amyloidogenic peptides and membranes (Fig. 2). These mechanisms include adsorption of peptide monomers or oligomers on the membrane surface, insertion of the peptide in the bilayer as a cluster, and insertion of a group of peptides that form a pore or channel in the lipid structure. The aforementioned mechanisms can lead to

disruption of cell membrane integrity, very similar to the previously reported scenarios for antimicrobial peptide interactions with the lipid bilayer [26]. QCM-D is a sensitive, label-free acoustic technique, capable of distinguishing between these membrane disruption pathways through measurement of mass change and viscoelasticity change of the bilayer [26,39].

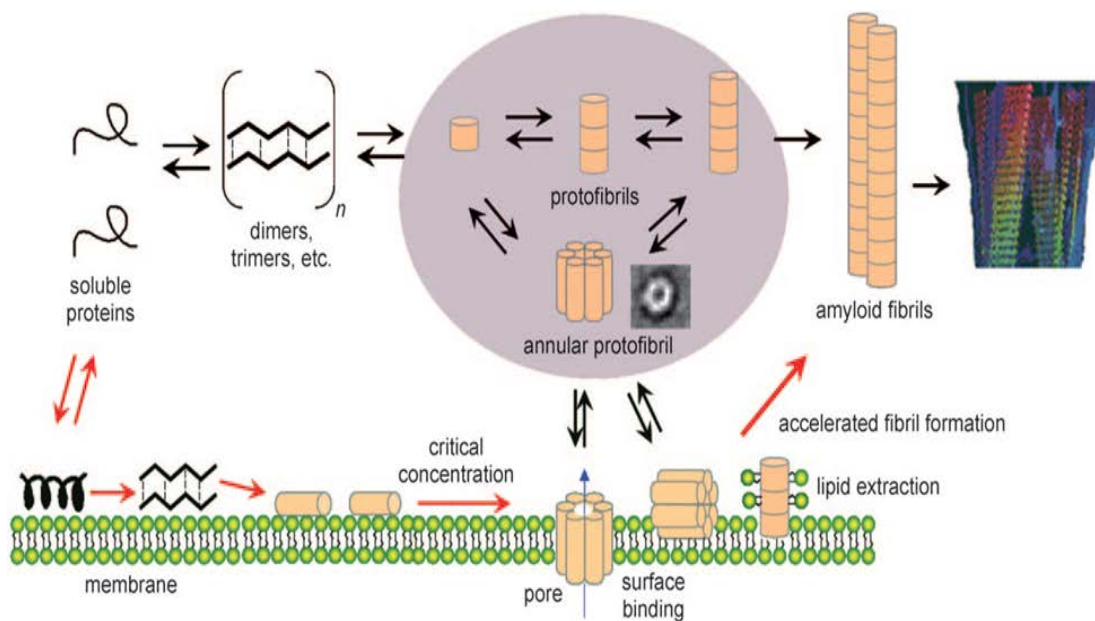


Figure 2. The process of amyloid-fibril formation in solution (top), the process of fibril formation in the presence of lipid membrane, and the mechanisms of cell membrane disruption. The figure is borrowed from Reference [20].

In the QCM-D technique, an applied voltage causes a gold-coated quartz crystal to oscillate, and the oscillation frequency and dissipation energy is recorded at different overtones of the natural frequency of the crystal. Change of frequency (Δf) is related to the mass change of the film on top of the crystal: an increase in frequency corresponds to mass loss and a decrease in frequency shows mass addition. The dissipation of energy is correlated with softness of the film and is defined as

$$D = -\frac{E_{lost}}{2\pi E_{stored}}, \quad (1)$$

where E_{lost} is the loss of energy in one oscillating cycle and E_{stored} is the total amount of initial energy stored in the oscillator [40]. When the film is rigid, the dissipation of energy is insignificant (less than 8×10^{-6} to 10×10^{-6} per 1 Hz of change in frequency [41]). The Sauerbrey model can describe the relationship between the adsorbed mass, Δm , and the corresponding frequency change, Δf [41,13]. The mass change can be calculated by the Sauerbrey equation, defined as

$$\Delta m = -C\Delta f, \quad (2)$$

where n is the number of the overtone and C is the sensitivity constant of the crystal ($17.7 \text{ ng cm}^{-2} \text{ Hz}^{-1}$) [40].

QCM-D, which has a sensitivity of $\sim 1.8 \text{ ng/cm}^2$ in liquid, is a strong tool for mechanistic assessment of membrane disruption resulting from peptide attachment to the membrane, peptide insertion into lipid bilayer, and mass removal during peptide exposure to a SLB [33].

In our experiment, after the formation of the SLB on the QCMD crystal, $A\beta$ solution flowed through the chamber until the volume of the chamber ($300 \mu\text{L}$) was filled with the peptide solution. Then the peptide was incubated and left to interact with the bilayer for about 24 hours, after which the surface was rinsed with the initial buffer solution. The QCM-D data are plotted in Fig. 3. In order to find the overall changes of mass and viscoelastic properties of the film, the frequency and dissipation values at the beginning of incubation period were subtracted from the F and D values obtained at the end of the incubation. The overall F and D changes were plotted in Fig. 4. Our QCM-D data showed that the bilayer remained rigid as ΔD was small ($< 5 \times$

10^{-6}) and the frequency signals of the different overtones almost overlapped. Therefore, the Sauerbrey model is applicable for calculation of mass change throughout the process.

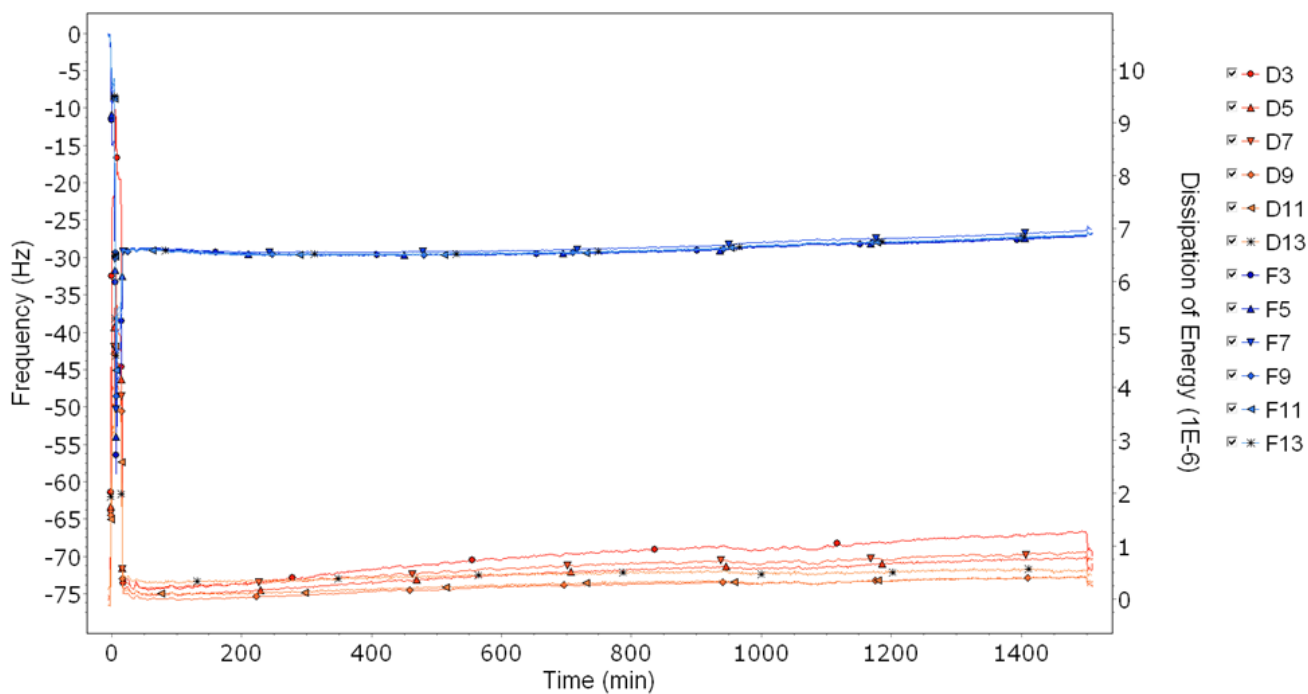


Figure 3. Representative QCM-D graph of SLB interacting with A β (1-42) with a concentration of 47 μ L. After setting the baseline in buffer, the vesicle solution was allowed to flow for 10 minutes resulting in the formation of a bilayer. After rinsing the bilayer with the buffer and allowing the peptide to flow, the flow was stopped and the SLB was incubated with the peptide for 24 hours and then washed with the buffer. The experiment was performed in 5 replicates. The blue and red curves correspond to frequency and dissipation values at different overtones.

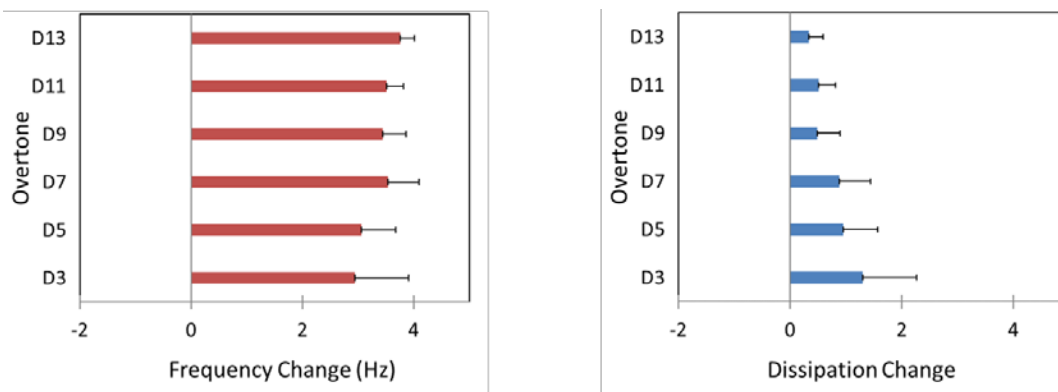


Figure 4. The overall change of frequency and dissipation of energy of the bilayer interacting with A β peptide. The data were collected at the following time points: 1 minute after introduction of the peptide and 1 minute before the end of incubation. The data are from 5 replicates. The error bars indicate the standard deviation.

Considering the overall mass and dissipation change of the film might be too simplistic to describe the peptide–membrane interaction because it only takes into account two time points in the experiment, while fibrillation is a complex, dynamic process. Previously, the QCM-D technique has been proposed to characterize the growth and elongation kinetics of amyloid peptide in the absence of a lipid membrane. Walters et al. proposed a possible mechanism for fibrillation of polyglutamine (polyQ) peptide associated with Huntington’s disease in which disordered polyglutamine monomers are added to a growing fibril continuously without requiring full consolidation to the β -sheet structure of the fibril [42]. It was concluded that eventually conformational rearrangement to a β sheet propagates through the elongating aggregate [42]. In another study, QCM-D measurement of glucagon peptide showed significant changes of F and D (~ 150 Hz and $\sim 30 \times 10^{-6}$, respectively) indicating fibril formation and elongation [41]. Three phases of monomer formation on the surface, fibril growth from nucleation sites, and end of fibril growth, were characterized [41]. The initial rigid phase was modeled by the simple Sauerbrey model, but due to the large dissipation of energy an extended Kelvin-Voigt model was applied to calculate the mass change of the film for the fibril elongation

and the end of growth (plateau) phases. A similar method was proposed by Buell et al. to study the elongation rate of three different amyloid peptides on the crystal surface and in the absence of lipid membrane [29]. In their method, a controlled number of seeds were deposited on the surface, and therefore the fibril elongation rate was directly characterized by the rate of frequency decrease. However, as mentioned before, when QCM-D is used for peptide aggregation in the presence of lipid bilayer the mechanism is more complicated, as the overall mass change of the film is a combination of the fibril formation and the potential lipid loss from the bilayer.

QCM-D has also been applied to study fibrillation in the presence of lipid membrane, but to our knowledge previous studies either did not observed any change to the mass and viscoelastic properties of membrane or the experiments were designed in conditions too far from pathologically relevant conditions. For instance, Kotarek and Moss conducted a QCM-D analysis to study the impact of phospholipid bilayer saturation on A β aggregation intermediate growth [13]. POPC and DPPC lipids were selected because they differ in the degree of carbon saturation within one of the two fatty acid chains but they both contain identical phosphocholine headgroups. It was concluded that the binding and subsequent growth of A β (1–40) aggregation intermediates occurred more readily on lipid bilayer surfaces containing a higher degree of lipid saturation. The initial state of A β peptides was already aggregated species referred as “aggregation intermediates”. However, as mentioned before, the focus Alzheimer’s disease research has shifted towards studying the initial steps of aggregation involving monomers or small (low-n) oligomers as the initiators of toxicity. Sasahara et al. used QCM-D technique in more pathologically relevant conditions to study the A β (1-42) aggregation on a bilayer with the same lipid composition as the one described here. They reported that F and D changes were

insignificant during monomer and oligomer interactions with the bilayer. The inconsistency of this report with our results might be due to the difference in duration of peptide incubation, as in the aforementioned study the peptide interacted with the bilayer for 90 min, whereas we incubated the peptide on top of the bilayer for about 24 hours. To our knowledge, none of the previous studies characterized interactions of a SLB with A β monomers and low-n oligomers in pathologically relevant conditions.

5.4.3 Peptide–membrane interaction kinetics characterized by QCM-D fingerprint

For further analysis, we used a D/F plot to characterize the kinetics of peptide–membrane interactions. D/F plots are known as QCM-D fingerprints, in which each point represents one time point [39,43]. When we plot ΔD on the y-axis and ΔF on the x-axis, the direction of the data from east to west corresponds to mass addition, and the direction of the data from south to north indicates a softer film. Any change in the slope of the curve indicates a change in the mechanism of the interactions. As our D/F graph shows, the process includes an initial adsorption step followed by a process of mass loss.

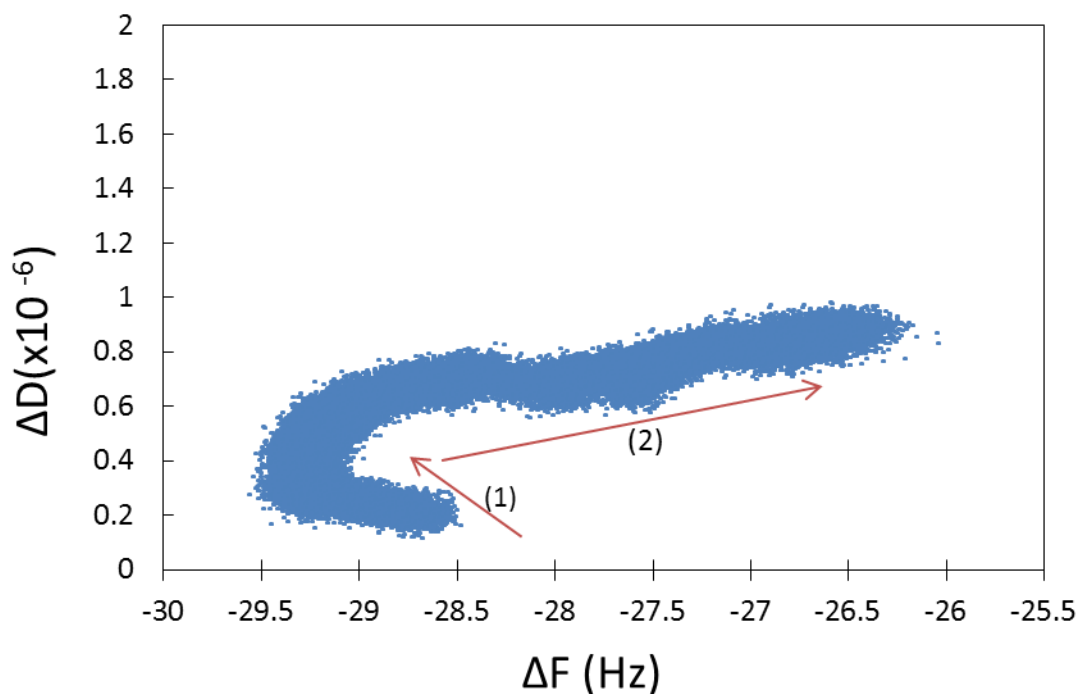


Figure 5. QCM-D fingerprint of A β (1-42) and SLB interactions. Peptide was dissolved in 50mM Tris buffer and 150mM NaCl (pH 7.2) with concentration of 47 μ M.

In the adsorption step, the frequency decreased about 1 Hz, while the dissipation values remained unchanged. If we assume that the mass change during this step is only due to the peptide adsorption and not the lipid removal, we can calculate the surface concentration of adsorbed A β molecules. Since the molecular weight of A β is 4.5 kDa, the frequency change of 1 Hz corresponds to 2.37×10^{12} A β molecules. Since the QCM-D chamber has a capacity of 300 μ L and the peptide concentration was 47 μ M, the total number of A β molecule in the bulk solution was $\sim 8.49 \times 10^{15}$. Dividing the number of A β in bulk solution the number of adsorbed A β indicates that only a small fraction of peptide ($\sim 0.028\%$) adsorbs on the membrane. This indicates that in our experiments, most of the peptide ($\sim 97\%$) remained in the bulk solution and

followed the same kinetic pathway that we obtained via ThT assay (Fig. 1) which means within the first 400 minutes all of the peptide transformed from disordered structure to β sheet structure.

In order to obtain a better understanding of peptide–membrane interaction, we calculate the P/L ratio based on the QCM-D results. Our data indicated that the frequency change for bilayer formation was -30.0 ± 0.1 Hz, which, according to the Sauerbrey equation (Eq. 3), corresponds to a mass change of 534 ng/cm^2 . This mass includes the mass of the bilayer and the hydration layer between the crystal and the bilayer. The mass of the hydration layer has been reported to be 102 ng/cm^2 [44,32]. Therefore, the mass of the bilayer is 432 ng . To calculate the number of lipid molecules on the surface, we can use the average molecular mass of the lipid based on the molecular weights of the lipids (Table1).

The average molecular weight is calculated by the following equation to be 714.95 g/mol ,

$$\sum C_i \cdot MW_i \quad (3)$$

Where, C_i and MW_i are the molar concentration and molecular weight of each lipid. Therefore the average molecular mass of the lipid is $1.188 \times 10^{-12} \text{ ng/molecule}$. Therefore, the number of lipid molecule per unit surface is $3.64 \times 10^{14} \text{ molecules/cm}^2$. Dividing the total number of peptides adsorbed on the bilayer (2.37×10^{12}) by this number indicates that the P/L ratio is about 1.3×10^{-2} . Note we obtained this number by assuming that in the first step, the peptide adsorption was the dominant process and we neglected the possible lipid removal at this stage. Since %3 of the lipid is GM1, the $A\beta$ /GM1 ratio was calculated to be 0.43.

We use Matsuzaki's model to propose a mechanism for peptide-bilayer interactions. As mentioned before, Matsuzaki et al. proposed a model for adsorption of $A\beta$ on membranes, based on which, the adsorption happens only on ganglioside clusters [22]. According to this model, at

A β /GM1 lower than 0.013, the peptide adsorbs on the membrane and remains in α -helical conformation. When the A β /GM1 value reaches 0.013 the peptide structure transforms to parallel β sheets composed of 15 monomers which is stable and does not aggregate to form fibrils. A β /GM1 ratios higher than 0.044, the structure changes to anti-parallel β -sheets which is known to be the most toxic aggregate species and has the capability of growing to fibrils [19]. Supported by this model, the A β /GM1 of 0.43 in our experiments confirms the formation of toxic aggregates with conformation of anti-parallel β -sheets which were potentially growing to form mature fibrils. QCM-D data indicates that in the second step of the process, the frequency increased about 3 Hz which corresponds to the mass loss of $\sim 54 \text{ ng cm}^{-2}$ (based on Eq. 2). The mass loss is possibly due to the formation of pores and detachment of some lipid and possibly some peptides from the bilayer. Note that this mass loss is the net mass change of the bilayer and since the peptide is growing simultaneously, the actual lipid removal is possibly larger than this value. Small change in dissipation of energy ($< 2 \times 10^{-6}$) indicates that the fibrillation causes some lipid removal from the bilayer but it does not change the viscoelastic properties of the film, significantly.

5.5 Conclusions

The mechanism of A β toxicity leading to the onset of Alzheimer's disease has not been fully discovered yet, due to the complex, time-dependent nature of peptide aggregation, dependence of the aggregation process on the initial state of the peptide, and also the lack of a reproducible technique as a platform for systematic studies. In this study, we showed that the QCM-D technique is a promising tool to conduct systematic studies on the mechanism of interactions between A β peptide and lipid membranes. To our knowledge, this was the first time

QCM-D was utilized for characterization of A β fibrillation from monomer states to the formation of mature fibrils. The data indicate that peptide–membrane interactions follow a two-step kinetic pathway starting with the adsorption of peptide and progressing until all the adsorption sites on the surface are saturated. In the second step, the membrane structure is destabilized as the result of interaction with peptide aggregates, which leads to lipid loss from the surface. Consistency of the results with the data obtained via other techniques substantiates QCM-D technique as a robust approach to answer the remaining unanswered questions in the field of Alzheimer’s disease.

5.6 Acknowledgements

We would like to thank Dr. Amy Peterson for use of the QCM-D instrument for the experiment, Dr. Arne Gericke for helpful discussions and also use of the Zetasizer Nano ZS instrument for DLS measurement, and Prof. Susan Roberts for use of the ultracentrifuge in her lab. We thank Ian Smith (WPI) for his help with the QCM-D experiments. We would like to thank Diego Vargas Blanco (WPI) and Ivan Ding (WPI) for discussions and help with the fluorescence spectroscopy plate reader.

5.7 References

- [1] P. Walsh, G. Vanderlee, J. Yau, J. Campeau, V.L. Sim, C.M. Yip, S. Sharpe, The mechanism of membrane disruption by cytotoxic amyloid oligomers formed by prion protein(106-126) is dependent on bilayer composition., *J. Biol. Chem.* 289 (2014) 10419–30. doi:10.1074/jbc.M113.515866.
- [2] C.G. Glabe, Common mechanisms of amyloid oligomer pathogenesis in degenerative

- disease., *Neurobiol. Aging*. 27 (2006) 570–5. doi:10.1016/j.neurobiolaging.2005.04.017.
- [3] S. Eleuteri, S. Di Giovanni, E. Rockenstein, M. Mante, A. Adame, M. Trejo, W. Wrasidlo, F. Wu, P.C. Fraering, E. Masliah, H. a Lashuel, Novel therapeutic strategy for neurodegeneration by blocking A β seeding mediated aggregation in models of Alzheimer's disease., *Neurobiol. Dis.* 74 (2015) 144–57. doi:10.1016/j.nbd.2014.08.017.
- [4] C.M. Yip, A. a Darabie, J. McLaurin, Abeta42-peptide assembly on lipid bilayers., *J. Mol. Biol.* 318 (2002) 97–107. doi:10.1016/S0022-2836(02)00028-1.
- [5] D.L. Mobley, D.L. Cox, R.R.P. Singh, M.W. Maddox, M.L. Longo, Modeling amyloid beta-peptide insertion into lipid bilayers., *Biophys. J.* 86 (2004) 3585–97. doi:10.1529/biophysj.103.032342.
- [6] E. Dawkins, D.H. Small, Insights into the physiological function of the β -amyloid precursor protein: beyond Alzheimer's disease., *J. Neurochem.* 129 (2014) 756–69. doi:10.1111/jnc.12675.
- [7] I.W. Hamley, The amyloid beta peptide: a chemist's perspective. Role in Alzheimer's and fibrillization., *Chem. Rev.* 112 (2012) 5147–92. doi:10.1021/cr3000994.
- [8] S. A Kotler, P. Walsh, J.R. Brender, A. Ramamoorthy, Differences between amyloid- β aggregation in solution and on the membrane: insights into elucidation of the mechanistic details of Alzheimer's disease., *Chem. Soc. Rev.* 43 (2014) 6692–700. doi:10.1039/c3cs60431d.
- [9] D.M. Walsh, D.J. Selkoe, A beta oligomers - a decade of discovery., *J. Neurochem.* 101 (2007) 1172–84. doi:10.1111/j.1471-4159.2006.04426.x.

- [10] H. Ueno, T. Yamaguchi, S. Fukunaga, Y. Okada, Y. Yano, M. Hoshino, K. Matsuzaki, Comparison between the aggregation of human and rodent amyloid beta-proteins in GM1 ganglioside clusters, *Biochemistry*. 53 (2014) 7523–7530. doi:10.1021/bi501239q.
- [11] L.O. Tjernberg, D.J.E. Callaway, A. Tjernberg, S. Hahne, C. Lilliehook, L. Terenius, J. Thyberg, C. Nordstedt, A Molecular Model of Alzheimer Amyloid -Peptide Fibril Formation, *J. Biol. Chem.* 274 (1999) 12619–12625. doi:10.1074/jbc.274.18.12619.
- [12] W. Qiang, W. M.M. Yau, J. Schulte, Fibrillation of β amyloid peptides in the presence of phospholipid bilayers and the consequent membrane disruption, *Biochim. Biophys. Acta.* 1848 (2014) 266–276. doi:10.1016/j.bbamem.2014.04.011.
- [13] J. A. Kotarek, M. A. Moss, Impact of phospholipid bilayer saturation on amyloid-beta protein aggregation intermediate growth: a quartz crystal microbalance analysis., *Anal. Biochem.* 399 (2010) 30–8. doi:10.1016/j.ab.2009.12.016.
- [14] J. A. Kotarek, K.C. Johnson, M. A. Moss, Quartz crystal microbalance analysis of growth kinetics for aggregation intermediates of the amyloid-beta protein., *Anal. Biochem.* 378 (2008) 15–24. doi:10.1016/j.ab.2008.03.022.
- [15] M. Vestergaard, T. Hamada, M. Takagi, Using model membranes for the study of amyloid beta:lipid interactions and neurotoxicity., *Biotechnol. Bioeng.* 99 (2008) 753–63. doi:10.1002/bit.21731.
- [16] R.M. Murphy, Kinetics of amyloid formation and membrane interaction with amyloidogenic proteins, *Biochim. Biophys. Acta - Biomembr.* 1768 (2007) 1923–1934. doi:10.1016/j.bbamem.2006.12.014.

- [17] E.Y. Chi, C. Ege, A. Winans, J. Majewski, G. Wu, K. Kjaer, K.Y.C. Lee, Lipid membrane templates the ordering and induces the fibrillogenesis of Alzheimer's disease amyloid-beta peptide., *Proteins*. 72 (2008) 1–24. doi:10.1002/prot.21887.
- [18] G.P. Gorbenko, P.K.J. Kinnunen, The role of lipid-protein interactions in amyloid-type protein fibril formation., *Chem. Phys. Lipids*. 141 (2006) 72–82.
doi:10.1016/j.chemphyslip.2006.02.006.
- [19] K. Matsuzaki, How do membranes initiate alzheimers disease? Formation of toxic amyloid fibrils by the amyloid ??-protein on ganglioside clusters, *Acc. Chem. Res.* 47 (2014) 2397–2404. doi:10.1021/ar500127z.
- [20] S.M. Butterfield, H. a Lashuel, Amyloidogenic protein-membrane interactions: mechanistic insight from model systems., *Angew. Chem. Int. Ed. Engl.* 49 (2010) 5628–54. doi:10.1002/anie.200906670.
- [21] K. Matsuzaki, Physicochemical interactions of amyloid β -peptide with lipid bilayers, *Biochim. Biophys. Acta - Biomembr.* 1768 (2007) 1935–1942.
doi:10.1016/j.bbamem.2007.02.009.
- [22] K. Matsuzaki, Physicochemical interactions of amyloid beta-peptide with lipid bilayers., *Biochim. Biophys. Acta*. 1768 (2007) 1935–42. doi:10.1016/j.bbamem.2007.02.009.
- [23] J. Fantini, N. Yahi, Molecular insights into amyloid regulation by membrane cholesterol and sphingolipids: common mechanisms in neurodegenerative diseases., *Expert Rev. Mol. Med.* 12 (2010) e27. doi:10.1017/S1462399410001602.
- [24] K. Sasahara, K. Morigaki, K. Shinya, Effects of membrane interaction and aggregation of

- amyloid β -peptide on lipid mobility and membrane domain structure., *Phys. Chem. Chem. Phys.* 15 (2013) 8929–39. doi:10.1039/c3cp44517h.
- [25] H. Ding, J. A. Schauerte, D.G. Steel, A. Gafni, β -Amyloid (1-40) peptide interactions with supported phospholipid membranes: a single-molecule study., *Biophys. J.* 103 (2012) 1500–9. doi:10.1016/j.bpj.2012.08.051.
- [26] K.F. Wang, R. Nagarajan, T. A Camesano, Differentiating antimicrobial peptides interacting with lipid bilayer: Molecular signatures derived from quartz crystal microbalance with dissipation monitoring., *Biophys. Chem.* 196 (2015) 53–67. doi:10.1016/j.bpc.2014.09.003.
- [27] A. Jan, D.M. Hartley, H. a Lashuel, Preparation and characterization of toxic A β aggregates for structural and functional studies in Alzheimer's disease research, *Nat. Protoc.* 5 (2010) 1186–1209. doi:10.1038/nprot.2010.72.
- [28] T.C. Eugene, C. Hall, W. Virginia, P.O. Box, W. Virginia, U. States, Preparation protocols of A β (1 – 40) promote the formation of polymorphic aggregates and altered interactions with lipid bilayers, *Biochemistry* 53 (2014) 7038-50.
- [29] A. K. Buell, C. M. Dobson, M. E. Welland, measuring the kinetics of amyloid fibril elongation using quartz crystal microbalances., *Amyloid proteins: methods and protocols*, New York: Humana Press (2012) 100-121.
- [30] Y. Barenholz, D. Gibbes, B.J. Litman, J. Goll, T.E. Thompson, R.D. Carlson, A simple method for the preparation of homogeneous phospholipid vesicles., *Biochemistry.* 16 (1977) 2806–10.

- [31] R.P. Richter, A.R. Brisson, Following the formation of supported lipid bilayers on mica: a study combining AFM, QCM-D, and ellipsometry., *Biophys. J.* 88 (2005) 3422–33. doi:10.1529/biophysj.104.053728.
- [32] P.S. Cremer, S.G. Boxer, Formation and Spreading of Lipid Bilayers on Planar Glass Supports, *J. Phys. Chem. B.* 103 (1999) 2554–2559. doi:10.1021/jp983996x.
- [33] A. Mechler, S. Praporski, K. Atmuri, M. Boland, F. Separovic, L.L. Martin, Specific and selective peptide-membrane interactions revealed using quartz crystal microbalance., *Biophys. J.* 93 (2007) 3907–16. doi:10.1529/biophysj.107.116525.
- [34] K. Matsuzaki, T. Noguch, M. Wakabayashi, K. Ikeda, T. Okada, Y. Ohashi, M. Hoshino, H. Naiki, Inhibitors of amyloid beta-protein aggregation mediated by GM1-containing raft-like membranes., *Biochim. Biophys. Acta.* 1768 (2007) 122–30. doi:10.1016/j.bbamem.2006.09.014.
- [35] A.K. Buell, C.M. Dobson, T.P.J. Knowles, M.E. Welland, Interactions between amyloidophilic dyes and their relevance to studies of amyloid inhibitors., *Biophys. J.* 99 (2010) 3492–7. doi:10.1016/j.bpj.2010.08.074.
- [36] T. Shimanouchi, N. Kitaura, R. Onishi, H. Umakoshi, R. Kuboi, Secondary nucleation of A β fibrils on liposome membrane, *AIChE Journal*, 58 (2012) 1–3. doi:10.1002/aic.
- [37] A. Cuco, B. Saramago, A.P. Serro, J. P. Farinha, B. Saramago, A. G. da Silva, Interaction of the Alzheimer A β (25–35) peptide segment with model membranes, *Colloids and Surfaces B: Biointerfaces* 141 (2016) 132–138.
- [38] E. Hellstrand, B. Boland, D.M. Walsh, S. Linse, Amyloid β -protein aggregation produces

- highly reproducible kinetic data and occurs by a two-phase process, *ACS Chem. Neurosci.* 1 (2010) 13–18. doi:10.1021/cn900015v.
- [39] G. A. McCubbin, S. Praporski, S. Piantavigna, D. Knappe, R. Hoffmann, J.H. Bowie, F. Separovic, L.L. Martin, QCM-D fingerprinting of membrane-active peptides., *Eur. Biophys. J.* 40 (2011) 437–46. doi:10.1007/s00249-010-0652-5.
- [40] O. Furman, S. Usenko, B.L.T. Lau, Relative importance of the humic and fulvic fractions of natural organic matter in the aggregation and deposition of silver nanoparticles., *Environ. Sci. Technol.* 47 (2013) 1349–56. doi:10.1021/es303275g.
- [41] M.B. Hovgaard, M. Dong, D.E. Otzen, F. Besenbacher, Quartz crystal microbalance studies of multilayer glucagon fibrillation at the solid-liquid interface., *Biophys. J.* 93 (2007) 2162–9. doi:10.1529/biophysj.107.109686.
- [42] R.H. Walters, K.H. Jacobson, J. a Pedersen, R.M. Murphy, Elongation kinetics of polyglutamine peptide fibrils: a quartz crystal microbalance with dissipation study., *J. Mol. Biol.* 421 (2012) 329–47. doi:10.1016/j.jmb.2012.03.017.
- [43] N. Y. Lu, K. Yang, J. L. Li, B. Yuan, Y. Q. Ma, Vesicle deposition and subsequent membrane-melittin interactions on different substrates: a QCM-D experiment., *Biochim. Biophys. Acta.* 1828 (2013) 1918–25. doi:10.1016/j.bbamem.2013.04.013.
- [44] C.M. Bailey, A. Tripathi, A. Shukla, Effects of Flow and Bulk Vesicle Concentration on Supported Lipid Bilayer Formation, *Langmuir.* 33 (43) (2017) 11986-97
acs.langmuir.7b02764. doi:10.1021/acs.langmuir.7b02764.

Chapter 6

Conclusions and Future Directions

Supported lipid bilayers (SLBs) have become important model systems to study the biophysical properties of lipid membranes as well as molecular-level interactions between various biomolecules and the membranes. The studies presented in this thesis provide a mechanistic approach to understanding the interactions of membranes with nanoparticles, natural polymers and peptides via QCM-D analysis. QCM-D with the mass sensitivity of the nanogram scale is a great tool for characterization of the SLB by monitoring ΔF and ΔD which correspond to the SLB mass and viscoelastic properties.

In the context of cytotoxicity of nanomaterials, SLB is an important model membrane to isolate a unique mechanism of toxicity and obtain more fundamental knowledge about NP toxicity. Assessing nanomaterial hazards has proven to be challenging due to the vast diversity of nanomaterials of different properties, such as molecular composition, size, surface area, and shape. In addition, there is a range of biological systems (cell type and cellular molecules) which could be studied and which can respond in differing ways. Many combinations of nano-bio interactions need to be examined in order to develop a complete understanding of nanoparticle-cell interactions. In this work, we used QCM-D analysis of a simple zwitterionic lipid bilayer (egg PC) to isolate the mechanism of membrane disruption as the potential root-cause of gold NPs toxicity. Our systematic study revealed the effects of several different parameters, such as NP size, NP surface functionalization, and the presence of polymers, on the NP-SLB interactions.

Our results showed that 2, 5, 10, and 40 nm diameter citric acid-stabilized gold NPs caused a small lipid loss from the bilayer. The dissipation changes were small enough to suggest that no significant perturbation of the membrane structure occurred. Since the lipid loss was

quite small, it was possible that pores were not large enough to permeabilize the membrane, implying that the NPs were not cytotoxic. However as we dissolved the NPs in a synthesized polymer (PMAA), to mimic the environmental conditions, the mass change was more significant for the larger NPs. A simple model was proposed to describe the NP-SLB interactions, based on which, the competition between the particle-bilayer adhesion energy, the SLB bending energy, and the interfacial energy at bilayer defect edges allows the larger and more adhesive NPs to be engulfed by the SLB and leave the crystal surface, causing a mass loss. This large mass change can be associated with membrane disruption, suggesting that even if gold NPs are intrinsically not cytotoxic, they can become cytotoxic in the presence of other organic additives through manipulation of their adhesive interactions with the bilayer.

To have a closer look at the toxicity of NP in the environment, we expanded the work to include natural polymers, known as natural organic matters (NOMs), in the experiments. Humic substances (humic acids and fulvic acids) are the main component of NOMs. In this study, four NOMs were examined; commercially available humic acid provided by Sigma-Aldrich (HA), humic acid extracted from Elliott soil (ESHA), humic acid extracted from the Suwannee River (SRHA), and fulvic acid extracted from the Suwannee River (SRFA). The low molecular weight humic substances (SRFA and SRHA) had the ability to adsorb to the bilayer, while the high molecular weight humic substances (HA and ESHA) did not interact with the bilayer. The presence of SRFA and SRHA led to adsorption of NPs to the bilayer, while the presence of HA and ESHA did not have any effect on NP-SLB interactions. This study again demonstrated the importance of investigating NP-SLB interactions in environmentally-relevant conditions as the molecular properties of NOMs can have a significant impact on NP-SLB interactions.

In the context of SLBs application for therapeutics design and development, we characterized the interactions of SLB with A β , the peptide associated with AD. The mechanism of A β toxicity which leads to the onset of AD is not fully discovered yet. The first step in the design of effective therapeutics is to understand how interactions of A β with cell membrane lead to death of the brain cells. The first event in the cascade of events leading to AD, starts with the aggregation of A β on membrane liquid-ordered microdomains (the so-called “lipid rafts”), enriched in cholesterol and sphingomyelin. Our first aim was to establish a robust method for the formation of a raft-containing SLB model that could serve as a template for the AD research.

Formation of multi-component bilayer containing sphingomyelin and cholesterol is challenging because it often leads to the adsorption of the intact vesicles on the substrate without rupturing and forming of the bilayer. In this study, we developed a robust QCM-D protocol for formation of the SLB composed of 1,2-Dioleoyl-sn-glycero-3-phosphocholine (DOPC), 1,2-dioleoyl- sn-glycero-3-phospho-L-serine (DOPS), cholesterol (Chol), sphingomyelin (SM), and ganglioside (GM1). Different experimental variables were tested to induce the vesicle fusion, such as pH, temperature, osmotic pressure, and vesicle size. The key parameter in forming the bilayer was found to be an osmotic pressure applied by NaCl concentration gradient across the vesicle membrane. Here, we reported the effects of each tested variable on the adsorption and the fusion of the raft-containing vesicles, and we explained the data based on the mechanisms of vesicle-vesicle and vesicle-substrate interactions.

In the last chapter, we characterized the interactions of A β with the raft-containing SLB which occurred during a complex dynamic process. In this process, SLB-A β interactions lead to both peptide fibrillation and membrane destabilization. The data indicated that the peptide–membrane interactions followed a two-step kinetic pathway starting with the adsorption of

peptide until the surface adsorption sites become saturated. In the second step, the membrane structure was destabilized which led to the lipid loss from the surface. To our knowledge, this was the first time QCM-D was utilized for characterization of A β aggregation from monomer states to the mature fibrils.

This study demonstrated that QCM-D analysis of SLB offers a novel approach to answer the remaining unanswered questions in the field of Alzheimer's disease. A robust protocol was established to form and characterize a pathologically-relevant SLB. We designed and developed this method to ultimately study the effect of each lipid component on the A β -SLB interactions. Unfortunately, there are still many unanswered questions about the onset of and progression of AD that should be addressed before we can design the effective therapeutics for AD. For instance, the role of cholesterol in the cause of AD has been questioned, repeatedly in the literature, but the contradictory results from random studies cannot fully answer the question yet. Clinical studies identified the high-cholesterol diets as a risk factor of the disease [1], but at the molecular interaction level, the presence of cholesterol is reported to increase the membrane stiffness stability against perturbations [2]. The method that we developed in this study can be easily applied to variety of experimental conditions to conduct systematic studies on the role that each lipid component plays the toxicity of A β peptide.

References

- [1] C.M. Yip, A. A. Darabie, J. McLaurin, Abeta42-peptide assembly on lipid bilayers., *J. Mol. Biol.* 318 (2002) 97–107. doi:10.1016/S0022-2836(02)00028-1.

- [2] W. Gibson Wood, Amyloid beta-protein interactions with membranes and cholesterol: causes or casualties of Alzheimer's disease, *Biochim. Biophys. Acta - Biomembr.* 1610 (2003) 281–290. doi:10.1016/S0005-2736(03)00025-7.